OPTOGENETIC DISSECTION OF PHRENIC PREMOTOR NETWORKS

by

JARED MICHAEL CREGG

Submitted in partial fulfillment of the requirements

for the degree of Doctor of Philosophy

Dissertation advisor: Jerry Silver, PhD

Department of Neurosciences

CASE WESTERN RESERVE UNIVERSITY

January 2018

CASE WESTERN RESERVE UNIVERSITY

SCHOOL OF GRADUATE STUDIES

We hereby approve the thesis/dissertation of

JARED MICHAEL CREGG

candidate for the degree of Doctor of Philosophy*.

Committee Chair:

Lynn T. Landmesser, PhD

Committee Members:

Warren J. Alilain, PhD

Evan S. Deneris, PhD

Thomas E. Dick, PhD

Jerry Silver, PhD

November 2nd, 2017

* We also certify that written approval has been obtained for any proprietary material contained therein.

Contents

List of Tables

Chapter 3

List of Figures

Chapter 2

Chapter 3

List of Abbreviations

ACh	Acetylcholine
AChR	Acetylcholine Receptor (nicotinic)
ANS	Autonomic Nervous System
AR	Adrenergic Receptor (α_1- or β-)
Atoh1	Atonal Homologue 1
CCHS	Central Congenital Hypoventilation Syndrome
ChAT	Choline Acetyltransferase
ChR2	Channelrhodopsin-2
CNS	Central Nervous System
CPG	Central Pattern Generator
Cre	Recombinase (Causes recombination)
DAMGO	[D-Ala^2, *N*-MePhe^4, Gly-ol]-enkephalin
Dbx1	Developing Brain Homeobox 1
E	Embryonic Day
Egr2	Early growth response 2 (Krox20)
EYFP	Enhanced Yellow Fluorescent Protein
f	Frequency
GABA	γ-Aminobutyric Acid
$GABA_AR$	$GABA_A$ receptor
Gad1	Glutamate Decarboxylase 1
GlyR	Glycine Receptor
GlyT2	Glycine Transporter 2
GPCR	G-Protein Coupled Receptor

KCC2	Potassium-chloride co-transporter 2
LacZ	β-Galactosidase
Nalcn	Sodium Leak Channel
OR	Opioid Receptor
P	Post-natal Day
pF	Parafacial
pFRG	Parafacial Respiratory Group
Phox2b	Paired-like Homeobox 2b
PICo	Post-inspiratory Complex
Piezo2	Piezo Type Mechanosensitive Ion Channel Component 2
PMN	Phrenic Motor Neuron
PN	Phrenic Nerve
PRAZ	Prazosin
preBötC	preBötzinger Complex
PROP	Propranolol
PTX	Picrotoxin
R26R	Rosa26 Reporter
RTN	Retrotrapezoid Nucleus
SCI	Spinal Cord Injury
STRYCH	Strychnine
Vgat	Vesicular GABA Transporter
Vglut2	Vesicular Glutamate Transporter 2

Optogenetic Dissection of Phrenic Premotor Networks

Abstract

by

JARED MICHAEL CREGG

A fundamental goal in systems neuroscience is to understand how behaviors are executed by the nervous system. Respiration is an essential behavior which we perform hundreds of millions of times over our lifespan. Given that deficits in respiration underlie a variety of human diseases and conditions, the neural mechanisms which control respiration are the subject of active investigation. Here, using an *ex vivo* model of mouse respiration combined with optogenetic and pharmacological approaches, I examined how central neural networks control phrenic motor neurons—which are the primary motor output associated with inspiration.

Inspiratory bursts are generated in a medullary structure termed the preBötC, and relayed via descending bulbospinal projections to phrenic motor neurons, which reside in cervical spinal cord levels C3-5/6. Spinal cord injury (SCI) above cervical level 4 disrupts these descending fibers and leads to permanent loss of diaphragm function. In this body of work, I found that after complete cervical SCI, spontaneous and bilaterally coordinated phrenic bursting could be initiated by blockade of fast inhibitory synaptic transmission. Here, glutamatergic neurons were sufficient and necessary for induction of phrenic

bursts. Direct stimulation of phrenic motor neurons was insufficient to evoke phrenic burst activity. Therefore, I identify a recurrent excitatory network which can direct phrenic motor bursting in the absence of medullary input. Transection and pharmacological manipulations indicated that this propriospinal network is dissociable from medullary circuits which generate *bona fide* inspiration, suggesting a novel non-respiratory function. Thus, these results demonstrate that phrenic motor neurons can be controlled by two independent premotor networks: the classical inspiratory network of the preBötC, and a second "latent" network which may initiate phrenic motor activity in physiological situations of increased network excitability.

The preBötC is required for generation of inspiratory bursts, and therefore changes in inspiratory frequency are ultimately coordinated by the preBötC. How is inspiratory frequency controlled? In the simplest model, excitation increases inspiratory frequency and inhibition causes apnea. To test this model, I used an optogenetic approach to stimulate select populations of hindbrain neurons and characterize how they modulate inspiratory frequency. I found that stimulation of excitatory Phox2b-lineage, putative CO_2-chemosensitive neurons dramatically increased frequency. Surprisingly, however, this effect was completely abolished by blockade of fast inhibitory synaptic transmission, indicating an essential role for inhibitory neurons in increasing inspiratory rate in response to elevated CO_2. To investigate inhibitory mechanisms which increase inspiratory frequency, I stimulated Vgat+ neurons and found that *phasic inhibition* can actually drive increases in inspiratory frequency via a rebound-like mechanism. I further found

that the parafacial oscillator, which generates expiration, likely acts as a source of phasic activity during stimulation of Phox2b+ neurons. These data argue that generation of inspiratory rhythm occurs in two functionally distinct modes—a low-frequency mode which is generated by excitatory circuits of the preBötzinger complex, and a high-frequency mode which requires inhibition. We propose a model whereby high frequency inspiratory bursts are generated as a product of inhibitory coupling between multiple excitatory oscillators.

Chapter 1: Introduction

Central Pattern Generators are the Neural Basis for Repetitive Motor Actions

Both the invertebrate and vertebrate nervous systems generate a variety of rhythmic behaviors independent of sensory input. These rhythmic behaviors include locomotion, respiration, mastication, micturition, postural control, swallowing, saccadic eye movements, and many others (Grillner, 2006; Marder, 2001). The networks underlying these stereotyped motor outputs are referred to as central pattern generators (CPGs). CPGs are thought to exhibit common underlying principles which govern their operation, including similar mechanisms of rhythm generation and modes of recruitment by higher-order circuits (Grillner, 2006). Understanding the core logic underlying CPG organization in a variety of systems is expected to allow insight into how the nervous system gives rise to complex processes, such as human behavior—what we actually do. These studies represent a “reverse engineering” approach to understanding our brains—if we understand motor output, we might work backwards to understand more complicated structures of the brain (e.g. basal ganglia, cortex).

The appreciation that central networks govern the *generation* of rhythmic motor output, however, has not always been the standard model (Marder, 2001). Early studies on locomotion posited that peripheral sensory input was the driving factor underlying both initiation and maintenance of locomotion (Guertin, 2012). In this model, peripheral inputs from exteroceptive organs in the skin and

proprioceptive organs of the muscles, joints, and tendons are integrated by central networks in successive order, allowing for movement to be coordinated continuously between flexor/extensor muscles of the right and left sides. This model for generation of movements is called the “chain of reflexes” model (Marder, 2001).

Although it seems obvious that our movements are not controlled in an “outside in” manner by our environments, formal proof was lacking until the formative studies of Thomas Graham Brown (Brown, 1911, 1914; Guertin, 2012; Stuart and Hultborn, 2008). To summarize briefly, Brown found that animals under a certain anesthetic plane did not exhibit proprioceptive or exteroceptive reflexes. Nonetheless, when lying on their sides (and not bearing weight), these animals would exhibit spontaneous and rhythmic hindlimb movements upon transection of the thoracic cord (Brown, 1911, 1914; Guertin, 2012). Brown thus proposed a “half-center” model where rhythms could be generated as a result of reciprocal inhibition between the left and right sides. Although these and other early experiments provided evidence for central generation of locomotor rhythms, the ideas of Brown would not gain traction for many years. Specifically, Anders Lundberg resurrected these studies, providing formative evidence for central generation of locomotor rhythms using intracellular recording combined with pharmacological manipulations in transected cats (Guertin, 2012; Jankowska et al., 1967; Stuart and Hultborn, 2008). Thus, it is now widely appreciated that CPGs govern the generation of all motor rhythms (Grillner, 2006; Marder, 2001), while sensory feedback helps to modulate these rhythms in a sophisticated way.

Respiration is Generated by a Central Neural Network Located in the Medulla

Respiration is an especially interesting motor behavior because, in contrast to other mammalian motor behaviors such as locomotion, mastication, micturition, etc.—which are episodic, respiration must be maintained continuously through life to maintain O_2/CO_2 homeostasis.

Respiration is a very complex act, involving the coordination of primary and accessory "pump" muscles, such as the diaphragm and intercostal muscles, as well as laryngeal and pharyngeal muscles which allow passage of air within the upper airway. Muscles which control inspiration—the act of drawing air into the lungs—must be coordinated not only with muscles that control expiration, but also with muscles that control a variety of orofacial behaviors, including vocalization, mastication, swallowing, etc. Thus, although it is tempting to say that there is a CPG or nervous center for breathing, these terms are vastly oversimplified. Nonetheless, respiration as a complex behavior can be broken down into discrete motor actions (e.g. inspiration, expiration).

As early as 1858, Pierre Flourens proposed that respiration was generated by a "vital node" within the medulla oblongata—the so-called *noeud vital* for respiration (Flourens, 1858; Ramirez, 2011). Soon afterward, however, several other investigators would report observing respiratory movements after spinal transection, suggesting that there was a spinal origin for respiration too (Brown-Séquard, 1860; Langendorff, 1880; Wertheimer, 1886). The initial explanation for variable reports of respiratory movements after spinal transection

was that spinal shock following transection often inhibited respiratory activity within the cord (Ghali, 2017). Thus, Porter undertook a series of experiments aimed at showing that phrenic motor neurons were not subject to inhibition derived from spinal shock, finding that increasing respiratory drive could augment inspiratory motor activity ipsilateral to a cervical spinal hemisection (Porter, 1895). By demonstrating that loss of phrenic inspiratory motor activity was not the result of inhibition caused by spinal shock, and instead that this loss of activity could be attributed to loss of bulbospinal impulses, these results provided strong support for a supraspinal (medullary) origin of respiratory rhythm (Porter, 1895).

With the advent of intracellular recording in the mid-20th century, studies on the "neurogenesis" of breathing flourished (Cohen, 1979; von Euler, 1983; Ezure, 1990; Long and Duffin, 1986; Richter, 1982). It was quickly determined from phrenic and intercostal nerve recordings that respiration exhibits three distinct phases: expiration, inspiration, and post-inspiration (von Euler, 1983; Richter, 1982). Expiration is normally passive—meaning that expiratory breaths are normally the result of elastic recoil of the ribcage following inspiration. Forceful recoil of the ribcage, however, is prevented by active post-inspiratory phrenic inspiratory activity which serves as a type of "brake" on expiration (von Euler, 1983). Unit and intracellular activity recorded from single neurons of the medulla could be correlated with distinct phases of the respiratory cycle, confirming that the respiration does, indeed, have a three-phase basis centrally (Richter, 1982).

Much of the experimental work during this period of time—and the models constructed as a result—were based on characterization and classification of unit and intracellular recordings from the ventrolateral medulla. Interpretations and models from these early studies should be cautioned in that many were the result of inference rather than hypothesis-driven experimentation. For example, a lack of activity by specific inspiratory-associated neurons was often attributed to inhibition (Richter, 1982), but it was not known at the time that single neurons of the ventrolateral medulla could exhibit pacemaker-like properties. “Pacemaker” neurons, or neurons which exhibit bursting in synaptic isolation, were only discovered within the ventrolateral medulla much later (Johnson et al., 1994).

Thus, many early studies modeled respiratory rhythmogenesis as a “network” phenomenon in which rhythm was the result of sequential phase transitions between expiratory, inspiratory, and post-inspiratory neurons, transitions which were presumably mediated by inhibitory synaptic transmission (von Euler, 1983; Richter, 1982). Indeed, a whole nomenclature has been established surrounding the characterization of these neurons and the relationships between them (Ezure, 1990), and some of these models are still being used by investigators today (Richter and Smith, 2014). In the late 80s, however, the discovery that inspiration could be generated in the absence of synaptic inhibition (Feldman and Smith, 1989), would lead to a “kernel” model for respiratory rhythmogenesis (Feldman et al., 1990; Smith et al., 1990).

The Pre-Bötzinger Complex: a Medullary Nucleus Which Generates Inspiration

Anatomical Identification of the Pre-Bötzinger Complex

Until 1991, a discrete population of neurons responsible for generating mammalian respiratory rhythm—the hypothesized *noeud vital*—had not been identified. Indeed, up until the late 80s, respiratory rhythm was thought to be a network-wide phenomenon (Richter, 1982). The discovery that inhibition was not critical for respiratory rhythmogenesis *per se* (Feldman and Smith, 1989), led to the hypothesis that a “kernel” of excitatory neurons underlies the generation of respiratory rhythm (Feldman et al., 1990). While this “kernel” had been localized to the ventrolateral medulla, technical limitations associated with adult rodent models prevented further anatomical definition of these circuits.

Development of the *en bloc* preparation in the 1970s and 80s granted neurophysiologists greater experimental access to hindbrain and spinal cord circuits (Landmesser et al., 1983; McClellan, 1984; Otsuka and Konishi, 1974; Rovainen, 1983; Smith and Feldman, 1987; Suzue, 1984; Suzue and Jessell, 1980), ultimately leading to anatomical identification of rhythmogenic respiratory circuits in the medulla (Smith et al., 1991).

Briefly, an *en bloc* preparation consists of the caudal neuroaxis—including the pons, medulla, and spinal cord—dissected free and bathed in oxygenated artificial cerebrospinal fluid (aCSF) perfusate. Here, tissue metabolism is supported by passive diffusion of O_2 and glucose into the parenchyma. Due to spatial limitations of diffusion, *en bloc* analyses of nervous tissue are limited to embryonic and early post-natal development in small mammalian species—including *mus musculus* and *rattus norvegicus*. Interestingly, the neonatal *en bloc*

preparation supports a robust respiratory-like rhythm termed fictive inspiration (Smith and Feldman, 1987; Suzue, 1984). Spontaneous rhythmic episodes of motor activity can be observed coincidentally in the phrenic nerve (which innervates the diaphragm), the C4 ventral root (which gives rise to the phrenic nerve), and the hypoglossal (XII) nerve—episodes which coincide with upward ribcage movements *in vitro* (Smith and Feldman, 1987; Suzue, 1984). Transection experiments demonstrate that this activity originates in the medulla (Smith and Feldman, 1987; Suzue, 1984). Thus, this neural activity is thought to be the *in vitro* correlate of *bona fide* respiration (Smith and Feldman, 1987; Suzue, 1984).

Using this *en bloc* model of respiration, Smith and colleagues went on in 1991 to define the medullary site of inspiratory rhythm generation (Smith et al., 1991). By performing sequential 75 µm vibratome sections in the rostrocaudal direction starting at the pontomedullary junction, Smith and colleagues identified a region caudal to the Bötzinger complex and rostral to the obex that generates inspiration. Removal of this region eliminated fictive respiratory activity from the C4 nerve (Smith et al., 1991). Additionally, sectioning in the rostral direction starting at the spinomedullary junction did not disrupt fictive respiration in more rostral cranial nerves X-XII until these sections came within 200 µm of that level which eliminated respiration in the rostrocaudal direction—thus indicating that this 200 µm slice of tissue is necessary for generation of inspiration. Indeed, *in vitro* recordings from a 500 µm slice that included this region indicated that this slice alone is sufficient for generating rhythmic hypoglossal inspiratory activity.

Furthermore, intracellular recordings indicated that the neurons which exhibit rhythmic bursting are located bilaterally in the ventrolateral region of the slice, ventral to the Nucleus Ambiguus and dorsal to the lateral reticular nucleus (Smith et al., 1991). Injection of CNQX, a AMPA/kainite receptor antagonist, into this region blocked inspiratory bursting. Thus it was proposed that this anatomically defined population of neurons—termed the pre-Bötzinger complex (preBötC)—is both sufficient and necessary for generating inspiration at least *in vitro* (Smith et al., 1991), representing an excitatory "kernel" or *noeud vital* for generation of respiratory rhythm.

Koshiya and Smith subsequently used Ca^{2+} imaging to visualize the generation of inspiratory rhythmogenesis in preBötC slices (Koshiya and Smith, 1999). Until these experiments, it had been hypothesized that individual "pacemaker" neurons generate bursting activity which is then synchronized at the population level through excitatory synaptic mechanisms (Ramirez et al., 1996; Rekling and Feldman, 1998; Smith et al., 1991). Given the inherent difficulty of performing intracellular recording from several neurons at once, this hypothesis was difficult to test experimentally. Koshiya and Smith used Ca^{2+} imaging to demonstrate that inspiratory bursts indeed arise via dynamic, coordinated action of a large population of excitatory neurons in the preBötC. Blocking excitatory synaptic coupling amongst this population by application of CNQX did not affect the generation of bursts by individual preBötC neurons, but largely eliminated coupling between individual neurons (Koshiya and Smith, 1999). CNQX application completely abolished inspiratory bursting at the level of hypoglossal

motor neurons (Koshiya and Smith, 1999; Smith et al., 1991). These data provided strong evidence that the preBötC acts as the site for inspiratory rhythm generation (at least *in vitro*) in that they provided a mechanistic explanation for the origin or genesis of spontaneous inspiratory burst activity.

Although extensive *in vitro* physiological data support the hypothesis that inspiration is generated by the preBötC, there has, nonetheless, been debate in the past as to whether observations made in reduced (i.e. *en bloc* or slice) paradigms can be generalized to eupneic breathing in the whole animal—especially intact, awake adults (St John, 2009). Medullary-spinal cord preparations and preBötC slices exhibit highly rhythmic inspiratory bursting; however, the motor output is aberrant in that it exhibits decrementing (rather than incrementing) activity as well as an unusual synchronization of inspiratory motor output between cranial and cervical/thoracic spinal nerves (Smith et al., 1990; Suzue, 1984), both of which are reminiscent of “gasping” observed *in vivo* (St John, 1990, 2009). Furthermore, only during progressive anoxia and/or “gasping” does respiration exhibit such a slow inspiratory frequency and such a long expiratory phase without generation of any significant spontaneous expiratory motor discharge (Macefield and Nail, 1987). Indeed, although late expiratory unit activity can be observed in the glossopharyngeal nerve *in vitro* (Smith et al., 1990), there is a marked lack of either intercostal expiratory unit activity or downward ribcage movements (Smith and Feldman, 1987; Smith et al., 1990; Suzue, 1984). “Gasping” observed during anoxia was thus proposed to manifest in *in vitro* preparations due to an “anoxic core” forming within the tissue as a

result of poor oxygenation (Brockhaus et al., 1993; Okada et al., 1993). These data have led to criticism that studies on generation of inspiration *in vitro* cannot be generalized to eupnea in the intact adult animal *per se*.

Nonetheless, there are many arguments that *in vitro* modes of inspiratory rhythmogenesis are representative of *bona fide* inspiration (Smith et al., 1990). *In vitro* preparations exhibit an abnormally long inspiratory burst duration as well as a low frequency of inspiratory bursting (Hilaire et al., 1997; Smith and Feldman, 1987; Smith et al., 1990; Suzue, 1984). However, these differences in burst frequency and duration can be largely attributed to the lack of peripheral vagal sensory afferent feedback *in vitro* as well as the reduced recording temperature necessary to keep the preparation from becoming anoxic; preparations warmed to 35 ^{o}C exhibit an inspiratory burst frequency and burst duration similar to that observed in vagotomized neonatal rats *in vivo* (Smith et al., 1990). Furthermore, vagotomized neonatal rats exhibit decrementing inspiratory motor discharge *in vivo* (Smith et al., 1990). Finally, generation of inspiratory rhythm *in vitro* is sensitive to known modulators of inspiration: The frequency of spontaneous inspiratory burst episodes is augmented by acidic pH, the opioid receptor antagonist naloxone, and the NK1R agonist substance P (Gray et al., 1999; Suzue, 1984), and furthermore, is depressed by alkaline pH or enkephalin-based opioid receptor agonists (Gray et al., 1999; Suzue, 1984).

Feldman and colleagues thus proposed the “kernel model” of inspiratory rhythmogenesis (Feldman et al., 1990; Smith et al., 1990). In this “kernel model”, the mechanisms generating inspiratory rhythm *in vitro* represent a kernel of the

system which generates inspiratory rhythm *in vivo*. In the intact animal, this "kernel" would be embedded within a much larger framework which would serve largely to modulate the basic rhythm generated by this "kernel". These modulatory elements would include pontine, chemosensory, vagal sensory feedback, as well as others. Thus, it was proposed that basic mechanisms underlying rhythmogenesis could be studied *in vitro*, and were the same as those underlying rhythm generation *in vivo* (Feldman et al., 1990).

Does the "kernel" which generates inspiration *in vitro* also generate inspiration *in vivo*? Two experiments performed in 1996 and 1997 provided evidence toward this end. First, Koshiya and Guyenet performed bilateral injections of the $GABA_A$ receptor agonist muscimol into the rostral aspect of the caudal ventrolateral medulla in adult rats, injection sites which overlapped with the reported location of the preBötC (Koshiya and Guyenet, 1996). Upon injection of muscimol, respiratory activity in the phrenic, hypoglossal, and vagus nerves was eliminated (Koshiya and Guyenet, 1996). Second, Ramirez and colleagues performed injections of ω-conotoxin, a N-type Ca^{2+} blocker which eliminates Ca^{2+} entry into presynaptic terminals, into the preBötC of adult cats (Ramirez et al., 1998). Unilateral injection of ω-conotoxin caused a decrease in phrenic nerve burst amplitude bilaterally which sometimes disappeared altogether, indicative of apnea. Indeed, subsequent experiments with unilateral injection of tetrodotoxin (TTX) into the preBötC of adult cats eliminated respiratory activity, inducing persistent apnea (Ramirez et al., 1998). These

experiments demonstrated that the preBötC is necessary for inspiratory bursting *in vivo*.

Molecular Identification of the Pre-Bötzinger Complex

The positive anatomical identification of the preBötC as the site for respiratory rhythm generation was initially problematic given its location in the reticular formation of the medulla—a diffusely organized, heterogeneous region of gray matter (Ramirez, 2011). While the preBötC had been identified functionally (Koshiya and Guyenet, 1996; Ramirez et al., 1998; Smith et al., 1991), it's molecular identity remained ambiguous until formative immunohistochemical studies of the late 1990's and early 2000's (Gray et al., 1999; Stornetta et al., 2003).

In 1999, Gray and colleagues found that the peptides substance P and DAMGO, neurokinin-1 receptor (NK1R) and μ-opioid receptor (μ-OR) agonists, respectively, had dramatic effects on inspiratory frequency (Gray et al., 1999). Given that the effects of substance P and DAMGO were insensitive to GABA/glycine receptor agonists, the authors reasoned that it was likely that substance P and DAMGO had direct effects on excitatory rhythmogenic neurons of the preBötC and/or upstream neuronal populations. The authors subsequently performed immunohistochemical analyses, finding that neurons of the preBötC expressed NK1R and μ-OR whereas adjacent neurons of the BötC or rVRG, cholinergic neurons, and catecholaminergic neurons did not express NK1R or μ-OR (Gray et al., 1999). The authors further found that the so-called type 1

rhythmogenic neurons of the preBötC expressed both NK1R and μ-OR, whereas type 2 neurons—which are not rhythmogenic—only expressed NK1R. The authors concluded that, since models of respiratory rhythmogenesis posit that excitation of type 1 neurons increases respiratory frequency and hyperpolarization of type 1 neurons decreases frequency, co-expression of NK1R and μ-OR uniquely identifies rhythmogenic neurons of the preBötC (Gray et al., 1999). These neurons were subsequently found to also exhibit expression of *Vglut2* and somatostatin (Stornetta et al., 2003).

Initial molecular identification of the preBötC would subsequently allow for further evidence that the preBötC acts as the sole site for generation of inspiration *in vivo* (Gray et al., 2001; McKay et al., 2005; Tan et al., 2008). In 2001, Gray and colleagues went on to show that specific ablation of NK1R neurons *in vivo* dramatically disrupted respiration (Gray et al., 2001). Unilateral injection of substance P conjugated with saporin, a cytotoxic agent which inhibits ribosomal protein synthesis, effectively ablated the NK1R-expressing neurons of the preBötC in the injected side but not in neurons of the contralateral side. Bilateral injections of substance P-saporin eliminated approximately 80% of NK1R neurons of the preBötC, and resulted in progressive, severe respiratory ataxia (Gray et al., 2001). Thus, consistent with previous studies which used non-specific methods to block activity within the preBötC (Koshiya and Guyenet, 1996; Ramirez et al., 1998), specific ablation of molecularly defined, rhythmogenic neurons within the preBötC dramatically disrupted eupneic respiration (Gray et al., 2001). These initial studies would subsequently be

complemented by follow-up work demonstrating that progressive ablation of NK1R neurons of the preBötC first disrupts respiration specifically during sleep (McKay et al., 2005). This data suggested that neurodegeneration and loss of neurons within the preBötC could lead to sleep-disordered breathing (Hayes et al., 2012; McKay et al., 2005), such as might occur during sleep apnea. Furthermore, silencing somatostatin-expressing neurons in the preBötC induced fatal central apneas (Tan et al., 2008), indicating a central role for the preBötC control of inspiration *in vivo*.

Using these descriptions of the preBötC in both mice and rats (Gray et al., 1999; Stornetta et al., 2003), Schwarzacher and colleagues subsequently carried out neuroanatomical characterization of the preBötC in humans (Ramirez, 2011; Schwarzacher et al., 2011). These authors found a substantial population of NK1R positive and somatostatin positive neurons in the ventrolateral medulla in a region which did not overlap with neighboring populations of motor neurons or catecholaminergic neurons, and within a region consistent with that described in mice and rats. Furthermore, humans with multiple systems atrophy exhibited a substantial reduction in the number of NK1R positive and somatostatin positive neurons in within the putative preBötC (Schwarzacher et al., 2011), suggesting that breathing deficits associated with multiple systems atrophy might result from neuroanatomical abnormalities in the preBötC. Nonetheless, neuroanatomical deficits in other regions of the brainstem are also likely to contribute to impaired respiration in these patients (Benarroch, 2007; Ramirez, 2011; Schwarzacher et al., 2011).

Although much progress had been made in the 2000's toward molecular identification of the preBötC (Gray et al., 1999, 2010; Stornetta et al., 2003), less was known about its transcriptional specification (Gray, 2008). This would change in 2010 with Bouvier and colleagues' discovery of *Dbx1* as a critical determinant of respiratory rhythmogenesis (Bouvier et al., 2010), which we review in detail below (see Respiration: Insights From Molecular Genetics).

Mechanisms of Inspiratory Rhythm Generation

First attempts at understanding cellular modes of inspiratory rhythm generation were carried out in the *en bloc* preparation (Feldman and Smith, 1989). These early results indicated that inhibition and Cl^--mediated conductances (such as those mediated by GABA and glycine receptors), while being essential for determining inspiratory burst amplitude and duration, were dispensable for generation of inspiratory rhythm (Feldman and Smith, 1989). Thus, mechanisms of rhythm generation which depend on reciprocal inhibition were categorically excluded as explanations for the origin of respiratory rhythm (Perkel and Mulloney, 1974; Skinner et al., 1994)—although this assumption would be revisited again numerous times by these authors and others in subsequent decades (Janczewski et al., 2013; Marchenko et al., 2016; Sherman et al., 2015). Instead, these early studies indicated that excitatory pacemaker neurons may underlie generation of respiratory rhythm (Feldman and Smith, 1989).

Pacemaker Neurons

What is a pacemaker neuron? A pacemaker neuron is defined as a neuron which exhibits rhythmic bursting in synaptic isolation (in low Ca^{2+} or after blockade of glutamate and GABA/glycine receptors using CNQX, APV, bicuculline, and STR). In 1994, it was found that single neurons in the preBötC exhibit rhythmic bursting after synaptic isolation from the network in which they are embedded (Johnson et al., 1994), and thus it was proposed that synchronization of pacemaker neurons through mutually excitatory interactions may underlie the generation of respiratory rhythm (Rekling and Feldman, 1998).

Which membrane currents underlie rhythmic bursting in pacemaker neurons? Persistent sodium current (I_{NaP}) and Ca^{2+}-activated nonspecific cation current (I_{CAN}) were proposed to be the two primary currents underlying initiation of bursting in pacemaker neurons (Del Negro et al., 2001, 2002a, 2005; Peña et al., 2004; Rybak et al., 2003; Thoby-Brisson and Ramirez, 2001). While pacemaker neurons contribute to bursting activity within the preBötC, they actually account for only a small percentage (<10%) of the total number of preBötC neurons (Del Negro et al., 2005).

Group Pacemaker Hypothesis

Although pacemaker currents contribute to rhythmic activity within single neurons of the respiratory network, it was initially unknown whether pacemakers were essential for generation of respiratory rhythm. In the 1990s, two alternative models had been proposed for generation of inspiratory bursts by excitatory

neurons of the preBötC (Rekling and Feldman, 1998). In the first model, pacemaker neurons exhibit rhythmic bursting in synaptic isolation. Bursting amongst several pacemaker neurons becomes synchronized through mutual excitatory connections. In the second model, termed the “group pacemaker” model, bursting by individual neurons is dispensable for generation of network-wide bursts. Instead, bursting is a result of extensive recurrent excitatory connectivity amongst a group of neurons with no intrinsic capability of generating bursts by themselves. Here, it is predicted that stimulation of single neurons would not be sufficient for generating a network-wide burst, and instead, stimulation of at least a few excitatory neurons at the same time would be required for evoking a burst (Rekling and Feldman, 1998).

To distinguish between these alternatives, the Feldman lab sought to examine whether inspiration (motor activity of XII) was abolished after blockade of intrinsic bursting in pacemaker neurons of the preBötC (Del Negro et al., 2002b, 2005). In 2002, Del Negro and colleagues found that blockade of persistent sodium current (I_{NaP}) abolished bursting in individual pacemaker neurons of the preBötC, but did not eliminate inspiration (Del Negro et al., 2002b); application of riluzole completely abolished I_{NaP}-dependent bursting from individual pacemaker neurons but did not block bursting from the preBötC (Del Negro et al., 2002b). Thus, pacemaker neurons did not appear to be essential for respiratory rhythmogenesis, and instead it was proposed that respiratory rhythmogenesis is an “emergent network property”.

Around the same time, it was proposed that calcium or non-specific cation currents might also underlie bursting of a subset of pacemaker neurons in certain contexts (Peña et al., 2004; Thoby-Brisson and Ramirez, 2001), which might explain why elimination of I_{NaP} alone did not terminate inspiration. In 2005, Del Negro and colleagues found that elimination of both I_{NaP} and I_{CAN} did indeed abolish bursting of individual pacemaker neurons and inspiratory bursts at-large. Nonetheless, application of substance P, which promotes neuronal excitability by activation of sodium leak channels (Gray et al., 1999; Shi et al., 2016; Yeh et al., 2017), could re-initiate inspiratory bursts (Del Negro et al., 2005). This data indicated that blockade of I_{NaP} and I_{CAN} suppressed inspiratory bursting by reducing overall excitability. Thus, bursting properties of individual pacemaker neurons were not essential for initiation of network-wide bursts (Del Negro et al., 2005).

These results would subsequently lead to pursuit of "emergent" mechanisms underlying a so-called "group pacemaker hypothesis" for respiratory rhythmogenesis (Feldman and Del Negro, 2006; Del Negro and Hayes, 2008; Del Negro et al., 2008), current models for which depend on calcium-activated nonspecific cation current, synaptic depression, and/or synaptic facilitation (Guerrier et al., 2015; Kottick and Del Negro, 2015; Del Negro et al., 2011; Pace et al., 2007; Rubin et al., 2009). Although "emergent" mechanisms can be implicated through negative experimental data, I think it is worth noting that "emergent" mechanisms are intrinsically difficult to test experimentally.

Inhibitory Neurons in Control of Inspiration: Rhythm or Pattern?

Going back to some of the earliest work examining cellular mechanisms of respiratory rhythm generation, it was quickly determined that inhibition is not required for generation of inspiratory bursts or respiratory rhythm *per se* (Feldman and Smith, 1989). Indeed, it is very clear from results in both the *en bloc* preparation and in preBötC slice preparations that global blockade of inhibitory synaptic transmission does not block the generation of inspiratory bursts (Feldman and Smith, 1989; Gray et al., 1999). Deletion of *Vglut2* results in failure to initiate inspiratory bursts at birth (Wallen-Mackenzie et al., 2006). Thus, it has been proposed that the core group of neurons which generate inspiratory rhythm are excitatory (Janczewski et al., 2013).

Owing to the fact that these results were obtained in reduced preparations (Feldman and Smith, 1989; Gray et al., 1999), it was argued that inhibitory neurons might nonetheless be critical for respiratory rhythm generation *in vivo* (Abdala et al., 2015; Richter and Smith, 2014; Shevtsova et al., 2014). These are arguments of state dependence—which are likely to be contested depending on specifics of any given experimental paradigm. Nonetheless, is was posited that the most important state to measure was that of the *in vivo* animal (Richter and Smith, 2014). Thus, in 2013 Janczewski and colleagues sought to determine whether inhibition was critical for respiratory rhythm generation *in vivo* (Janczewski et al., 2013). Bilateral injection of the preBötC with bicuculline and strychnine in adult rats did not cause termination of respiratory rhythm, but did

cause a decrease in respiratory frequency attributed to blockade of inhibitory vagal feedback associated with the Hering-Breuer reflex (Janczewski et al., 2013). The authors concluded that while inhibition is very important for patterning inspiratory bursts, inhibition is dispensable for the generation of inspiratory rhythm *in vivo*.

Given that blockade of inhibitory neurons can result in homeostatic mechanisms which cause the appearance of alternate forms of rhythm (Moult et al., 2013), it was important to extend these studies using optical approaches for making precise and transient manipulations to the preBötC (Sherman et al., 2015). Indeed, at the time it was known that a subset of GlyT2+ neurons in the preBötC exhibited pacemaker properties (Morgado-Valle et al., 2010), and thus more transient manipulations might uncover fundamentally new circuit dynamics. In 2015, Sherman and colleagues infected GlyT2+ neurons in the preBötC with excitatory and inhibitory opsins and examined ventilatory responses to photostimulation in awake mice (Sherman et al., 2015). Photostimulation of ChR2-expressing GlyT2+ neurons within the preBötC immediately caused apnea for the duration of the photostimulus. After termination of the photostimulus, inspiration resumed with a consistent latency—a mechanism termed “respiratory reset” (Sherman et al., 2015). Stimulation of archaerhodopsin-expressing GlyT2+ neurons augmented inspiration, where amplitude of individual inspiratory breaths was larger and respiratory frequency was increased (Sherman et al., 2015). The authors concluded that glycinergic preBötC neurons modulate inspiratory pattern but do not contribute to the generation of inspiratory rhythm.

Interestingly, injection of $GABA_AR$ and GlyR antagonists in the BötC can dramatically suppress inspiration (Marchenko et al., 2016). Marchenko and colleagues proposed that this experimental paradigm blocked inhibitory synapses within the BötC derived from preBötC projections, causing an increase in BötC inhibition to the preBötC (Marchenko et al., 2016). This sort of feedback loop highlights how network models of inspiration are important for understanding respiratory control. Nonetheless, these data are largely consistent with a model in which excitatory neurons of the preBötC generate rhythmic inspiratory bursts, and inhibitory neurons serve largely to shape inspiratory burst pattern (Janczewski et al., 2013; Marchenko et al., 2016; Sherman et al., 2015).

To be clear, although the role of inhibition in generation of rhythm versus modulation of respiratory pattern is still under debate, it is widely accepted that inhibitory neurons are critical for respiration and play an essential role in allowing for antagonistic phasing between expiration, inspiration, and post-inspiration (Abdala et al., 2015; Anderson et al., 2016; Janczewski et al., 2013; Richter and Smith, 2014; Sherman et al., 2015). From an outsider's perspective, a clearer definition of what type of inhibitory circuit conformations are inherently rhythmogenic would help to define experiments that support or rule out the specific involvement of inhibitory neurons in respiratory rhythmogenesis.

Modularity in Respiratory Control

Modular Organization of Zebrafish and Mammalian Locomotor Systems

Locomotor systems in the zebrafish and mammalian spinal cord are thought to exhibit modular organization, that is, specific rhythmic burst “modules” exert control over specific muscles and/or groups of related muscles (Bagnall and McLean, 2014; Hagglund et al., 2013; McLean and Dougherty, 2015). Here, rhythm is a property of specific burst modules and motor pattern arises via coordination between modules.

In zebrafish, this sort of “modular” organization can allow for complex modes of swimming behavior, such as axial rotation—which is controlled by specific engagement of modules controlling ventral muscles on one side (e.g. the left side) and dorsal muscles on the opposite side (Bagnall and McLean, 2014). Evidence for modular organization of lumbar locomotor circuits in the mammalian spinal cord has also been uncovered (Hagglund et al., 2013). Here, optogenetic stimulation of Vglut2+ interneurons in small regions of the spinal cord could evoke rhythmic motor output, and these rhythms did not cause recruitment of neighboring modules (Hagglund et al., 2013). This data indicates that locomotor rhythms are the property of discrete rhythmogenic structures, and that motor pattern arises via interactions between these rhythmogenic modules.

Nonetheless, organization of motor behaviors into discrete rhythmogenic modules does not explain modes of rhythmogenesis for every motor system. In stark contrast to modular organization proposed for both the zebrafish and mammalian locomotor systems (Bagnall and McLean, 2014; Hagglund et al., 2013; Kiehn, 2016; McLean and Dougherty, 2015), right/left swimming behavior in *Xenopus* tadpoles is organized by a “half-center” rhythmogenic structure (Li

and Moult, 2012; Moult et al., 2013). Here, inhibitory coupling between neurons of the right and left side allows for generation of a rhythmic swimming behavior (Moult et al., 2013).

How can inhibitory coupling be intrinsically rhythmogenic? In the simplest model, two inhibitory neurons with reciprocal connectivity exhibit antiphasic patterning (that is neuron A fires while neuron B is inhibited). Adding rebound kinetics to this system causes the output of each neuron to become rhythmic (Perkel and Mulloney, 1974; Skinner et al., 1994). Thus, in this configuration, motor rhythm (rhythmogenic output of each neuron) and motor pattern (antiphasic pattern of each output) are network features that are inherently yoked. In *Xenopus* tadpoles, fast silencing of one side (e.g. the left side) of the spinal cord abruptly disrupts output of the other side (Moult et al., 2013). This effect is due to the loss of post-inhibitory rebound excitation following an inhibitory synaptic volley from the opposite site. Thus, in *Xenopus*, right/left swimming does not necessarily exhibit modular organization, and instead, locomotor rhythm is coordinated at a higher level (Moult et al., 2013).

Evidence for Modularity in Respiration

Respiration has three distinct phases: expiration, inspiration, and post-inspiration (Anderson et al., 2016; von Euler, 1983; Feldman et al., 1990; Huckstepp et al., 2016, 2015; Lawson et al., 1991; Richter, 1982; Richter and Smith, 2014; Smith et al., 1991). Whereas inspiration is generated by rhythmogenic circuits of the preBötC (Smith et al., 1991), expiration is thought to

be generated by the pF oscillator (Huckstepp et al., 2016, 2015; Onimaru et al., 2003; Pagliardini et al., 2011; Thoby-Brisson et al., 2009) and post-inspiration is generated by the post-inspiratory complex (PICo) (Anderson and Ramirez, 2017; Anderson et al., 2016). Thus, three distinct rhythmogenic substrates are thought to form the basis for three distinct phases of mammalian respiration (Anderson and Ramirez, 2017).

Interestingly, the frequency of inspiration and expiration can be manipulated independently using μ-opioid receptor-directed perturbations (Janczewski and Feldman, 2006; Mellen et al., 2003), and the frequency of post-inspiration can be manipulated independently of inspiration by application of nor-epinephrine (Anderson et al., 2016). These data suggest that oscillations in motor output generated by the preBötC, the pF, and the PICo operate independently, and one phase of respiration is not essential to drive a subsequent phase. Thus, these experiments demonstrate that respiration can be modular, that is, specific modules can be recruited to control groups of expiratory/inspiratory/post-inspiratory muscles without affecting the generation of rhythms controlling antagonistic muscle groups.

Modularity in respiratory control could allow for considerable flexibility to meet behavioral needs, including vocalizations, sigh, swallow, etc. For example, if certain vocalizations require one to perform several expiratory breaths in sequence, a modular system could accommodate this behavioral need by allowing for several bursts of expiratory activity without induction of inspiratory bursts. Nevertheless, the same investigators which have proposed that

respiration is modular (Janczewski and Feldman, 2006; Mellen et al., 2003) have also proposed that respiration is not modular (Huckstepp et al., 2016), suggesting that inspiration might actually cause expiration and *vice versa* (Huckstepp et al., 2016). These hypotheses would appear to be incongruent, and thus merit further investigation.

Development of Respiratory Circuits

A hallmark feature of the nervous system is its ability to give rise to complex patterns of neural activity based on membrane excitability and network interactions. Neural activity first appears within networks of the hindbrain and spinal cord shortly after neurogenesis. As early as E12—prior to development of synaptic inhibition—the spinal cord generates low frequency/long duration burst activity which propagates amongst developing spinal networks via excitatory synaptic transmission and electrical coupling (Czarnecki et al., 2014; Hanson and Landmesser, 2003; Jean-Xavier et al., 2007; Myers et al., 2005), but is also facilitated by GABA and glycine which both initially act to depolarize postsynaptic neurons (Jean-Xavier et al., 2007). Voltage imaging at E12.5-13.5 demonstrates that these depolarizing waves arise from both the cervical and lumbar enlargements and propagate into the medulla (Momose-Sato et al., 2012a, 2012b).

Interestingly, phrenic motor neurons exhibit activity-dependent innervation of the diaphragm during this early stage of embryogenesis (E12.5-13.5). The

phrenic nerve enters the diaphragm at E12.5 and the basic pattern of intramuscular nerve branching and innervation is largely complete by E13.5 (Brandon et al., 2003), which is prior to the emergence of respiratory rhythm (Thoby-Brisson et al., 2005). Here, evoked ACh release from phrenic motor neurons (rather than spontaneous vesicle fusion) is thought to regulate diaphragm innervation (Usiak and Landmesser, 1999; Varoqueaux et al., 2005; Washbourne et al., 2002); knockout of either choline acetyltransferase (ChAT) or the alpha1 subunit of the muscle nAChR causes severe defasciculation and branching of intramuscular nerves, hyperinnervation, and a failure of terminal PMN axonal arbors to be restricted to the middle of the muscle (An et al., 2010; Brandon et al., 2003; Misgeld et al., 2002). These changes are apparent by E13.5 (Brandon et al., 2003). Since activation of phrenic motor neurons by the preBötC occurs much later at E15-15.5 (Thoby-Brisson et al., 2005, 2009), propagating waves of activity arising from the cervical or lumbar cord are likely what cause evoked phrenic motor neuron activity between E12.5 and E14.5 (Hanson and Landmesser, 2003; Momose-Sato et al., 2012a, 2012b). Thus, in addition to its role in directing the development of neural circuits in other aspects of the CNS (Kastanenka and Landmesser, 2010, 2013; Myers et al., 2005), early activity is thought to be essential for specification and development of respiratory circuits too.

Propagating burst activity generated by cholinergic networks of the spinal cord disappears around E14-14.5 in a period coinciding with development of the first inhibitory synapses (Momose-Sato et al., 2012a, 2012b). Interestingly,

around this same period in embryonic development, the primary excitatory neurotransmitter in the spinal cord switches from ACh to glutamate (Myers et al., 2005). Also around E14.5, a group of excitatory neurons within the parafacial nucleus begins to generate oscillatory activity which is thought to be the embryonic correlate of expiration (Huckstepp et al., 2016, 2015; Onimaru et al., 2003; Pagliardini et al., 2011; Thoby-Brisson et al., 2009). Early embryonic oscillatory activity exhibited by the so-called embryonic pF oscillator is generated by a riluzole-sensitive persistent sodium current (Thoby-Brisson et al., 2009).

At E15.5 the embryonic correlate of the preBötC begins to exhibit oscillatory activity too (Thoby-Brisson et al., 2005), establishing fetal breathing movements in the embryo (Greer and Martin-Caraballo, 2017; Greer et al., 2006). In order to secure adequate respiration at birth, fetal breathing movements are thought to be involved in circuit maturation—including the acquisition of neuronal membrane electrical properties and maturation of skeletal muscle (Feldman et al., 2009; Greer and Martin-Caraballo, 2017; Greer et al., 2006).

Interestingly, at least during embryonic development (~E15.5), the pF oscillator and the preBötC exhibit synchronous activity—that is, the pF oscillator and the preBötC give rise to burst activity at the same time (Thoby-Brisson et al., 2009). Nonetheless, the frequency of each oscillator can be manipulated independently; riluzole (which non-specifically blocks I_{NaP}) selectively depresses the oscillatory activity of the pF oscillator, while the μ-opioid agonist DAMGO selectively depresses the oscillatory activity of the preBötC (Thoby-Brisson et al.,

2009). These data indicate that post-natal respiration is derived from an early embryonic network composed of at least two distinct oscillators which exhibit synchronous activity.

Of particular note, a hallmark feature of embryonic networks is that they exhibit relatively synchronous activity (Hanson and Landmesser, 2003; Thoby-Brisson et al., 2009), owing to extensive recurrent excitatory connections and limited maturity of inhibitory synaptic transmission (Hanson and Landmesser, 2003; Ren and Greer, 2006; Ritter and Zhang, 2000; Talpalar et al., 2011). So, although the pF oscillator and the preBötC exhibit synchronous activity at E15.5 (Thoby-Brisson et al., 2009), development and maturation of inhibitory synapses is thought to give rise to a respiratory rhythm which exhibits multiple independent phases (Feldman et al., 2009). These observations have led to the (perhaps fallacious) idea that excitatory circuits generate respiratory rhythm, and synaptic inhibition shapes respiratory pattern (Cui et al., 2016; Feldman et al., 2009; Janczewski et al., 2013; Sherman et al., 2015).

Respiration: Insights from Molecular Genetics

Over the last 30 years, several genes have been identified which are essential for respiration (Gaultier et al., 2004; Gray, 2008, 2013; Grossmann et al., 2010). Knockout of critical genes usually leads to respiratory failure at birth or during a short perinatal time window thereafter. This period is defined by transition from fetal breathing movements, liquid-filled lungs, and maternal dependency for

O_2/CO_2 homeostasis, to breathing (Turgeon and Meloche, 2009). Indeed, failure in the transition to respiration is a significant cause of perinatal mortality in humans (Turgeon and Meloche, 2009). Discovery of genes critical for respiration has led to several unique insights into anatomical and functional organization of hindbrain respiratory circuits. Here I review a few of these genes in detail with the goal of demonstrating how their discovery has changed how we think about respiratory control. Listed in alphabetical order:

Atoh1

In 1997, the Zoghbi lab generated an *Atoh1* (*Math1*; drosophila *atonal* homologue) knockout mouse, and found that *Atoh1* was essential for development of cerebellar granule neurons (Ben-Arie et al., 1997). Interestingly, *Atoh1* null mice also exhibited perinatal lethality due to respiratory failure; *Atoh1* knockout mice were born alive but quickly developed cyanosis due to failure to initiate respiration (Ben-Arie et al., 1997). Given that *Atoh1* expression is confined primarily to the central nervous system (Akazawa et al., 1995; Ben-Arie et al., 1996), the authors concluded that a central mechanism was likely to explain respiratory failure in *Atoh1* null mice (Ben-Arie et al., 1997). This was subsequently confirmed in medullary-spinal cord preparations *in vitro*, where *Atoh1* null mice exhibited a very slow spontaneous inspiratory frequency (Rose et al., 2009).

What population of hindbrain Atoh1+ neurons is essential for respiration at birth? Early analysis indicated that *Atoh1* is expressed by a variety of hindbrain

populations, including neurons of the pFRG/RTN and parabrachial complex (Rose et al., 2009). In *Atoh1* null mice, Atoh1-lineage neurons failed to migrate ventrally to their final position in the RTN/pFRG, and furthermore, an Atoh1-lineage marked axonal tract that projected along the ventral surface of the medulla to the preBötC was lost (Huang et al., 2012). These data suggested that Atoh1-lineage derived structures within the medulla are important for respiration. Consistent with this hypothesis, conditional deletion of *Atoh1* using a *HoxB1*^{Cre} allele, which allows for recombination in all tissues caudal to the rhombomere 3/4 boundary, resulted in 50% neonatal lethality at birth (Maricich et al., 2009). Furthermore, conditional deletion of *Atoh1* using a *HoxA4*^{Cre} allele, which allows for recombination in all tissues caudal to the rhombomere 6/7 boundary, a region which includes the preBötC (Borday et al., 2006; Hayes et al., 2017), does not result in respiratory failure at birth. This data indicates that a population of Atoh1-lineage neurons derived from the rhombomeres 3/4-6/7 is important for respiration at birth, a region which includes the RTN/pFRG (Gray, 2013; Huang et al., 2012)

Given that Atoh1-lineage neurons of the RTN/pFRG also express *Phox2b* (Dubreuil et al., 2009), Huang and colleagues used a *Phox2b*^{Cre} allele to specifically delete *Atoh1* from Phox2b-lineage neurons (Huang et al., 2012). Consistent with previous data from Maracich and colleagues, Huang et al. found that these mice exhibited 43% lethality in the first post-natal day. Surprisingly, a large contingent of these *Atoh1*^{Phox2bCKO} mice survived to adulthood, and exhibited similar ventral Atoh1-lineage RTN/pFRG migration defects as the

germline knockouts (Huang et al., 2012). Although these results indicate that a ventral population of Phox2b-lineage derived Atoh1-expressing neurons is critical for respiratory fitness at birth, these results nonetheless do not explain the full penetrance of respiratory failure in the germline *Atoh1* knockouts (Huang et al., 2012).

In addition, these results indicate heterogeneity amongst Atoh1-lineage and Phox2b-lineage neurons of the RTN/pFRG. Phox2b-null mice die at birth due to respiratory failure, and this phenotype can be completely attributed to CO_2 sensitive neurons of the pFRG (Kumar et al., 2015); RTN/pFRG specific deletion of *Phox2b* using an $Egr2^{Cre}$ or $Lbx1^{Cre}$ allele results in nearly 100% penetrance of the neonatal lethality phenotype (Dubreuil et al., 2009). Moreover, Huang and colleagues found that $Atoh1^{Phox2bCKO}$ mice did not exhibit defects in CO_2 chemosensitivity *per se* because $Atoh1^{Phox2bCKO}$ *in vitro* preparations still responded to an acidic pH challenge mimicking metabolic acidosis (Huang et al., 2012). $Atoh1^{Phox2bCKO}$ preparations nonetheless exhibited a blunted inspiratory response to acidic pH *in vitro* and a blunted ventilatory response to hypercapnia *in vivo*, indicating that while CO_2 sensitivity is maintained, downstream executional circuitry may be compromised (Huang et al., 2012).

Since 2012, the contributions of different transcriptionally-defined populations of RTN/pFRG neurons have not become any clearer. From a variety of conditional approaches targeting Egr2-, Islet1-, Lbx1-, Phox2b-, and Atoh1-lineage derived neurons of the RTN/pFRG (Dubreuil et al., 2009; Huang et al., 2012; Ruffault et al., 2015), it is clear that there is functional heterogeneity within

this brainstem region, but unifying principles have been difficult to define. In my opinion, CO_2-sensitive neurons are Phox2b-lineage derived and are not derived from an overlapping population of Atoh1-lineage neurons; deletion of Atoh1 within Phox2b-lineage neurons does not affect CO_2 chemosensitivity (Huang et al., 2012). However, as stated above, it does appear that Atoh1-lineage neurons are important in downstream elements of the circuit essential for sustaining the full respiratory response to elevated CO_2. Indeed, it is known that Atoh1-lineage neurons of the RTN/pFRG exhibit increased firing in response to acidic pH (Ruffault et al., 2015). Although this experiment does not shed light on whether Atoh1-lineage neurons exhibit CO_2 chemosensitivity themselves, it does indicate that they may play some role in the central response to hypercapnia.

Although neonatal lethality phenotypes of a variety of different conditional mutants have been informative, accompanying electrophysiological analysis of such mutants has not kept pace. This is likely owing to the difficulty in obtaining a robust number of mutants as well as the relatively specialized skillset needed for electrophysiological analyses. Indeed, many of these mutants have been analyzed using calcium imaging during prenatal timepoints in which networks favor excitation (Ruffault et al., 2015; Thoby-Brisson et al., 2009), making it hard to understand how findings during these early time points of analysis (E14.5-15.5) correlate with post-natal periods during which GABA/glycine become inhibitory (Feldman et al., 2009; Hübner et al., 2001; Ren and Greer, 2006; Ritter and Zhang, 2000; Rivera et al., 1999; Stein et al., 2004). Indeed, although expiration is thought to be generated within substructures of the RTN/pFRG and

act out-of-phase with inspiration (Huckstepp et al., 2016, 2015; Pagliardini et al., 2011), the RTN/pFRG and the preBötC oscillate in synchrony during early embryogenesis (Thoby-Brisson et al., 2009). Synchronous activity is a hallmark feature of early excitatory embryonic networks (Hanson and Landmesser, 2003) and purely excitatory networks at large (Anderson et al., 2016; Talpalar et al., 2011).

Can electrophysiological analysis of *Atoh1* mutants shed light on the role of Atoh1-lineage neurons in respiration? Interestingly, in 2014, Tupal and colleagues found that *Atoh1* mutants—derived from E18.5 embryos—exhibited a lack of temporal separation between expiration, inspiration, and post-inspiration (Tupal et al., 2014). These results suggested that Atoh1-lineage neurons are responsible for setting up a “phase-delay” between independent respiratory oscillators. Although the mechanism of “phase-delay” was not understood, it is very likely that this mechanism involves inhibition given that purely excitatory networks usually operate in synchrony (Anderson et al., 2016; Talpalar et al., 2011).

Much of the interest surrounding an Atoh1-lineage role in respiration has focused on medullary structures (Huang et al., 2012; Rose et al., 2009; Ruffault et al., 2015; Tupal et al., 2014); however, it is important to note that a population of neurons rostral to the rhombomere 3/4 boundary is critical for the full penetrance of the Atoh1-null neonatal lethality phenotype (Maricich et al., 2009). Although it is not clear what population this might include, the pontine parabrachial complex and Kolliker-Füse nuclei are Atoh1-lineage derived (Huang

et al., 2012), are situated close to the rhombomere 3/4 boundary (Gray, 2008), and are known to play a role in respiration (Dutschmann and Dick, 2012; Dutschmann and Herbert, 2006). Interestingly, removal of these pontine structures *in situ* causes expiratory/inspiratory/post-inspiratory motor outputs to operate in synchrony (Jones and Dutschmann, 2016). These data together suggest a critical role for the pons in orchestrating triphasic respiratory motor outputs and respiration more generally, but mechanisms underlying pontine control of respiration are still poorly understood (Dutschmann and Dick, 2012).

Dbx1

How do transcriptional networks specify development of the preBötC? *Mafb* mutants exhibit impaired respiratory rhythmogenesis associated with disrupted *Mafb* expression in the preBötC (Blanchi et al., 2003); however, given the broad expression of *Mafb* in the caudal hindbrain, it was unclear whether impaired respiration was specifically caused by abnormal development of the preBötC. In 2010, Bouvier and colleagues discovered that Dbx1 more specifically specifies the development of the preBötC and loss of Dbx1 results in an absence of inspiratory rhythmogenesis (Bouvier et al., 2010).

Coordination of bilaterally synchronous activity between the right/left preBötC nuclei is thought to arise from excitatory commissural axonal projections (Koshiya and Smith, 1999; Wallen-Mackenzie et al., 2006). Neurons which coordinate behavior across the midline had been most well-characterized in locomotion generating circuits of the lumbar cord, for which it was known that

commissural neurons exhibit expression of *Dbx1*, *Nkx2.2*, and *Sim1* (Lanuza et al., 2004). Bouvier and colleagues found that *Dbx1*-null mice die at birth due to respiratory failure, where *Dbx1*-null mice failed to exhibit activity at the level of C4 or XII motor output and at the level of the preBötC. Importantly, Dbx1-null mice still exhibited oscillatory activity associated with the pF nucleus (Bouvier et al., 2010), which synchronizes its output with the preBötC at E15.5 (Thoby-Brisson et al., 2009), indicating that lack of *Dbx1* selectively impairs the development of the preBötC (Bouvier et al., 2010). Interestingly, commissural connectivity was disrupted in *Dbx1*-null mice, an effect which could be recapitulated in mutants with conditional deletion of *Robo3* in Dbx1-lineage neurons (Bouvier et al., 2010). These data indicate a *Robo3*-dependent commissural axon guidance program is necessary for right/left synchrony of respiration (Bouvier et al., 2010).

Since 2010, the importance of Dbx1-lineage neurons in establishing rhythmic output from the preBötC has been well-documented (Cui et al., 2016; Koizumi et al., 2016; Kottick and Del Negro, 2015; Vann et al., 2016; Wang et al., 2014). Indeed, optogenetic stimulation of channelrhodopsin-2 expressing Dbx1-lineage neurons evokes inspiratory bursts in rhythmic preBötC slice preparations (Kottick and Del Negro, 2015) as well as in adult mice (Cui et al., 2016), and optogenetic silencing of Dbx1-lineage neurons of the preBötC disrupts generation of inspiratory bursts in adult mice (Koizumi et al., 2016; Vann et al., 2016).

Interestingly, downstream inspiratory premotor nuclei, including the rostral ventral respiratory group (rVRG) and the premotor nucleus of XII are also derived

from a Dbx1-lineage (Revill et al., 2015; Wu et al., 2017). In the case of the rVRG, Dbx1-directed commissural connectivity between the left/right rVRG appears to be important for sustaining right/left burst synchrony during transmission of bursts from the preBötC to phrenic motor neurons (Wu et al., 2017).

Egr2

Transcription factor programs direct hindbrain specification from early development (mouse E7.5) through birth. A hallmark feature of hindbrain development is its segmentation into 9 rhombomeres (Lumsden and Krumlauf, 1996), which is defined by expression of segmentation factors, most notably, the *Hox* genes (Lumsden and Krumlauf, 1996; Philippidou and Dasen, 2013). Gene regulatory networks within each rhombomere lead to the specification of more specialized nuclei later during development, and therefore studying hindbrain segmentation is expected to yield insight into how networks function post-natally (Chatonnet et al., 2007). Indeed, during chick embryogenesis, individual rhombomeres exhibit discrete rhythmogenic substrates which give rise to more complex interactions during later developmental periods (Fortin et al., 1999).

Deletion of *Egr2* (also known as *Krox20*) disrupts development of hindbrain rhombomeres 3 and 5 (Schneider-Maunoury et al., 1993; Swiatek and Gridley, 1993), and results in ~60-70% lethality within the first postnatal day (Jacquin et al., 1996; Schneider-Maunoury et al., 1993; Swiatek and Gridley, 1993). Plethysmograph recordings from neonatal mice indicated that perinatal

lethality could be attributed to impaired respiratory function (Jacquin et al., 1996); Egr2-null mice could initiate inspiratory bursts, but exhibited significantly more apneas and a reduced basal respiratory frequency (Jacquin et al., 1996). Incomplete penetrance of the neonatal lethality phenotype is consistent with data from other mutant mice which indicate that the perinatal period is especially sensitive to defects in hindbrain development (Huang et al., 2012; Yeh et al., 2017); if mutants do survive the perinatal period they can often grow to adulthood (Huang et al., 2012). Indeed, the authors found that administration of naloxone, a μ-opioid antagonist, improved survival of Egr2-null mice past the perinatal period as old as 2 weeks of age (Jacquin et al., 1996).

Clearly a rhombomere 3 or 5 population of neurons is critical for respiration (Jacquin et al., 1996), but given that these rhombomeres underlie development of a large number of medullary and pontine nuclei (Gray, 2008, 2013), what population of Egr2-lineage neurons is causative? Previous work had indicated that an Egr2-dependent parafacial respiratory group could strongly modulate inspiratory activity (Coutinho et al., 2004; Onimaru et al., 2003). To investigate this in greater detail, Thoby-Brisson and colleagues examined developmental origin of the pF respiratory group (Thoby-Brisson et al., 2009). Using an *Egr2*^{Cre} allele as a tool for fate-mapping of Egr2-lineage cells, Thoby-Brisson and colleagues found that Egr2-lineage neurons of the parafacial nucleus generate oscillatory activity as early as E14.5. This parafacial oscillator synchronizes with the preBötC around E15.5, suggesting a dual-origin of respiratory rhythm at least during early embryonic development when networks

are purely excitatory (Thoby-Brisson et al., 2009). This oscillator is thought to represent the embryonic correlate of expiration (Feldman et al., 2009; Huckstepp et al., 2016, 2015; Mellen et al., 2003; Pagliardini et al., 2011).

Given that *Egr2* more broadly specifies r3 and r5 development (Schneider-Maunoury et al., 1993; Swiatek and Gridley, 1993), additional roles for *Egr2* in respiratory control have been proposed. These roles include organization of pontine structures (Chatonnet et al., 2007; Jacquin et al., 1996), as well as specification of Egr2-lineage serotonergic neurons (Brust et al., 2014; Ray et al., 2013). Indeed, Egr2-lineage serotonergic neurons may play an important role in the central response to CO_2 (Brust et al., 2014; Corcoran et al., 2009; DePuy et al., 2011; Hodges et al., 2008; Ray et al., 2011, 2013), although serotonergic neurons are not thought to act as central CO_2 chemoreceptors *per se* (DePuy et al., 2011; Guyenet and Bayliss, 2015; Guyenet et al., 2010).

Nalcn

Although ionic mechanisms (e.g. persistent sodium current) play a formative role in respiratory control (McCrimmon et al., 2001), surprisingly few genes encoding membrane channels have been associated with respiratory dysfunction. This perhaps highlights redundancy amongst ion channel subunits contributing to different ionic currents and mechanisms underlying rhythmogenesis. Nonetheless, in 2007, it was found that *Nalcn* knockout mice exhibit neonatal lethality due to respiratory failure (Lu et al., 2007). *Nalcn* encodes a sodium “leak” channel which contributes to resting membrane

excitability independent of membrane voltage (Lu et al., 2007). Indeed, neuronal resting membrane potential in *Nalcn* knockout mice is insensitive to changes in extracellular [Na^+], indicating that *Nalcn* is the chief contributor to Na^+ leak conductance in the brain. Plethysmography and *in vitro* recordings in medullary spinal cord preparations confirmed that *Nalcn* knockout mice exhibit a substantially reduced respiratory frequency compared with wild-type controls (Lu et al., 2007).

Although a variety of hindbrain neurons express *Nalcn* (Shi et al., 2016; Yeh et al., 2017), discovery of *Nalcn* as critical for respiration was especially salient owing to the known modulation of *Nalcn* via substance P (Lu et al., 2009). Substance P had been previously discovered as a respiratory-active peptide which modulates preBötC output via direct action on the neurokinin-1 GPCR (Gray et al., 1999; Hayes and Del Negro, 2007; Ptak et al., 2009). Indeed, it was subsequently found that substance P augments the firing of respiratory neurons in an *Nalcn* dependent manner (Shi et al., 2016; Yeh et al., 2017).

Several conditional *Nalcn* mutants have been described (Flourakis et al., 2015; Yeh et al., 2017). Although most conditional *Nalcn* knockout mice generated to-date have survived past the post-natal period, Dbx1-lineage specific knockout results in ~33% respiratory lethality within the first day of birth (Yeh et al., 2017). This is consistent with a preBötC-specific role for *Nalcn*. Additionally, Atoh1-lineage specific knockout of *Nalcn* results in an increase in spontaneous apneas both in the first post-natal day as well as in both awake and anesthetized mice 7 weeks old (Yeh et al., 2017), although Atoh1-lineage specific knockout of

Nalcn does not result in post-natal lethality by itself. Interestingly, Phox2b-lineage specific knockout of *Nalcn* did not cause neonatal lethality or result in increases in spontaneous apneas, suggesting an RTN-independent role for *Nalcn* (although functional heterogeneity within the RTN is poorly understood, see *Atoh1* discussion above). These data suggested that a lack of *Nalcn* expression in pontine Atoh1-lineage structures might underlie increased apneas, an interpretation which was further supported by recapitulation of apneas in mice with Engrailed-1-lineage specific deletion of *Nalcn* (Yeh et al., 2017). Importantly, only neural wide (Nestin-lineage) or glutamatergic (Vglut2-specific) deletion recapitulated the full penetrance of the neonatal lethality phenotype associated with germline deletion of *Nalcn* (Yeh et al., 2017), suggesting that there are other as-yet unexplored populations of respiratory neurons which depend on *Nalcn*.

Piezo2

Of the genes required for respiratory function, the importance of *Piezo2* in respiration has only been recently ascribed (Nonomura et al., 2017). It has long been known that the vagus nerve relays mechanosensory afferent feedback: the lungs and airway are innervated by vagal sensory neurons of the jugular-nodose ganglion complex, and the vagus nerve carries sensory fibers which are characterized as mechanosensitive, that is, they exhibit activity related to the extent of lung inflation (Zhang et al., 2006). Furthermore, the vagus nerve mediates the Hering-Breuer reflex—a reflex which prevents over-inflation of the lung (Lee and Yu, 2014; Zhang et al., 2006). Thus, sensory neurons in the lungs

and airway have stretch receptors and/or a mechanosensitive apparatus, although the mechanism underlying mechanosensitivity was not known until recently (Nonomura et al., 2017). In addition to serving a role in specific mechanosensory reflexes, vagal mechanosensory feedback is thought to be important for respiratory control more generally; upon vagotomy, the frequency of respiration drops by ~50% (Cui et al., 2016; Janczewski et al., 2013; Kaczyńska and Szereda-Przestaszewska, 2013; Smith et al., 1990). The functional significance of vagal mechanosensory feedback in adults, however, is still under debate (Dutschmann et al., 2014).

In 2010, *Piezo1* and *Peizo2* were identified as mechanically activated cation channels (Coste et al., 2010). It was quickly found that *Piezo2* (but not *Piezo1*) was essential for mechanotransduction in Merkel cells (Woo et al., 2014), which are responsible for light touch. Furthermore, *Piezo2* was found to act as the major channel responsible for low-threshold mechanosensation in sensory systems more generally (Ranade et al., 2014). Interestingly, *Piezo2* mutants exhibit neonatal lethality (Dubin et al., 2012), suggesting that *Piezo2* serves an essential life-supporting perinatal role possibly related to its function in mechanosensitivity.

Nonomura and colleagues investigated whether the lethality of *Piezo2* null mice could be specifically attributed to respiratory failure (Nonomura et al., 2017). *Piezo2* null mice are born in the expected ratio, but die within 24 h of birth. *Piezo2* null mice exhibit signs of respiratory distress including cyanosis, gasping, decreased blood oxygen saturation, and reduced respiratory frequency

(Nonomura et al., 2017). Interestingly, in plethysmograph recordings from neonatal mice the authors observed that *Piezo2* null mice exhibit reduced expiration (although no deficits in initiation of inspiration), suggesting that inhibitory mechanosensory feedback may facilitate the inspiratory-expiratory phase transition (Nonomura et al., 2017).

Nonomura and colleagues generated several tissue-specific conditional *Piezo2* knockout mice, and found that conditional deletion of *Piezo2* in the nodose ganglion alone was not sufficient to recapitulate respiratory failure observed in *Piezo2* knockouts; however, deletion of *Piezo2* in all neural-crest derived lineages (including the jugular-nodose ganglion complex) recapitulated respiratory failure in *Piezo2* knockouts (Nonomura et al., 2017). These data suggest that the entire jugular-nodose ganglion complex is required for mechanosensory feedback at birth (as opposed to just the nodose ganglion). The authors were not able to demonstrate that deletion of Piezo2 specifically in the jugular-nodose ganglion complex recapitulates respiratory failure observed in the germline knockout (Nonomura et al., 2017). Nonetheless, the authors went on to demonstrate that stimulation of Piezo2+ neurons in the jugular-nodose complex suppresses respiration similar to the Hering-Breuer reflex, and conditional deletion of *Piezo2* reduces vagal nerve firing in response to lung inflation in adult mice (Nonomura et al., 2017).

Interestingly, Nonomura and colleagues found that while conditional deletion of *Piezo2* in the nodose ganglion abolished the lung inflation-induced Hering-Breuer reflex, *Piezo2* and the Hering-Breuer reflex were dispensable for

normal respiration in adult animals (Nonomura et al., 2017). First, deletion of *Piezo2* in Phox2b-lineage neurons did not cause neonatal lethality, yet it abolished the Hering-Breuer reflex in adult animals. Second, conditional deletion of *Piezo2* in adult neural crest-lineage neurons abolished the Hering-Breuer reflex but did not cause any changes in basal respiratory frequency (Nonomura et al., 2017). There are several possibilities here, a few of which I list here: First, it is possible that there are differential roles for *Piezo1* and *Piezo2* in adult animals, such that *Piezo2* mediates rapidly-adapting lung-inflation induced mechanical stimuli while *Piezo1* is responsible for slowly-adapting stimuli as might occur during basal conditions (Coste et al., 2010). However, expression of *Piezo1* in sensory endings of the lung has not been characterized, and furthermore, this does not explain why *Piezo2* is essential at birth. Second, it is known that the Hering-Breuer reflex habituates with post-natal maturation (Dutschmann et al., 2014), so it is possible that there are no changes in basal respiratory frequency because it is not essential for respiration at least in awake animals. Nevertheless, the Hering-Breuer reflex is still thought to be important during anesthesia. Third, it is possible that conditional knockout of *Piezo2* does affect respiratory frequency, but there is slow compensation by other systems (such as by CO_2 chemosensitive neurons). Here, it would be very informative to see whether frequency drops after vagotomy in Piezo2-conditional knockout mice. Finally, it is possible that vagal effects on respiratory frequency are independent of inhibitory mechanosensory feedback altogether, as recent

genetic dissection has revealed unexpected complexity of vagal sensory afferents in their ability to control respiratory frequency (Chang et al., 2015)

Together these data provide a mechanistic basis for vagal mechanosensory feedback associated with the Hering-Breuer reflex (Cui et al., 2016; Janczewski et al., 2013; Kaczyńska and Szereda-Przestaszewska, 2013; Smith et al., 1990).

Phox2b

Central congenital hypoventilation syndrome (CCHS, or Ondine's curse) is a life-threatening disorder associated with impaired ventilatory response to hypercapnia, and is also more generally associated with dysfunction and tumors of the autonomic nervous system (ANS). Due to the well-known role of the transcription factor *Phox2b* in development of the ANS (Brunet and Pattyn, 2002; Pattyn et al., 1999), Amiel and colleagues considered *Phox2b* a candidate gene for CCHS (Amiel et al., 2003). Sequencing *Phox2b* in humans with CCHS revealed frameshift and polyalanine expansion mutations in *Phox2b* (Amiel et al., 2003), strongly suggesting that mutations in *Phox2b* cause CCHS. This was subsequently confirmed by experiments using mouse genetics, where a mouse carrying a human CCHS mutation in *Phox2b* exhibited a lack of CO_2 chemosensitivity (Dubreuil et al., 2008). Discovery of *Phox2b* as the cause of CCHS has facilitated significant insight into central CO_2 chemosensation.

In 2004, the laboratory of Patrice Guyenet discovered that ventral hindbrain neurons of the retrotrapezoid/parafacial nucleus (RTN/pFRG) are

exquisitely sensitive to CO_2 (Mitchell, 2004; Mulkey et al., 2004), and soon thereafter found that these neurons express *Phox2b* (Kang et al., 2007; Stornetta et al., 2006). ChR2 photostimulation of *Phox2b*-expressing neurons in the RTN/pFRG caused rapid respiration *in vivo* (Abbott et al., 2009), suggesting that *Phox2b*-expressing neurons of the RTN/pFRG are *bona fide* CO_2 chemosensitive neurons. Although a small number of neurons of the RTN also express *Atoh1* (Ruffault et al., 2015; see discussion above), it is thought that Atoh1+ neurons of the RTN are not *bona fide* CO_2 chemosensitive neurons.

What is the molecular mechanism underlying CO_2 chemosensitivity of Phox2b+ neurons? The mechanism of chemosensitivity could be relatively non-specific, where CO_2 or protons act to alter pH—and thus the conformation—of membrane channels. This mechanism is unlikely, however, owing to the specific and exquisite sensitivity of pFRG/RTN neurons (Mulkey et al., 2004). Alternatively, CO_2 or protons might act as ligands for specific membrane proteins. Indeed, pH-sensitive GPCRs (OGR1 and GPR4) and potassium channels (TASK-1-3) had been previously identified (Bayliss et al., 2001; Ludwig et al., 2003).

TASK-1 and TASK-3 are acid-sensitive potassium channels which are expressed in a variety of brainstem neurons (Bayliss et al., 2001; Talley et al., 2001; Washburn et al., 2002, 2003), and contribute to their pH sensitivity (Bayliss et al., 2001; Mulkey et al., 2007; Washburn et al., 2002). Nevertheless, TASK-1 and TASK-3 are dispensable for central CO_2 chemosensitivity; both the ventilatory response to CO_2 and the sensitivity of RTN neurons to acidic pH is

maintained in TASK-1 and TASK-3 double knockout mice (Mulkey et al., 2007). Moreover, knockout of TASK-1 and TASK-3 abolished the pH-sensitivity of raphe neurons (Mulkey et al., 2007). These results indicate that central chemosensitivity is mediated primarily by Phox2b+ neurons of the RTN, and that the mechanism underlying chemosensitivity is independent of acid-sensitive TASK channels.

In 2010, Gestreau and colleagues unexpectedly found that TASK-2, an alkaline-sensitive potassium channel, is involved in central CO_2 chemosensitivity (Gestreau et al., 2010). TASK-2 had not been considered as a candidate for CO_2 chemosensitivity due to its weak and/or absent expression in the brain (Reyes et al., 1998). Nonetheless, Gestraeu et al. used a *TASK-2*$^{LacZ/+}$ knockin-knockout allele to characterize expression from the *TASK-2* locus, and found that a few hindbrain nuclei do exhibit LacZ+ cells (Gestreau et al., 2010). Of nuclei situated along the ventral surface of the hindbrain, only the RTN/pFRG exhibited a prominent population of LacZ+ neurons (Gestreau et al., 2010). The authors further found an absence of LacZ+ neurons in the pFRG after crossing the *TASK-2*$^{LacZ/+}$ allele to a mouse carrying a humanized CCHS mutation in *Phox2b*, strongly suggesting that *TASK-2* is expressed in Phox2b+ neurons of the RTN/pFRG. Finally, Gestreau and colleagues found that *TASK-2* null mice exhibit a diminished respiratory response to hypercapnia (Gestreau et al., 2010). In comparison with mice carrying a humanized CCHS mutation in *Phox2b*, *TASK-2* null mice do not exhibit neonatal lethality due to respiratory failure and still exhibit a partial response to CO_2 (Dubreuil et al., 2008; Gestreau et al.,

2010). This data suggested that additional pH-sensitive proteins may contribute to central CO_2 chemosensitivity. Indeed, although in some RTN/pFRG neurons pH sensitivity could be completely accounted for by loss of *TASK-2*, several neurons exhibited an additional pH-sensitive current which was independent of *TASK-2* (Wang et al., 2013).

In 2015, Kumar and colleagues found that *GPR4*, a GPCR with known proton sensitivity (Ludwig et al., 2003), was the other major determinant of CO_2 sensitivity in Phox2b+ neurons (Kumar et al., 2015). Hindbrain GPR4 expression is restricted primarily to Phox2b+ neurons of the RTN/pFRG. Similar to *TASK-2* null mice, *GPR4* null mice exhibited a blunted respiratory response to hypercapnia. Furthermore, compared with wild type mice, GPR4 null mice exhibited a larger percentage of Phox2b+ neurons in the RTN/pFRG which were insensitive to acidic pH (Kumar et al., 2015). In *GPR4* null mice, exogenous lentiviral-mediated expression of GPR4 in Phox2b+ neurons of the RTN/pFRG rescued the ventilatory response to hypercapnia. Finally, $GPR4^{-/-}$;$TASK\text{-}2^{-/-}$ mice largely phenocopied mice which carried a humanized CCHS mutation in *Phox2b*; double knockout mice did not exhibit a ventilatory response to hypercapnia and exhibited reduced survival past the neonatal period (Kumar et al., 2015).

Discovery of mutations in *Phox2b* as the cause of human CCHS has led to a comprehensive understanding of central CO_2 chemosensitivity at the cellular and molecular level (Bayliss et al., 2015; Guyenet and Bayliss, 2015; Guyenet et al., 2016). Nevertheless, how Phox2b+ neurons of the RTN/pFRG ultimately

increase tidal volume and respiratory frequency at the circuit level is still largely unknown (Guyenet and Bayliss, 2015).

Vgat

The vesicular GABA transporter (*Vgat*, also known as *Viaat* or *Slc32a1*) is required for synaptic vesicle loading of both GABA and glycine (Wojcik et al., 2006). *Vgat* null mice die from respiratory failure at birth (Wojcik et al., 2006), indicating an essential role for GABA/glycine transmission in respiratory control. This observation is not surprising given that inhibition is thought to be critical for respiratory pattern formation, including vagal mechanosensory feedback and control of inspiratory burst duration (Janczewski et al., 2013). Nevertheless, a variety of mice with knockout of genes associated with inhibitory synaptic transmission exhibit variable penetrance of respiratory failure, indicating heterogeneity amongst inhibitory neurons in their acquisition of terminal inhibitory identity features and importance for respiration.

Inhibitory synaptic transmission is initiated by expression of KCC2, a potassium-chloride co-transporter which establishes an outward-in chloride gradient late during embryonic development (Rivera et al., 1999). KCC2 knockout mice exhibit respiratory failure at birth (Hübner et al., 2001), indicating that synaptic inhibition mediated by GABA/glycinergic transmission—rather than excitatory GABA/glycinergic transmission which is observed during embryogenesis (Jean-Xavier et al., 2007)—is essential for respiration at birth. Even so, the GABA/glycinergic system is thought to continue to mature post-

natally during periods where KCC2 expression is continually upregulated in accordance with neuronal maturation (Stein et al., 2004). In respiratory circuits, inversion of the membrane chloride gradient is thought to begin during embryogenesis (Ren and Greer, 2006), and continue post-natally at least for a few days in mice and rats (Ren and Greer, 2006; Ritter and Zhang, 2000).

Glycine transporters *GlyT1* and *GlyT2* are responsible for uptake of glycine from the extracellular space (Harvey and Yee, 2013). *GlyT1* is primarily expressed by glia, where it functions to keep the extracellular concentration of glycine low; *GlyT1* knockout mice exhibit respiratory failure at birth due to excessive extracellular glycine and GlyR-mediated inhibitory currents (Gomeza et al., 2003a). In contrast, neuronal *GlyT2* is important for refilling of glycine vesicles and glycine neurotransmission (Harvey and Yee, 2013). Interestingly, congenital mutations in *GlyT2* have been associated with life-threatening neonatal apnea in humans (Rees et al., 2006). Nonetheless, *GlyT2* is dispensable for respiration; *GlyT2* knockout mice do not exhibit respiratory failure at birth (Gomeza et al., 2003b). Given that glycine transmission is highly reduced in *GlyT2* knockouts at birth, and furthermore, that there does not seem to be compensation by GABA in *GlyT2* null mice (Latal et al., 2010), these data suggest that GABA is the predominant inhibitory neurotransmitter associated with respiratory control. This hypothesis is supported by evidence from the *Gad1* (or *Gad67*) null mouse—where Gad1 is the primary enzyme associated with GABA synthesis in the hindbrain/spinal cord—which exhibit perinatal lethality due to respiratory failure (Asada et al., 1997).

Several lines of evidence indicate that the GABA and glycine transmitter systems exhibit extensive overlap at the single neuronal level. Inhibitory neurons can co-release both GABA and glycine at a single synapses (Jonas et al., 1998; Rahman et al., 2013; Russier et al., 2002). Additionally, although *GlyT2* null mice do not exhibit respiratory failure at birth (Gomeza et al., 2003b), deletion of *Vgat* from GlyT2+ neurons causes perinatal respiratory lethality (Rahman et al., 2015). The extent to which these neurotransmitter systems exhibit complete overlap; however, is unclear and is likely to vary depending on the specific group of neurons under investigation.

Vglut2

Glutamatergic neurons usually express only one of three glutamate transporters (Fremeau et al., 2004). Vesicular glutamate transporter 2 (*Vglut2*, also known as *Slc17a6*) is the primary glutamate transporter expressed by neurons of the hindbrain and spinal cord (Fremeau et al., 2004; Hägglund et al., 2010; Oliveira et al., 2003). Excitatory *Vglut2*-expressing neurons are thought to form the essential “kernel” which gives rise to inspiratory bursting (Janczewski et al., 2013). Indeed, deletion of *Vglut2* causes respiratory failure at birth (Talpalar et al., 2011; Wallen-Mackenzie et al., 2006), which can be attributed at least in part to the failure of the preBötC to give rise to bursts (Wallen-Mackenzie et al., 2006).

Interestingly, in the case of spinal locomotor circuits, flexor-extensor motor rhythms can be generated in the absence of glutamate transmission (Talpalar et

al., 2011; Wallen-Mackenzie et al., 2006). Although normal locomotion is thought to depend on excitatory rhythmogenic neurons in the lumbar spinal cord (Caldeira et al., 2017; Dougherty et al., 2013; Hagglund et al., 2013; Hägglund et al., 2010; Talpalar et al., 2011), stimulation of inhibitory circuits by bath application of NMDA/5HT is, nonetheless, sufficient to evoke flexor/extensor rhythms (Talpalar et al., 2011; Wallen-Mackenzie et al., 2006). Here, networks of Ia inhibitory neurons mediate reciprocal inhibition between muscle Ia afferents and antagonistic motor neurons (Talpalar et al., 2011). Thus, tonic excitation of a *purely inhibitory* network is sufficient to generate both flexor-extensor motor rhythm and pattern (Talpalar et al., 2011).

Dysfunction in Respiratory Control: Spinal Cord Injury

A significant amount of effort has gone into understanding how the nervous system controls respiration. One goal of these studies is to shed light on how the brain functions more generally (Feldman and Kam, 2015), yet these efforts hold direct clinical implications as well. Diseases associated with respiratory dysfunction include amyotrophic lateral sclerosis (Lepore et al., 2008), sudden infant death syndrome (Garcia et al., 2013; Gaultier et al., 2004), central congenital hypoventilation syndrome (Amiel et al., 2003; Dubreuil et al., 2008), Rett syndrome (Abdala et al., 2016, 2010; Hülsmann et al., 2016; Katz et al., 2009; Ramirez et al., 2013a), central sleep apnea syndrome (Ramirez et al., 2013b), and spinal cord injury (as well as other diseases too). In this section I will

specifically focus on reviewing respiratory dysfunction after spinal cord injury (SCI), as certain outstanding questions in the organization of phrenic premotor circuits are pertinent to the present body of work and our laboratory's longstanding interest in promoting recovery of diaphragm function after SCI (Alilain and Silver, 2009; Alilain et al., 2008, 2011).

Spinal cord injury has an annual incidence in the US of 17,000 cases per year, with approximately 282,000 people in the US living with SCI. Nearly 60% of SCIs cause incomplete or complete tetraplegia, which results from an injury sustained to the cervical spinal cord (National Spinal Cord Injury Statistical Center, 2016). Cervical SCI, especially when occurring rostral to the level of phrenic motor pools, interrupts descending bulbospinal pathways and results in severe respiratory weakness. In point, the leading cause of death among people sustaining spinal cord injury is pneumonia and septicemia (National Spinal Cord Injury Statistical Center, 2016), which are caused by an inability to clear the airway and reliance on a mechanical ventilator. Thus there is considerable interest in understanding how different types of strategies could maximize regeneration following spinal cord injury (Cregg et al., 2010; Gardner et al., 2015; Hilton et al., 2012; Hurtado et al., 2011; Lang et al., 2015; Niemi et al., 2016; Wang et al., 2009a, 2010). In the context of respiration, these interventions are primarily focused on restoring bulbospinal input to or augmenting the output of motor neurons controlling primary (i.e. phrenic) or accessory (e.g. abdominal, intercostal) respiratory muscles (Alilain et al., 2008, 2011; Warren and Alilain, 2014; Warren et al., 2014).

Inspiration is generated by the preBötC and relayed to phrenic motor motor neurons in spinal cord levels C3-5/6 via a medullary premotor nucleus termed the rostral ventral respiratory group rVRG (Wu et al., 2017). Thus, it is widely thought that inspiration originates in the medulla, and that phrenic motor neurons are controlled directly by the rVRG and indirectly by the preBötC (Davies et al., 1985; Dobbins and Feldman, 1994; Duffin and van Alphen, 1995; Ellenberger and Feldman, 1988; Ellenberger et al., 1990; Smith et al., 1991). Nonetheless, going back over a century (Brown-Séquard, 1860; Langendorff, 1880; Wertheimer, 1886), there has been evidence of phrenic nerve discharge generated by the spinal cord itself (Coglianese et al., 1977; Ghali and Marchenko, 2016; Reinoso et al., 1996; Viala et al., 1979; Zimmer and Goshgarian, 2007). The nature of this activity has always been a mystery, but we have found that after certain manipulations aimed at restoring function after cervical spinal cord injury, PMNs can exhibit strange activity that is not explained by the classic model of PMN control (i.e. preBötC → rVRG → PMNs) (Alilain et al., 2008, 2011). Thus, in order to effectively promote regeneration and restoration of diaphragm function, it will be important to understand conceptually how this spinal-cord-derived activity manifests—chiefly, whether this activity can manifest as a result of hyperexcitability of motor neurons themselves or whether this activity is generated by an excitatory network which evades or is subservient to control of the preBötC.

Summary and Research Aims

Through this introduction I have provided the reader with a general impression of the way I think about and approach studies in respiratory control. I have also highlighted several outstanding questions within the field along the way. In the present body of work (Chapters 2 & 3), I will address two outstanding questions specific to the control of phrenic motor neurons: In Chapter 2, I will examine premotor substrates which give rise to phrenic motor bursts. Although it is well established that the dominant premotor substrate which generates inspiratory bursts is the preBötC (Smith et al., 1991), this work revealed that a second excitatory substrate within the spinal cord can generate and evoke PMN bursts. Unexpectedly, I found that these two burst-generating substrates (i.e. preBötC and spinal cord) do not exhibit functional interaction (Cregg et al., 2017a). In Chapter 3, I will examine how inspiratory frequency is controlled. Though most models posit that inspiratory (and respiratory) frequency are determined by a balance of excitatory/inhibitory synaptic inputs to the preBötC, I unexpectedly found that inhibition can actually promote generation of inspiratory bursts through a rebound-like mechanism. Furthermore, I found that inhibition was required for sustaining increases in frequency as would occur physiologically in response to elevated CO_2 (Cregg et al., 2017b). In Chapter 4, I discuss how these discoveries lead to exciting new hypotheses regarding 1) the physiological significance of spinal cord derived PMN bursts and 2) the generation of inspiratory (and respiratory) rhythms over a large frequency range.

Chapter 2: A Latent Propriospinal Network Can Restore Diaphragm Function after High Cervical Spinal Cord Injury

Abstract

Spinal cord injury (SCI) above cervical level 4 disrupts descending axons from the medulla which innervate phrenic motor neurons, causing permanent paralysis of the diaphragm. Using an *ex vivo* preparation in neonatal mice, we have identified an excitatory spinal network which can direct phrenic motor bursting in the absence of medullary input. After complete cervical SCI, blockade of fast inhibitory synaptic transmission caused spontaneous, bilaterally-coordinated phrenic bursting. Here, spinal cord glutamatergic neurons were both sufficient and necessary for induction of phrenic bursts. Direct stimulation of phrenic motor neurons was insufficient to evoke burst activity. Transection and pharmacological manipulations showed that this spinal network acts independently of medullary circuits which normally generate inspiration, suggesting a distinct non-respiratory function. We further show that this “latent” network can be harnessed to restore diaphragm function after high cervical spinal cord injury in adult mice and adult rats.

Introduction

Inspiration—the act of drawing air into the lungs—is executed primarily by the diaphragm, which contracts ~20,000 times per day and 10^8 times over the average human lifespan. The diaphragm is solely innervated by phrenic motor neurons (PMNs), which are anatomically positioned at spinal cord levels C3-5/6. Thus, injury to the cervical spinal cord severely compromises diaphragm function.

Excitatory circuits of the preBötzinger complex (preBötC), located in the ventrolateral medulla, generate inspiration and relay inspiratory drive to PMNs via a medullary premotor nucleus termed the rostral ventral respiratory group (rVRG; Smith et al., 1991). Neurons of the rVRG maintain bulbospinal projections that synapse directly with PMNs (Davies et al., 1985; Dobbins and Feldman, 1994; Duffin and van Alphen, 1995; Ellenberger and Feldman, 1988; Ellenberger et al., 1990) and, therefore, it is well established that rhythmic PMN bursts arise from circuits rostral to the spinomedullary junction. Evidence that rVRG axons make direct synaptic contact with PMNs comes from studies examining cross-correlation between rVRG units and phrenic nerve activity, which exhibit 1-2 ms latencies typical of monosynaptic connections (Davies et al., 1985; Duffin and van Alphen, 1995). Additional evidence comes from anatomical studies demonstrating close apposition of rVRG axons, identified by anterograde labeling, with the dendritic arbors of retrogradely labeled PMNs (Ellenberger and Feldman, 1988; Lane et al., 2008). Also, synapses between rVRG axon terminals

and PMNs have been identified at the ultrastructural level (Ellenberger et al., 1990).

The simplest model, which is widely accepted, is that PMN bursts are always directly evoked by rVRG input. Nonetheless, there is also data indicating that in the absence of supraspinal (rVRG) input, PMN activity can be initiated centrally by various pharmacological manipulations (Coglianese et al., 1977; Ghali and Marchenko, 2016; Reinoso et al., 1996; Viala et al., 1979; Zimmer and Goshgarian, 2007), or by electrical stimulation (Huang et al., 2016; Kowalski et al., 2013). Although it has been suggested that this activity might be generated by a spinal analogue of the preBötC (Ghali and Marchenko, 2016), the origin of this activity has always been elusive. Indeed, it is largely unclear whether this PMN activity is caused by pharmacologic/electrical action on PMNs themselves, or whether these manipulations engage propriospinal neurons which are also known to synapse with PMNs (Dobbins and Feldman, 1994; Lane et al., 2008; Lipski et al., 1993; Lois et al., 2009). Importantly, there is no existing evidence that when isolated from the medulla, propriospinal neurons can generate spontaneous PMN burst activity.

If there is a population of propriospinal neurons that can generate PMN bursts, then it is important to determine if these interneurons simply relay inspiratory drive from the preBötC (e.g. preBötC → rVRG → interneuronal burst population → PMNs), or whether these neurons act as part of some other independent system—and what relevance this system might have. In this study we establish an *ex vivo* model of spinal cord injury, and combine this model with

pharmacologic and optogenetic perturbations to investigate whether propriospinal circuits are capable of evoking PMN bursts. We identify a recurrent excitatory network that is both sufficient and necessary for PMN bursting in the absence of the medulla, and show that activity generated by this network is dissociable from *bona fide* inspiration. Furthermore, we demonstrate that this network can be used to promote diaphragm function after spinal cord injury in adult mice and rats.

Results

Blockade of Inhibitory Synaptic Transmission Initiates Persistent PMN Bursting

We first established an *ex vivo* model of cervical spinal cord injury for tractable interrogation of phrenic premotor network organization. Mouse *ex vivo* preparations exhibit fictive inspiration (Figure 2.1A). Inspiratory frequency in *ex vivo* preparations is depressed relative to *in vivo* conditions due to lack of vagal feedback as well as the relatively cooler temperatures required for maintaining the preparation during recording (23-26^{o}C). In these neonatal preparations (P2-4), we found that a C1 lateral hemisection eliminates phrenic nerve inspiratory burst activity on the side ipsilateral to the lesion (Figure 2.1B, n = 8), and that complete transection at C1 arrests fictive inspiratory activity in both phrenic nerves (Figure 2.1C, n = 8). Since these data phenocopy well-characterized physiology of the adult mammal after spinal cord injury (Alilain et al., 2008), we proceeded to use this *ex vivo* preparation to understand the functional organization of phrenic premotor circuits.

We first examined whether spinal premotor circuits are capable of generating PMN bursts given tonic excitatory input. After a C1 transection injury, we found that bath application of NMDA/5HT elicited very modest PMN unit activity in 50% of cases (Figure 2.2A, *n* = 2 of 4). This unit activity did not exhibit any noticeable patterning between the left and right phrenic nerves, and PMNs did not exhibit any clear bursts. In contrast, application of NMDA/5HT evoked robust locomotor-like bursting from the ventral roots of the L2 segment, which exhibited right/left alternation (Figure 2.2B).

To further address whether an excitatory stimulus could evoke PMN bursts in the absence of medullary input, we used an optogenetic strategy to stimulate cervical Vglut2+ neurons. We found that after complete C1 transection, 30 s of continuous photostimulation of the ventral cervical spinal cord of *Vglut2*^{Cre}*;R26R*^{ChR2} preparations generated only modest PMN unit activity at light onset, with unit firing tapering off over the course of the photostimulation paradigm (Figure 2.2C). We examined PMN responses at multiple light intensities (10-100%), different light stimulus frequencies (20 Hz, 50 Hz), and different pulse durations (20 ms, 100 ms), and found that continuous light generated the strongest response consisting solely of PMN unit activity but no PMN bursts (Figure 2.2C). In contrast, photostimulation of the lumbar cord evoked fictive locomotion (Hägglund et al., 2010), with alternating burst activity between right and left L2 ventral roots (Figure 2.2D). Together these results indicate that simply increasing excitation in the absence of medullary input does not evoke PMN burst activity.

These data suggest that either the contribution of interneurons to PMN output is diminutive, or that inhibition suppresses the action of excitatory interneurons under these conditions. To test these alternatives we examined PMN output after blockade of fast inhibitory synaptic transmission. Unexpectedly, bath application of picrotoxin (PTX) and strychnine (STRYCH) in the absence of the medulla initiated spontaneous bilaterally-coordinated PMN bursting (Figure 2.3B). The frequency of spontaneous PMN bursting caused by blocking inhibition was much slower than that of fictive inspiration (Figure 2.3C). Spinal cord derived PMN bursts also exhibited a significantly longer burst duration compared with fictive inspiratory bursts (Figure 2.3D). The duration of each individual spontaneous PMN burst did not predict the onset of subsequent bursts (Figure 2.3E). Finally, whereas fictive inspiration was highly rhythmic (Figure 2.3F, top), spontaneous PMN bursting observed in the absence of inhibition was not rhythmic (Figure 2.3F, bottom).

Excitatory Interneurons are Sufficient and Necessary for Spinal Cord Derived PMN Bursting

Spinal cord derived PMN bursting initiated by blockade of inhibitory synaptic transmission may be caused via two distinct mechanisms: First, bursts could arise from PMNs themselves via synchronization of subthreshold activity in electrically coupled dendritic arbors (Tresch and Kiehn, 2000). Previous electrophysiological analyses, however, have suggested that PMNs do not exhibit electrical coupling via gap junctions (Lipski, 1984). Second, PMN bursts

could arise from recurrent excitatory premotor networks. To distinguish between these possibilities we examined PMN burst generation after washing out Ca^{2+}, which is required for synaptic transmission. Ca^{2+} washout completely eliminated spinal cord derived PMN bursts (Figure 2.4A). Moreover, we found that blockade of NMDA and non-NMDA glutamate receptors also abolished spontaneous PMN bursting (Figure 2.4B). These data indicate that excitatory presynaptic input is required for spontaneous PMN bursting after blockade of inhibitory synaptic transmission.

We next tested whether PMN bursts could be evoked by stimulation of cervical glutamatergic interneurons. In PTX/STRYCH disinhibited preparations from *Vglut2^{Cre};R26R^{ChR2}* mice, a series of 200 ms photostimuli centered on the ventral cervical spinal cord was sufficient to evoke bilaterally coordinated PMN bursting (Figures 2.5A-5D). PMN bursting could be driven at a frequency similar to that of fictive inspiration (Figures 2.5D-F, ~5 bursts min^{-1}). The duration of individual burst episodes was significantly shorter during trains of photostimulation compared with those observed spontaneously (Figure 2.5G). Light-evoked PMN bursts do not simply reflect direct activation of PMNs by Vglut2+ sensory or bulbospinal fibers because stimulation of Vglut2+ fibers in the absence of PTX/STRYCH did not evoke PMN bursts (Figure 2C). Additionally, the brief 200 ms photostimulus caused activity which lasted on the order of seconds (Figures 2.5C, 2.5D, 2.5G, and 2.5H). This suggests that the stimulus is recruiting recurrent excitatory premotor networks.

Blockade of NMDA and non-NMDA glutamate receptors abolished light-evoked PMN burst activity (Figure 2.5H), indicating a presynaptic origin of light-evoked bursts. Although it is well known that lumbar motor neurons release glutamate and express Vglut2 (Mentis et al., 2005; Nishimaru et al., 2005; Talpalar et al., 2011), we observed only sparse *Vglut2*^{Cre} mediated recombination of an EYFP-reporter allele in putative PMNs (Figure 2.5B, arrow). To directly examine *Vglut2*^{Cre}-mediated recombination in PMNs, we retrogradely traced PMNs by intrapleural injection of CTB-555 (Figures 2.6A-C). PMNs labeled by CTB-555 were positioned between the medial and lateral motor columns in spinal cord levels C3-5 (Figures 2.7A,B). 27.2% of CTB-labeled PMNs expressed LacZ in *Vglut2*^{Cre};*Tau*$^{lsl\text{-}LacZ}$ mice (50/184 neurons, n = 4, Figures 6A-C).

We next performed *in situ* analysis to assess whether PMNs express *Vglut2* mRNA (Figures 2.6D-F). While some motor neurons of the lateral column expressed *Vglut2*, most PMNs lacked expression (n = 4, 4/104 neurons, Figures 2.6D-F). This data indicates that *Vglut2*^{Cre}-mediated recombination in a subset of PMNs is caused by transient rather than sustained *Vglut2* expression.

After Ca^{2+} washout, stimulation of ChR2-expressing PMNs in *Vglut2*^{Cre}*;R26R*^{ChR2} mice evoked only minor PMN unit activity but no PMN bursts (Figures 2.6I,J). These results indicate that light-evoked bursts arise from excitatory premotor networks rather than from direct stimulation of PMNs.

Direct Stimulation of PMNs is Not Sufficient to Evoke PMN Bursts

To further test whether stimulation of PMNs would be sufficient to evoke PMN bursts, we used a *ChAT*^{Cre} allele to allow motor neuron-specific expression of ChR2 (Figure 2.7B). 99.1% of PMNs expressed ChR2-EYFP in *ChAT*^{Cre}*;R26R*^{ChR2} mice (216/218 neurons, n = 7, Figures 2.6G,H). We also observed ChR2-EYFP expression in cholinergic interneurons (Figure 2.7B, arrows), which represent a small fraction of cervical spinal interneurons (Barber et al., 1984).

After C1 transection and blockade of inhibitory synaptic transmission, 200 ms *ChAT*^{Cre}*;R26R*^{ChR2} photostimulation resulted in PMN unit activity for 193 ± 6 ms, but did not evoke bursts which outlasted the stimulus duration (Figure 2.7C). In comparison, 200 ms photostimulation of Vglut2+ interneurons resulted in a burst of PMN activity that lasted for 3635 ± 556 ms (Figures 2.7C,D). We examined whether varying the stimulus duration in *ChAT*^{Cre}*;R26R*^{ChR2} preparations would lead to burst responses lasting longer than the light stimulus. Photostimuli of 200-4000 ms evoked PMN unit activity that lasted only for the duration of the photostimulus (Figures 2.7E,F). Since light-evoked PMN unit activity persisted after Ca^{2+} washout, it is caused by direct stimulation of PMNs rather than ChR2+ cholinergic interneurons (Figures 2.7E,F). Lastly, after Ca^{2+} washout, photostimulation of PMNs in *ChAT*^{Cre}*;R26R*^{ChR2} mice caused a much more robust unit response than photostimulation of PMNs in *Vglut2*^{Cre}*;R26R*^{ChR2} mice (Figures 2.6I,J). This is consistent with our anatomical data demonstrating that only a subset of PMNs exhibit *Vglut2*^{Cre}-mediated recombination (Figure 2.6C). Together these data indicate that direct stimulation of PMNs is not

sufficient to evoke sustained PMN bursts. We conclude that PMN bursts arise from recurrent excitatory premotor networks.

Dissociation of Spinal Cord Derived PMN Bursting from Bona Fide Inspiration

Our results provide evidence for an excitatory spinal cord network that can evoke PMN bursting. To address whether this network relays excitatory inspiratory drive from higher-order medullary nuclei (e.g., preBötC → rVRG → interneuronal burst population → PMNs), we examined PMN activity after blockade of inhibition in spinomedullary preparations. Interestingly, we observed two distinct modes of PMN bursting under these conditions: high frequency/short duration and low frequency/long duration (Figures 2.8A,B, +PTX/STRYCH). We reasoned that these distinct modes of PMN bursting reflect the action of two distinct premotor networks: PMN bursts of shorter duration are likely driven by the preBötC because they exhibit a frequency and duration similar to that of fictive inspiration (Figure 2.8B), and the longer PMN bursts are likely driven by excitatory spinal cord network activity which emerges following blockade of inhibition.

To test this, we performed a lateral C1 hemisection lesion to eliminate descending medullary input to PMNs on the right side. We found that a C1 hemisection eliminated short duration bursts only on the side ipsilateral to the lesion (Figure 2.8A, diamonds). Notably, synchronous long duration PMN bursts were retained on both sides (Figures 2.8A,B). We conclude that the high frequency/short duration bursts are of medullary origin, and long duration bursts

are of spinal cord origin. Importantly, these experiments demonstrate that in disinhibited preparations, excitatory medullary and spinal cord premotor networks do not interact; one type of bursting does not drive the other.

We next examined whether medullary and spinal cord premotor networks exhibit differential pharmacological sensitivity. Opioids are known to depress inspiration via direct action on preBötC circuits (Gray et al., 1999). In spinomedullary preparations, bursts of medullary origin exhibited slower frequency, smaller amplitude, and shorter duration in response to bath application of the μ-opioid agonist DAMGO (Figures 2.8A,C), whereas bursts of spinal cord origin were remarkably insensitive to DAMGO (Figures 2.8A,C). In contrast, spinal cord—but not medullary—derived PMN bursts were largely eliminated by application of riluzole, a non-selective drug that blocks persistent sodium current (I_{NaP}, Figures 2.9A-D). Consistent with previous data, riluzole application had no effect on medullary derived inspiratory burst frequency (Figures 2.9A,B; Thoby-Brisson et al., 2009), but shortened both the amplitude and duration of inspiratory bursts (Figures 2.9C,D; Peña et al., 2004). Together these pharmacological manipulations demonstrate that spinal cord derived PMN bursting is dissociable from *bona fide* inspiration.

Spontaneous Spinal Cord Derived PMN Bursts Originate in the Thoraco-Lumbar Cord

To further examine the anatomical origin of spontaneous burst initiation after blockade of inhibitory synaptic transmission, we simultaneously recorded

from the phrenic nerve and the L2 ventral root (Figure 2.10A). Previous work in the lumbar spinal cord has demonstrated that blockade of inhibitory synaptic transmission initiates synchronous bursting across multiple ventral roots (Bracci et al., 1996). This synchronous burst activity has been attributed to excitatory premotor circuits associated with locomotion (Bracci et al., 1996; Hägglund et al., 2010; Talpalar et al., 2011). Upon application of PTX/STRYCH in C1 transected preparations, we found that PMNs exhibited long duration bursting synchronous with lumbar motor neurons in L2 (Figures 2.10A,B). Furthermore, PTX/STRYCH application caused similar bursting in the radial and musculocutaneous nerves (not shown), suggesting that long duration bursts generated by excitatory interneurons recruit motor neurons at every spinal level. Importantly, PMN bursting in the disinhibited cord was insensitive to application of the muscle AChR antagonist d-Tubocurarine (1.44 ± 0.35 min^{-1} before vs. 1.29 ± 0.35 min^{-1} after, n = 2), demonstrating that spontaneous PMN bursts are recruited directly by an excitatory premotor network rather than indirectly via intercostal muscle sensory afferents (Decima et al., 1969).

To better define the location of networks generating spontaneous bursts in the disinhibited spinal cord, we transected the spinal cord at T8. Interestingly, regions of spinal cord rostral and caudal to the transection both continued to generate bursts, but these bursts were no longer synchronous, and the frequency of the bursts rostral to T8 was reduced (Figures 2.10A-C). In a purely excitatory network, such as the early embryonic spinal cord or sinoatrial-atrioventricular node coupling in the heart, burst initiation is determined by the

most excitable population of cells. Our data suggests that the most excitable population of glutamatergic neurons in the disinhibited spinal cord resides caudal to T8, and that this population drives network-wide bursts. However, in their absence, other excitable populations of glutamatergic neurons rostral to T8 can take over and initiate network-wide bursts, albeit at a lower frequency (Figure 2.10C). We subsequently performed sequential rostral spinal cord transections and found that transection at C8 abolished spontaneous spinal cord derived PMN bursting (Figures 2.10A-C). Although C8 transection abolished *spontaneous* PMN bursting (Figures 2.10A-C), small PMN bursts could still be evoked by stimulation of cervical glutamatergic neurons in a subset of cases (n = 2 of 4 mice, Figures 2.10D,E). These data indicate that recurrent excitatory networks in the disinhibited spinal cord exhibit a gradient of excitability which is highest in the lumbar cord and lowest in the cervical cord (Figure 2.10F).

Spinal Cord Premotor Networks can Restore Diaphragm Function After Hemiparalysis

A few previous studies have demonstrated that blockade of inhibitory synaptic transmission can initiate PMN activity in adult rodents (Ghali and Marchenko, 2016; Zimmer and Goshgarian, 2007). Although the nature of this activity was largely unclear, it was suggested that this activity might represent a spinal cord origin for respiratory rhythm (Ghali and Marchenko, 2016). Given that hemisection lesions can dissociate spinal cord burst activity from *bona fide* inspiration (Figures 2.8A,B; also shown in Figure 2.11A for comparison with the

adult), we examined whether similar lesions would dissociate PTX/STRYCH initiated PMN activity from respiration in adult mice. In anesthetized mice >8 weeks old, C2 hemisection abolished diaphragm activity ipsilateral to the lesion (Figure 2.11B). Subsequent microinjection of PTX/STRYCH into the cervical spinal cord rapidly initiated activity in the paralyzed hemidiaphragm (Figure 2.11B, green arrows). This activity was largely independent of rhythmic inspiratory circuits of the preBötC because medullary driven inspiratory bursts did not evoke weak unit or burst activity ipsilateral to the lesion (Figures 2.11B,C; indicated by diamonds). However, given the fast dynamics of mouse respiration (~90 min^{-1}), we found that long spinal cord derived bursts almost always overlapped with medullary derived respiratory bursts to some degree (Figures 2.11B,C).

To demonstrate that long duration spinal cord derived bursts can occur independently of medullary derived bursts, we performed similar experiments in adult rats, which exhibited a slower respiratory rate than mice (~30 min^{-1}; Figure 2.11D). C2 hemisection lesions abolished diaphragm activity ipsilateral to the lesion (Figure 2.11D), and intrathecal application of PTX/STRYCH initiated spontaneous activity in the paralyzed hemidiaphragm (Figure 2.11D). Again, activity observed in the paralyzed hemidiaphragm (Figure 2.11D,E; green arrows) was independent of the preBötC because medullary driven inspiratory bursts did not evoke weak unit or burst activity ipsilateral to the lesion (Figures 2.11D,E; indicated by diamonds). Likely owing to the slower dynamics of rat respiration, we observed several long spinal cord derived bursts which were

clearly spaced in between medullary derived inspiratory bursts (Figures 2.11D,E). In both adult mice and rats, we observed ipsilateral diaphragm activity after administration of PTX/STRYCH at the cervical level, suggesting that recurrent excitatory networks rostral to C8 (see evoked activity in Figures 2.10D,E) may give rise to spontaneous burst activity *in vivo* due to enhanced neural dynamics (37^{o}C vs. 23-26^{o}C *ex vivo*). It is also likely that PTX/STRYCH diffused far beyond the initial site of application because we also noted spastic-like movements of the hindlimbs. These data are largely consistent with our *ex vivo* data (Figure 2.11A), indicating that the spinal network we characterize in neonatal preparations has a correlate in adult animals. Together these data demonstrate that spontaneous spinal cord derived PMN bursting is generated independently of respiratory rhythm in adult animals (Figure 2.12), and may be harnessed to promote diaphragm activity in the absence of descending bulbospinal input in the context of SCI.

Discussion

Our data puts to rest a lingering controversy—which has endured in the literature for more than a century—as to whether a "spinal respiratory rhythm generator" can initiate rhythmic inspiratory activity independent of supraspinal input (Brown-Séquard, 1860; Porter, 1895). Our data provides evidence against this hypothesis by demonstrating that while PMN bursts of spinal cord origin can occur, they 1) are not spontaneous and can only be evoked under certain pharmacological conditions, 2) are not rhythmic (Figure 2.3F), 3) are

anatomically and pharmacologically distinguishable from *bona fide* inspiratory circuits under the control of the preBötC, and 4) are likely derived from more caudal regions of the spinal cord associated with circuits of the locomotor CPG. The idea that a lack of inhibition could cause spontaneous PMN bursting is perhaps not surprising given that this occurs in premotor circuits of the lumbar cord, for which propriospinal circuits act as the basis for locomotion and effects of disinhibition are well described (Bracci et al., 1996). Nevertheless, these data are surprising in the context of a vast literature on PMNs, which are thought to derive their dominant excitatory input from supraspinal neurons of the rVRG. Our data thus lead to several exciting new hypotheses concerning physiological role(s) for episodic spinal cord derived PMN bursts.

One possibility is that a caudally-derived excitatory burst module is specifically associated with PMN control under certain circumstances. This could be related to premotor circuits anatomically positioned caudal to C8, such as those associated with control of sympathetic preganglionic neurons or intercostal motor neurons. Alternatively, an excitatory circuit that coordinates bilaterally symmetric motor neuron activity throughout the rostrocaudal extent of the spinal cord—but is dissociable from rhythmic respiratory circuits of the brainstem—might represent a substrate for innate behavioral responses such as startle. In point, hyperekplexia is an exaggerated startle disorder in humans associated with dysfunction of glycinergic transmission (Rees et al., 2006). In contrast to these hypothetical roles, there is strong evidence that such spinal cord derived PMN burst activity does occur in situations of increased network excitability. Two

well-described cases of increased network excitability exist physiologically: First, during embryogenesis, spinal circuits are highly excitable due to depolarizing action of GABA/glycine (Jean-Xavier et al., 2007). Second, spinal cord injury results in a variety of membrane and/or synaptic changes as well as anatomical remodeling that causes increased network excitability (Bellardita et al., 2017; Buttry and Goshgarian, 2014).

Low frequency, long duration bursts propagate within the spinal cord during embryogenesis as early as E12 (Hanson and Landmesser, 2003; Momose-Sato et al., 2012a, 2012b; Myers et al., 2005). Interestingly, PMNs exhibit activity-dependent intramuscular nerve branching and innervation of the diaphragm during this early stage of embryogenesis (E12.5-13.5; Brandon et al., 2003). Here, evoked ACh release from PMNs (rather than spontaneous vesicle fusion) regulates diaphragm innervation (Usiak and Landmesser, 1999; Washbourne et al., 2002). This evoked release is likely caused by spinal waves of propagating burst activity since activation of PMNs by the preBötC occurs much later at E15-15.5 (Thoby-Brisson et al., 2009). Although waves of propagating burst activity during embryogenesis exhibit a number of similarities to those we observe in the disinhibited spinal cord, a notable difference is that burst activity during embryogenesis is generated chiefly by excitatory cholinergic rather than glutamatergic synaptic transmission (Hanson and Landmesser, 2003; Momose-Sato et al., 2012a, 2012b). The mechanisms underlying transition from acetylcholine to glutamate as the primary excitatory neurotransmitter in the spinal cord are not understood; however, evidence that glutamatergic networks

compensate for loss of acetylcholine transmission in *ChAT*$^{-/-}$ embryos, and that proper assembly of locomotor networks is disrupted in *ChAT*$^{-/-}$ embryos, suggests that downregulation of cholinergic signaling may help to instruct the development of future glutamatergic premotor networks (Myers et al., 2005). These data lend support to the hypothesis that the diffuse excitatory spinal circuit which can generate PMN activity post-natally might represent a “latent” or “holdover” network from development.

Increased excitation after spinal cord injury can lead to adverse outcomes, including muscle spasticity and/or autonomic dysreflexia (Bellardita et al., 2017; Ueno et al., 2016). An emergent view is that spasticity is caused by recruitment of disparate populations of excitatory neurons into functional circuits—leading to enhanced excitation independent of motor neuron excitability or inhibition (Bellardita et al., 2017). Interestingly, cervical spinal cord injury in human C4 tetraplegic patients is sometimes accompanied by diaphragm spasticity (Silver and Lehr, 1981). Moreover, we have observed occasional diaphragm spasticity after spinal cord injury in the adult rat in the context of experimental manipulations aimed at restoring function to the chronically denervated phrenic motor pool (P.M. Warren, J. Silver, unpublished data). It has been difficult to understand why diaphragm spasticity occurs since premotor networks controlling phrenic bursting have been thought to reside in the medulla. These medullary networks should be relatively insensitive to lesion of the cervical spinal cord, suggesting a different origin of spastic activity. Recent transynaptic tracing experiments initiated in PMNs after C2 hemisection injury have demonstrated

extensive anatomical plasticity in PMN premotor networks (Buttry and Goshgarian, 2014). The origin of diaphragm spasticity after adult spinal cord injury could thus be due to heightened engagement of a pre-existing spinal network which directs PMN bursting independently of descending bulbospinal input.

Excitingly, the same mechanisms that cause network dysfunction and/or spasticity might also be harnessed toward restoration of normal circuit function. In recent years, restoring diaphragm function after SCI has become a model system for understanding functional regeneration beyond the glial scar (Alilain et al., 2011; Cregg et al., 2014), because normal function of PMNs is controlled by direct monosynaptic connection with neurons of the rVRG (Davies et al., 1985; Duffin and van Alphen, 1995; Ellenberger and Feldman, 1988; Ellenberger et al., 1990). This model presents a somewhat simpler system (vs. locomotion or micturition) for understanding how regenerating axons engage circuits caudal to a spinal cord lesion. In two examples from our previous work, we observed recovery of diaphragm function after hemiparalysis which seemed to involve the contribution of interneuronal networks (Alilain et al., 2008, 2011). These results were perplexing at the time because we did not understand that a spinal cord network could evoke PMN bursting independently of *bona fide* inspiration as our present study has shown (Alilain et al., 2008, 2011). Thus, those attempting to enhance regeneration of axons and restoration of a “simple” motor behavior may need to consider the dynamic interplay between intact networks and networks that undergo dramatic reorganization caudal to a spinal lesion.

Finally, future experiments aiming to identify spinal PMN excitatory burst populations in more anatomical detail could lead to a diaphragm “pacing” device (Huang et al., 2016; Kowalski et al., 2013). We demonstrate pacing of spinal cord derived PMN bursting at a rate similar to fictive inspiration, and given considerable technical advancements, this proof-of-concept could be therapeutically relevant *in vivo* after cervical spinal cord injury. Toward identification of PMN excitatory burst populations, our finding that spontaneous PMN burst activity is eliminated upon transection at C8 may be useful. In point, Kowalski and colleagues recently demonstrated that PMN unit activity—as opposed to burst activity demonstrated here—could be evoked by epidural stimulation at spinal cord level T2 (Kowalski et al., 2013). Altogether, our data provides new insight into PMN premotor network organization and establishes a conceptual framework for targeting treatment and recovery of diaphragm function after cervical SCI.

Acknowledgments

Kevin A. Chu, Lydia E. Hager, Rachel S.J. Maggard, Daimen R. Stoltz, Michaela Edmond, Warren J. Alilain, Polyxeni Philippidou, Lynn T. Landmesser, and Jerry Silver contributed as co-authors to Chapter 2. This work was supported by NSF grant DGE-0951783 (to J.M.C.), start-up from the University of Kentucky College of Medicine (to W.J.A.), NIH grant NS101105 (to W.J.A.), start-up from Case Western Reserve University (to P.P.), the Mt. Sinai Foundation (to P.P.), NIH grant NS085037 (to P.P.), NIH grant NS074199 (to L.T.L.), and NIH grant

NS025713 (to J.S.). We thank Jing Qiang You for technical assistance and Thomas (TED) Dick, Philippa Warren, and Christopher Wilson for helpful commentary and discussion.

Methods

Contact for Reagent and Resource Sharing

Further information and requests for resources should be directed to and will be fulfilled by the Lead Contact, Jerry Silver (jxs10@case.edu).

Experimental Models

All animal procedures were performed in accordance with Case Western Reserve University or University of Kentucky College of Medicine Institutional Animal Care and Use Committee (IACUC) guidelines.

Vglut2^{Cre} (Jackson Laboratories, stock #016963, STOCK Slc17a6$^{tm2(cre)Lowl}$/J), *ChAT*^{Cre} (#006410, B6;129S6-Chat$^{tm2(cre)Lowl}$/J), *R26R*$^{ChR2\text{-}EYFP}$ (#012569, B6;129S-Gt(ROSA)26Sor$^{tm32(CAG\text{-}COP4*H134R/EYFP)Hze}$/J), *R26R*^{EYFP} (#007903, B6.Cg-Gt(ROSA)26Sor$^{tm3(CAG\text{-}EYFP)Hze}$/J), and *Tau*$^{lsl\text{-}LacZ}$ (#021162, B6.129P2-Mapt^{tm2Arbr}/J) mice were obtained from Jackson Laboratories and maintained on a mixed background. Genotyping was conducted according to Jax strain-specific genotyping protocols. *Vglut2*^{Cre} or *ChAT*^{Cre} mice were crossed to homozygous *R26R*$^{ChR2\text{-}EYFP}$ reporter mice to direct ChR2-EYFP expression to glutamatergic or cholinergic neurons, respectively. Given dense labeling of neuropil due to strong axonal trafficking of ChR2-EYFP in *Vglut2*^{Cre}*;R26R*$^{ChR2\text{-}EYFP}$ mice (data not shown), we used homozygous *R26R*^{EYFP} or *Tau*$^{lsl\text{-}LacZ}$ reporter mice to label glutamatergic neuronal soma with EYFP or LacZ, respectively. Animals heterozygous for Cre recombinase and heterozygous for ChR2-EYFP,

EYFP, or LacZ alleles were used for these experiments. We carried out experiments that did not require genetic perturbations in wild type C57BL/6J mice (#000664). Animals were assigned to groups based on genotype. Experiments and analysis were performed with prior knowledge of genotype. *Ex vivo* experiments were carried out in P2-4 male and female mice. Experiments in adult mice were performed in >8 week old male and female mice.

Sprague-Dawley rats were purchased from Charles River Laboratories, Inc. Rat experiments were performed in adult females >8 weeks old.

Dissection

P2-4 mice were cryoanesthetized and rapid dissection was carried out in 23-26 °C oxygenated Ringers solution. Solution was composed of 128 mM NaCl, 4 mM KCl, 21 mM $NaHCO_3$, 0.5 mM NaH_2PO_4, 2 mM $CaCl_2$, 1 mM $MgCl_2$, and 30 mM D-glucose and was equilibrated by bubbling in 95% O_2/5% CO_2. The hindbrain and spinal cord were exposed by ventral laminectomy, and phrenic nerves exposed and dissected free of connective tissue. Phrenic nerves were identified as the only medially projecting nerves arising from the brachial plexus. A transection at the pontomedullary boundary rostral to the anterior inferior cerebellar artery was used to initiate fictive inspiration. C1 transection/hemisection were performed at the level of the C1 ventral root, which is caudal to the obex.

Ex Vivo Electrophysiology and Photostimulation

Recording experiments were performed under continuous perfusion of oxygenated Ringers solution (14 ml min^{-1}, 23-26 °C). Suction electrodes were attached to phrenic nerves (rPN/lPN) and/or ventral roots from lumbar segment 2 (L2). Signal was band-pass filtered from 30 Hz to 1 kHz using Grass amplifiers, amplified 10,000-fold, and sampled at a rate of 50 kHz with a Digidata 1440A (Molecular Devices). A Polychrome V monochromator (Till Photonics) was used for photostimulation, where blue light (wavelength 473 nm, 10 nm bandwidth) was directed at the spinal cord using a fiberoptic light guide (Till Photonics). The spatial extent of light illumination and scatter in the transverse plane is represented in experimental schematics (Figures 2.2C, 2.2D, 2.5A, 2.6I, 2.7C, and 2.10D). Light intensity was measured with a photodiode (Cat# S120C, Thorlabs) coupled to a power meter (Cat# PM100D, Thorlabs). The light intensity used in this study was ~0.20 mW/mm^2.

Drugs

NMDA (7 µM, Sigma), 5-hydroxytryptophan (5HT, 8 µM, Sigma), picrotoxin (PTX, 10 µM, Sigma, $GABA_AR$ antagonist), strychnine hydrochloride (STRYCH, 0.3 µM, Sigma, GlyR antagonist), CNQX (20 µM, Sigma, non-NMDA glutamatergic receptor antagonist), AP5 (20 µM, Sigma, NMDAR antagonist), D-Ala^2-*N*-Me-Phe^4-$glycol^5$-enkephalin (DAMGO, 2 µM, Sigma, µ-opioid receptor agonist), riluzole (10 µM, Tocris), and d-Tubocurarine (10 µM, Tocris, AChR antagonist).

Retrograde Tracing

Retrograde tracing of PMNs was performed as described previously (Mantilla et al., 2009), but adapted to neonatal mice. P0 mice were cryoanesthetized, and a 33 gauge Hamilton syringe was used to deliver 10 µl of CTB-555 into the pleural space (ThermoFisher Cat# C34776, 2 mg/ml). Pups were allowed to recover on a heating pad before returning to their home cage.

Immunochemistry and X-Gal Staining

Spinal cord tissue from P4 mice was dissected free and fixed in 4% paraformaldehyde for 30 min. 20 µm thick transverse spinal cord sections were obtained using a cryostat. Sections were blocked for 2 h in 5% normal goat or donkey serum and 0.1% triton-X100, and subsequently incubated overnight with rabbit anti-GFP (ThermoFisher Cat# 11122, 1:500) and/or goat anti-ChAT (Chemicon Cat# AB144P) primary antibodies. After 3-4 washes in 1x PBS + 0.1% triton-X100, tissue was incubated overnight with appropriate Alexa fluor secondary antibodies from ThermoFisher or Jackson ImmunoResearch. After 3-4 more washes, coverslips were mounted using CITIFLOUR Af1 medium. For X-gal staining, spinal cord sections were washed in PBS and subsequently incubated overnight at 37^{o}C in X-gal staining buffer as follows: 1x PBS, 1:5000 IGEPAL CA-630, 5 mM potassium ferrocyanide (Sigma Aldrich, Cat# P9387), 5 mM potassium ferricyanide (Sigma Aldrich, Cat# P8131), 0.01 wt/v % sodium dodecyl sulfate (SDS), and 2.5 mM 5-bromo-4-chloro-3-indolyl β-D-galactopyranoside (X-gal, Sigma-Aldrich, B4252). X-gal stained sections were

washed in PBS, and slides were then mounted with coverslips. Imaging was performed on a Leica upright fluorescence/brightfield scope.

In Situ Hybridization

In situ hybridization was performed as described (Philippidou et al., 2012). P4 spinal cord was dissected free and fixed for 2 h in 4% paraformaldehyde. 20 µm thick transverse spinal cord sections were obtained using a cryostat. To generate an *in situ* probe for *Vglut2*, RNA was collected from P2 mouse spinal cord (Thermo Fisher Scientific Cat# AM1931), and reverse transcribed to cDNA (Applied Biosystems Cat# 4368814). A 710 bp template for *in vitro* transcription was amplified using platinum *Taq* polymerase with the following primers: 5'-tggagaagaagcaggacaac and 5'-TAATACGACTCACTATAGGGgccagaacatgtaccagacc, where the underlined sequence is the T7 promoter. A PCR cleanup was performed, and a DIG-labeled *Vglut2* probe was generated by *in vitro* transcription (Sigma-Aldrich Cat# 11175025910) followed by column purification (Sigma-Aldrich Cat# GE27-5330-01). Tissue sections were hybridized with the *Vglut2* probe, and subsequently incubated with an alkaline phosphatase labeled antibody against DIG (Sigma-Aldrich Cat# 11093274910). Color was developed using a NBT/BCIP solution (Sigma-Aldrich Cat# 11681451001).

C2 Hemisection and Diaphragm EMG

Mice were anesthetized with a ketamine (80 mg/kg) and xylazine (10 mg/kg) cocktail administered intraperitoneally. Rats were anesthetized with

urethane (1.2 g/kg) administered intraperitoneally in doses of 0.8 g/kg and 0.4 g/kg separated by 1 h. A laparotomy was performed to expose the diaphragm. Bipolar recording electrodes were inserted into the left and right hemidiaphragm to record baseline inspiratory activity. Signal was amplified using Grass amplifiers, and acquired in Spike2 using a CED1401 acquisition system (Cambridge Electronic Design, Ltd.). After baseline recording, a multilevel dorsal laminectomy was performed over the C2-5 spinal cord. The dura and arachnoid mater were opened, and a C2 hemisection was performed with angled microscissors just caudal to the C2 dorsal root. We established the completeness of the C2 hemisection lesion by diaphragm EMG recording. In mice, we used a Nanoject (Drummond Scientific) to deliver 250 nl of PTX (50 mM)/STRYCH (30 mM) at 3 sites in levels C3-5 on the side ipsilateral to the lesion. Injections were performed at a depth of 1 mm. In rats, we injected 10 ul PTX (50 mM)/STRYCH (30 mM) intrathecally at the level of the C2 hemisection.

Analysis

Data was recorded using pCLAMP 10 software (Molecular Devices) and analyzed in Spike2 (Cambridge Electronic Design, Ltd.). Signal was processed to remove DC drift. Poincaré plots in Figure 3.1 were used to examine variability in burst cycle. Using group data from 8 animals, we calculated IBI_n , IBI_{n+1} matrix values using a custom Perl script (available upon request), and plotted contours in Origin 8 (OriginLab Corporation). Raster plot in Figure 2 was constructed in R (R Project), where trials are aligned by light onset, and the timing and duration of individual bursts are represented by black rectangles (using the rect() function in

R). Gray boxes were used to highlight independent biological replicates. Burst probability was calculated continuously (averaged every 0.1 s over 24 trials, bin = 5 s) using a custom Perl script (available upon request). Phrenic motor neuron positioning in Figure 3 was quantified relative to the central canal (0,0) for both right and left phrenic motor pools. We combined right/left data by vertical transformation, calculated contour matrix values using a custom Perl script (available upon request), and plotted contours in Origin 8 (OriginLab Corporation). Burst amplitude in Figures 2.8 and 2.9 was quantified in rectified and integrated (time constant = 0.2 s) traces before/after drug application, and without movement of the recording electrode between conditions. To account for variability in recording signal between preparations, amplitude is presented as a percentage of pre-drug baseline (100%). Phase diagrams in Figure 2.5 were constructed as previously described (Kjaerulff and Kiehn, 1996), where 0 represents in-phase (synchronous) and π represents out of phase (asynchronous) bursting. In Figure 2.6, EKG artifact was reduced using ECGDelete script from Cambridge Electronic Design, Ltd.

Statistics

Statistical analysis was performed in JMP version 11 (SAS). Minimum sample size needed to obtain statistical significance was determined by power analysis, and experiments were performed with at least this minimum number of animals. A Shapiro-Wilk test was used to determine whether data sets exhibited a normal Gaussian distribution. For data not abiding to a normal distribution

(sometimes due to boundary constraints), a Mann-Whitney U test was used for pairwise comparisons. For data exhibiting a normal distribution, a Brown-Forsythe test was used to determine whether groups exhibited equivalent variance. In cases of equivalent variance, a two-tailed t-test was used for comparisons between 2 groups, and a one-way ANOVA test was performed for >2 groups. A Tukey-Kramer HSD test was used *post hoc* to compare individual pairs and assign levels of significance. If variances were unequal, Welch's ANOVA test was performed to account for unequal standard deviations. Bonferroni correction was used for multiple comparisons in Mann-Whitney U and Welch ANOVA. $P < 0.05$ was considered to be statistically significant, where $*P < 0.05$, $**P < 0.01$, $***P < 0.001$. Descriptive data is presented as mean ± standard error mean. Box and whisker plots were used to visualize data, where whiskers represent range excluding outliers. *n* represents the number of biological replicates (animals) for each group, unless stated otherwise. Details on statistical tests used for each experiment can be found can be found in the accompanying figure legend.

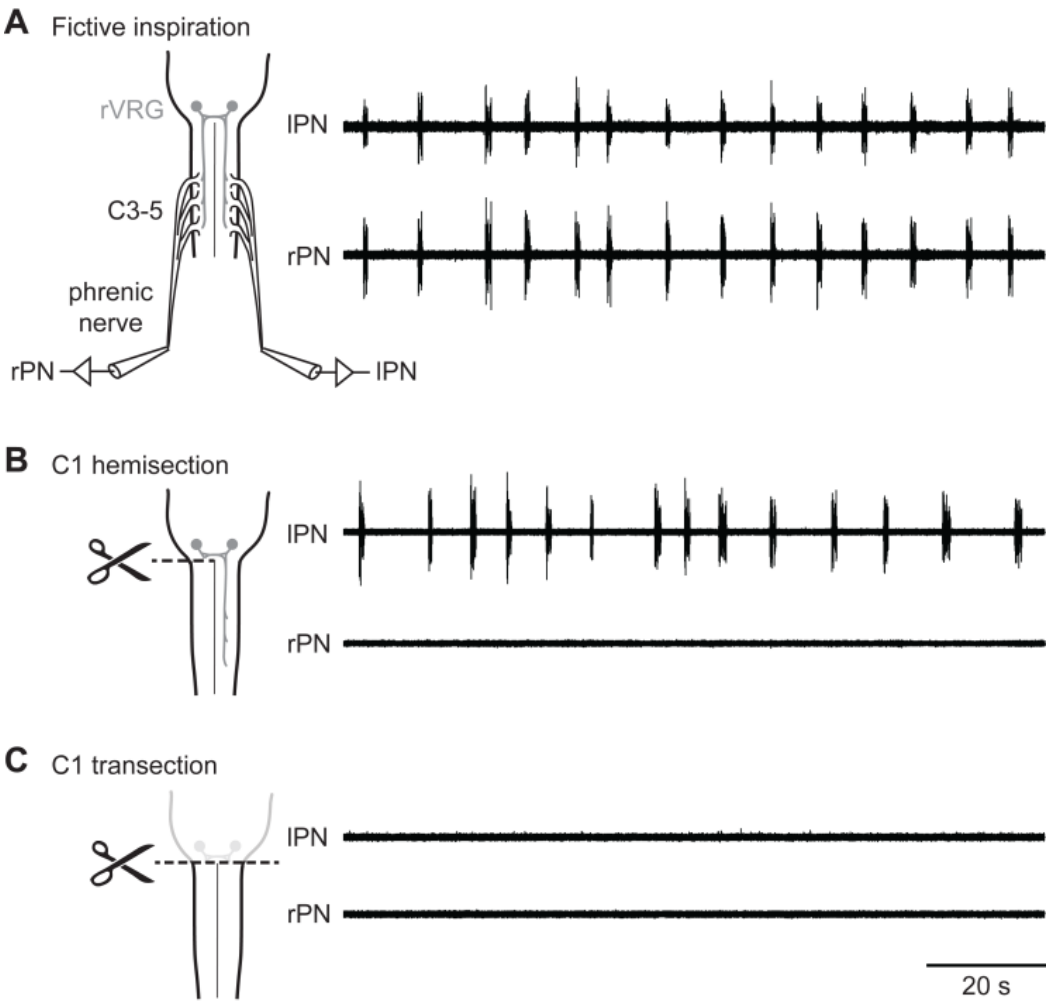

Figure 2.1: An *Ex Vivo* Model of Spinal Cord Injury Recapitulates Hallmark Features of the Adult Descending Respiratory System.

(A) In the *ex vivo* spinomedullary preparation, fictive inspiratory activity is observed from right and left phrenic nerves (*n* = 8), note synchronous left/right bursting. Inspiratory rate is depressed relative to *in vivo* conditions due to lack of vagal feedback as well a recording temperature of 23-26^{o}C.

(B) Right C1 hemisection eliminates fictive inspiration only on the side ipsilateral to the lesion (rPN, *n* = 8).

(C) Complete C1 transection eliminates fictive inspiratory activity in both phrenic nerves (n = 8).

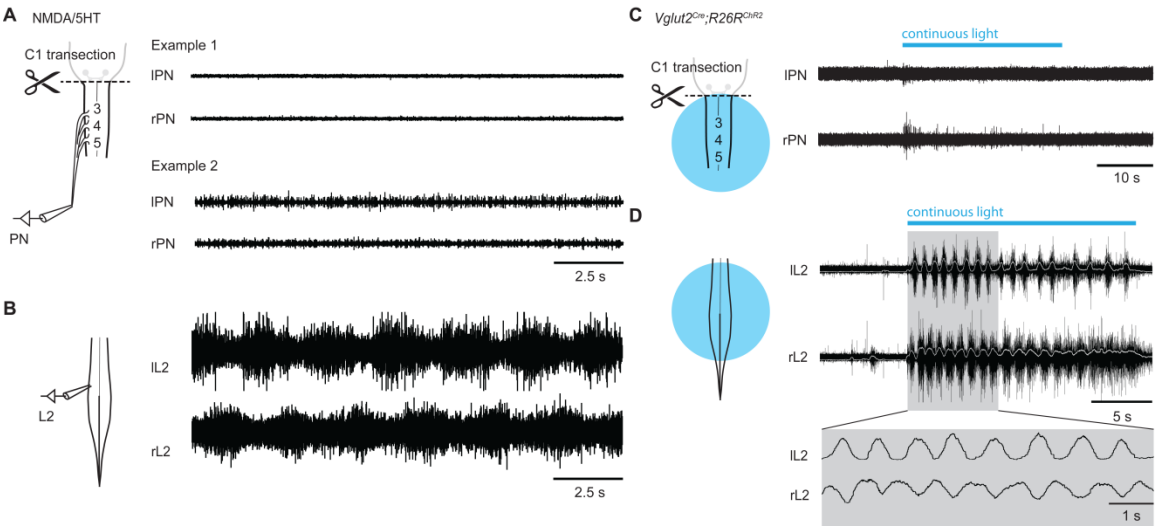

Figure 2.2: Increased Excitation Using Pharmacology or Optogenetics Results in Modest Unit Activity from PMNs.

(A) After C1 transection, bath application of NMDA/5HT resulted in PMN unit activity in 50% of cases (Example 2, *n* = 2/4). We did not observe any PMN burst activity in response to application of NMDA/5HT.

(B) In contrast, bath application of NMDA/5HT resulted in robust locomotor-like burst activity from lumbar roots (bottom); i.e. left/right alternation of bursts is observed.

(C) After C1 transection, photostimulation of cervical Vglut2+ interneurons evoked modest unit activity from PMNs (top; best example). No PMN burst activity was observed in response to stimulation of cervical Vglut2+ neurons.

(D) In contrast, photostimulation of lumbar Vglut2+ neurons immediately evoked fictive locomotor activity in L2 ventral roots (bottom). Left/right alternation of burst pattern is visible.

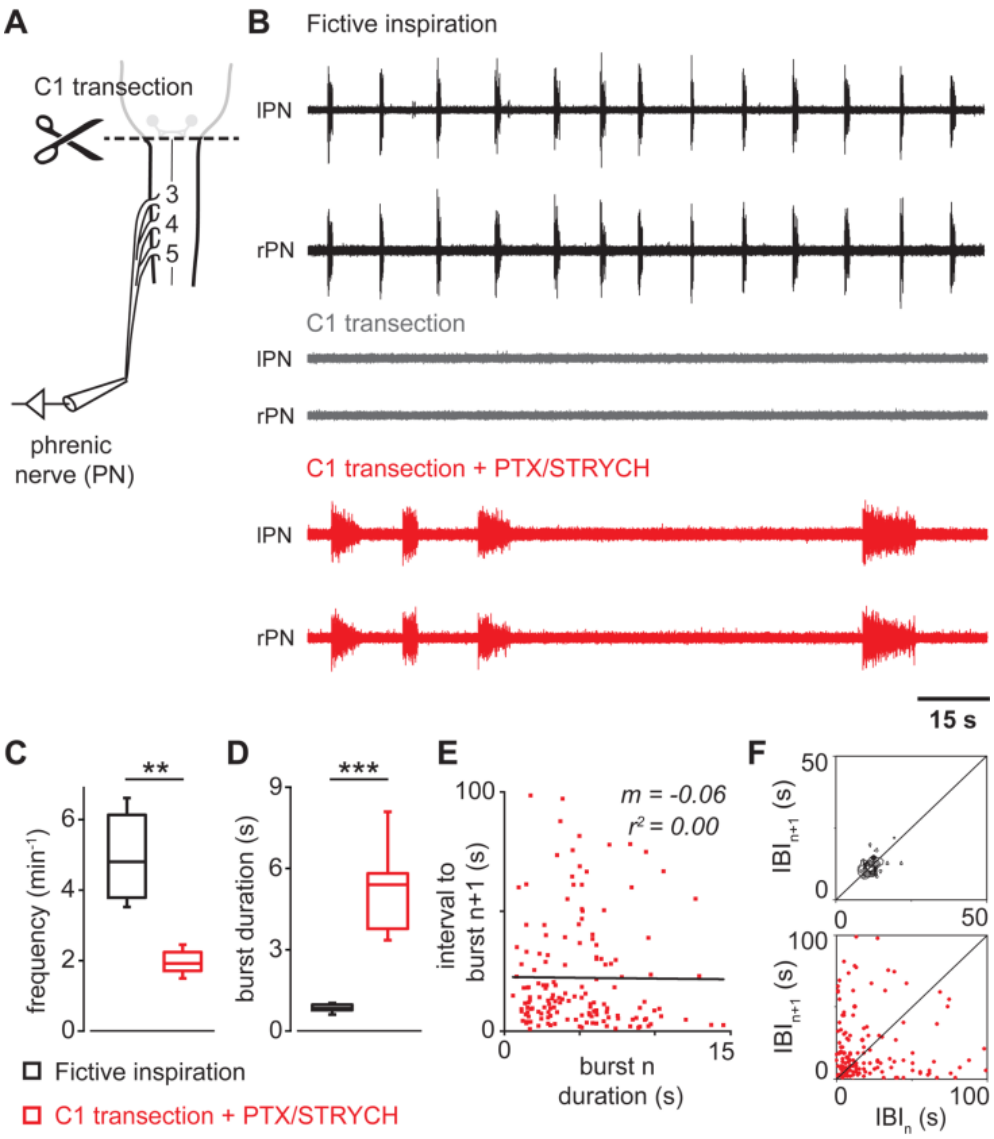

Figure 2.3: After C1 Transection, Blockade of Inhibitory Synaptic Transmission Initiates Persistent PMN Bursting.

(A) *Ex vivo* preparation (P2-4) consists of medulla and cervical through sacral spinal cord. Suction recording electrodes were placed on the phrenic nerves as they enter the pleural cavity.

(B) Spinal cord medullary preparations exhibit fictive inspiration. Phrenic nerve inspiratory activity is abolished after a C1 transection injury. Blockade of fast

inhibition (+PTX/STRYCH) initiates spontaneous PMN bursting in the absence of descending bulbospinal input.

(C) Spontaneous spinal cord derived PMN bursting initiated by blockade of fast inhibition exhibits a slower frequency as compared with fictive inspiration (n = 8 mice, $^{**}P$ = 0.0019, U = 62, Mann-Whitney U test).

(D) PMN bursting initiated by blockade of fast inhibition exhibits a significantly longer burst duration as compared with fictive inspiration (n = 8 mice, $^{***}P$ = 0.00009, $F_{1,7.1}$ = 62.1, Welch's ANOVA).

(E) Burst duration for individual PMN bursts (n) initiated by blockade of fast inhibition does not predict timing or onset of subsequent bursts (n + 1, m = -0.06, r^2 = 0.00).

(F) Poincaré analysis of variability in interburst interval (IBI). Fictive inspiration is highly rhythmic (contour plot falls on line of identity for IBI_n versus IBI_{n+1}). Spinal cord derived PMN bursting does not exhibit a stable rhythm (contours do not fall on line of identity).

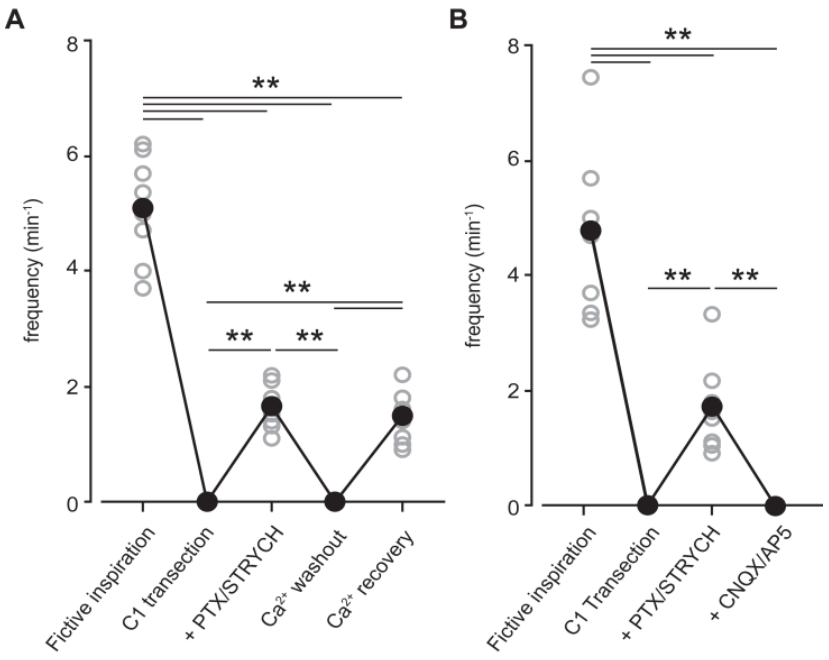

Figure 2.4: Spinal Cord PMN Bursting Requires Excitatory Presynaptic Input.

(A) Ca^{2+} washout abolishes spontaneous spinal cord derived PMN bursting evoked by blockade of fast inhibitory neurotransmission. *n* = 8 mice, *U* = 64 for each significant comparison where ***P* < 0.01, Mann-Whitney U test with Bonferroni correction for multiple comparisons.

(B) Bath application of antagonists of NMDA (AP5) and non-NMDA (CNQX) glutamate receptors abolishes spontaneous spinal cord derived PMN bursting. *n* = 8 mice, ***P* < 0.01, *U* = 62.5 for inspiration vs. PTX/STRYCH and *U* = 64 for every other significant comparison, Mann-Whitney U test with Bonferroni correction.

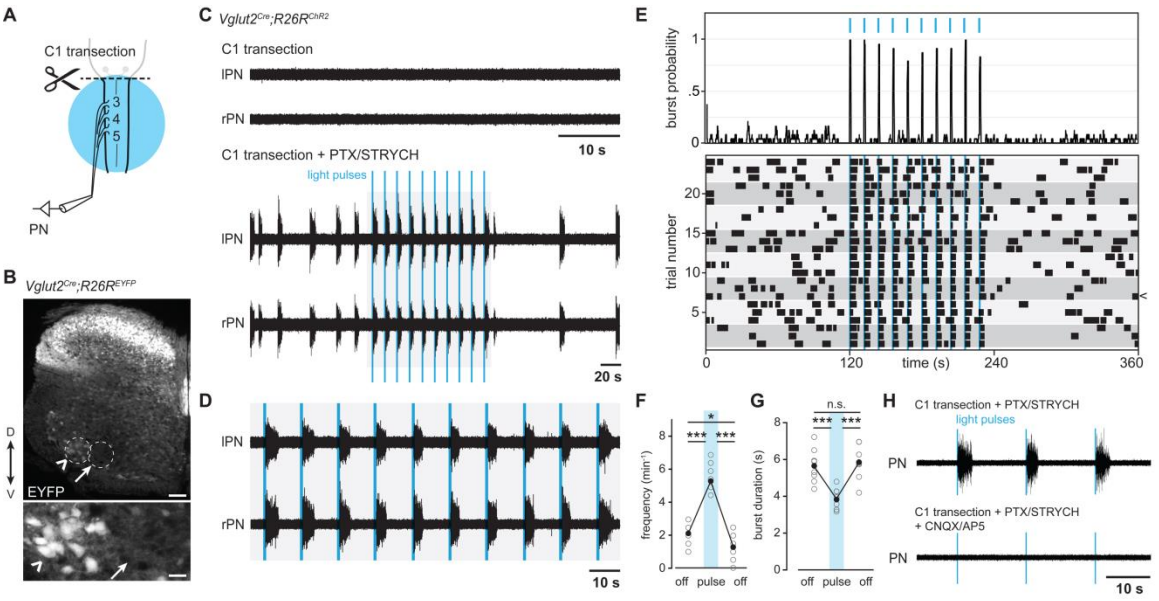

Figure 2.5: Excitatory Neurons are Sufficient and Necessary for PMN Burst Activity in the Absence of Bulbospinal Input.

(A) Experimental *ex vivo* paradigm for photostimulation of cervical Vglut2+ neurons.

(B) Distribution of neurons exhibiting *Vglut2*^{Cre} induced expression of EYFP from a *R26R*^{EYFP} reporter allele in cervical spinal cord level C5. Vglut2+ neurons are situated in spinal cord laminae I-X. Motor neurons identified by their position in lamina IX also exhibit Cre-induced expression of EYFP (arrowheads); however a region corresponding to the location of the phrenic motor nucleus lacked any Vglut2+ soma (arrows). Scale bars: top = 100 µm, bottom = 30 µm.

(C) After complete C1 transection, spinal cord preparations exhibit no PMN activity. PTX/STRYCH application induces bilaterally coordinated bursting of PMNs, and single bursts can be evoked by ChR2-mediated stimulation of

Vglut2+ glutamatergic neurons with 200 ms pulses of blue light. Light was pulsed at a frequency of 5 min^{-1}.

(D) Inset from (C).

(E) Burst probability plot and raster plot for PTX/STRYCH induced bursts. Individual trials are aligned by light onset and grey boxes are used to highlight independent biological replicates (3 trials per animal, n = 8 mice).

(F) Burst frequency is increased during photostimulation (n = 8 mice, ***P = 8.5 x 10^{-11} before vs. during photostimulation, ***P = 6.2 x 10^{-11} during vs. after photostimulation, *P = 0.013 before vs. after photostimulation, $F_{2,21}$ = 156.5, one-way ANOVA and *post hoc* Tukey-Kramer HSD).

(G) Burst duration is significantly reduced during photostimulation (n = 8 mice, ***P = 0.0007 before vs. during photostimulation, ***P = 0.0002 during vs. after photostimulation, $F_{2,21}$ = 14.6, one-way ANOVA and *post hoc* Tukey-Kramer HSD).

(H) PMN bursting evoked by stimulation of Vglut2+ neurons requires glutamate transmission (n = 2 mice).

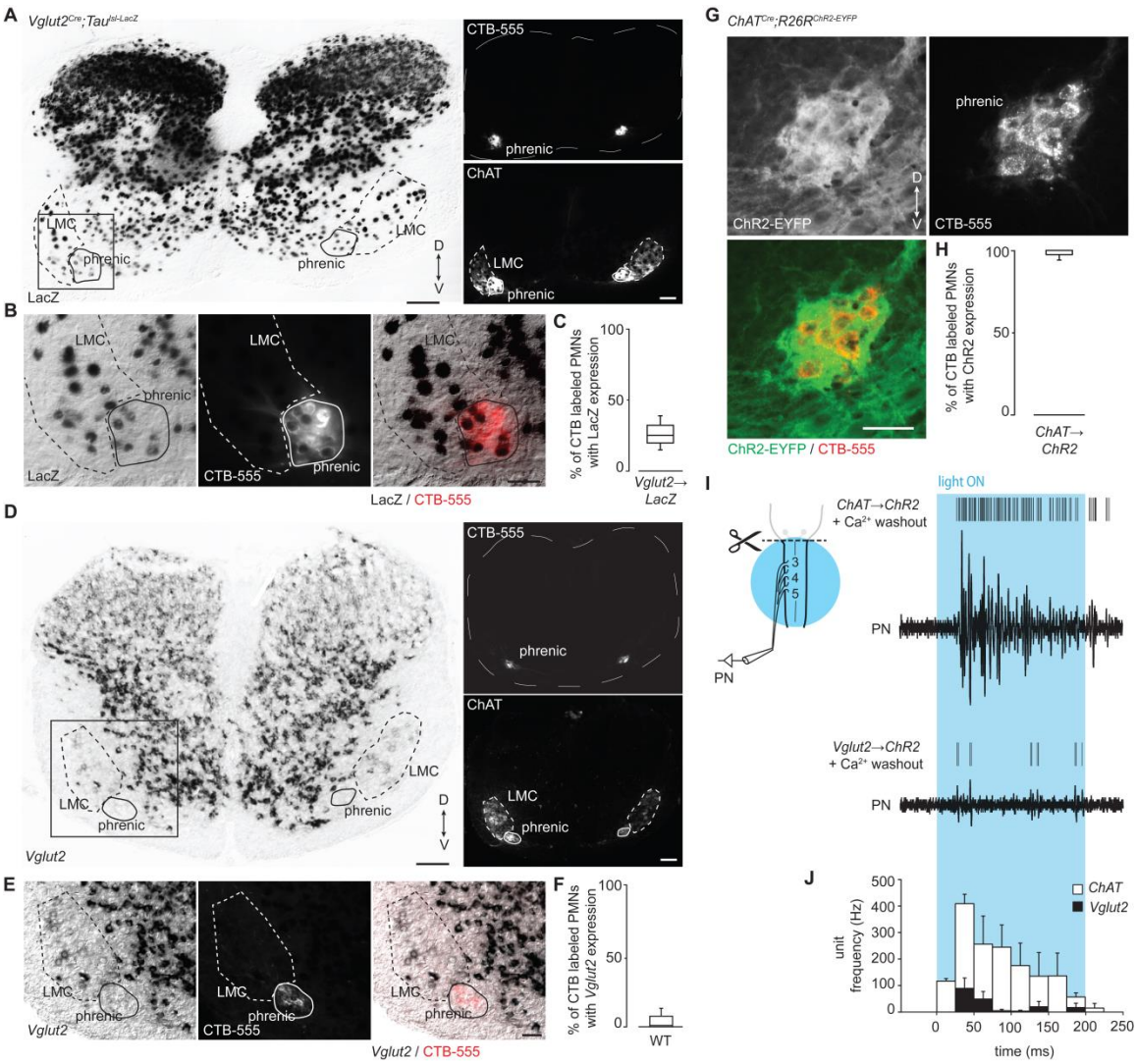

Figure 2.6: *Vglut2*^{Cre}- and *ChAT*^{Cre}-Mediated Recombination in PMNs.

(A) Characterization of *Vglut2*^{Cre} allele. *Vglut2*^{Cre}-mediated recombination of a *Tau*$^{lsl\text{-}LacZ}$ reporter allele leads to LacZ expression in Cre-positive neurons. The phrenic motor nucleus and lateral motor column (LMC) were defined based on backlabeling of PMNs with CTB-555 (right, top) and by ChAT immunochemistry (right, bottom). LacZ expression was observed in excitatory interneurons, as well as a subset of LMC motor neurons and PMNs. Scale bars = 100 µm.

(B) Inset from (A). A subset of CTB-labeled PMNs exhibited expression of LacZ. Scale bar = 50 µm.

(C) Percentage of CTB-labeled PMNs with LacZ expression. 50/184 neurons (27.2%), *n* = 4.

(D) *In situ* hybridization for *Vglut2* mRNA (left). The phrenic motor nucleus and lateral motor column (LMC) were defined based on CTB-555 labeling of PMNs (right, top) and ChAT immunochemistry (right, bottom) in an adjacent section. LMC motor neurons exhibited some expression of *Vglut2* mRNA whereas PMNs did not (representative image based on *n* = 4 animals). Excitatory interneurons exhibited much higher expression of *Vglut2* than motor neurons. Scale bars = 100 µm.

(E) Inset from (D). CTB-labeled PMNs in the same section probed for *Vglut2*. Scale bar = 50 µm.

(F) Percentage of CTB-labeled PMNs with *Vglut2* expression. 4/104 neurons (3.8%), *n* = 4.

(G) In $ChAT^{Cre};R26R^{ChR2\text{-}EYFP}$ mice, retrogradely labeled PMNs (CTB-555, red) exhibited expression of ChR2-EYFP (green, visualized by staining for GFP). Scale bar = 50 µm.

(H) Percentage of CTB-labeled PMNs in $ChAT^{Cre};R26R^{ChR2\text{-}EYFP}$ mice with ChR2-EYFP expression. 216/218 neurons (99.1%), *n* = 7.

(I) PMN unit activity evoked by photostimulation of $ChAT^{Cre};R26R^{ChR2}$ vs. $Vglut2^{Cre};R26R^{ChR2}$ PMNs. In the absence of Ca^{2+}, photostimulation of ChAT→ChR2 PMNs evoked robust unit activity (bars at top show units detected

in the raw trace below). In contrast, photostimulation of Vglut2→ChR2 PMNs evoked only modest PMN unit activity.

(J) Quantification of PMN units evoked by photostimulation of ChAT→ChR2 vs. Vglut2→ChR2 PMNs. *n* = 3 for $ChAT^{Cre}$;$R26R^{ChR2}$ preparations, and *n* = 4 for $Vglut2^{Cre}$;$R26R^{ChR2}$ preparations.

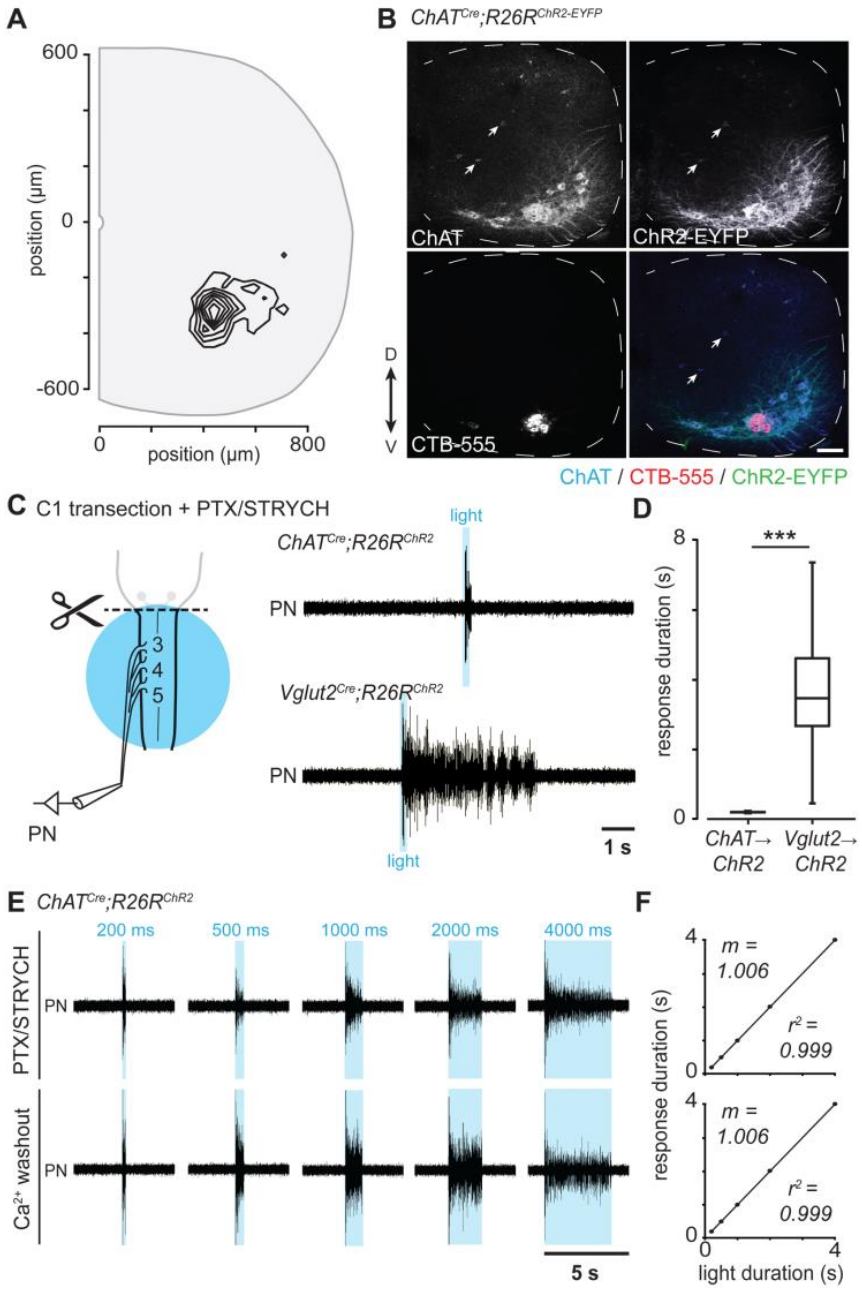

Figure 2.7: Direct Photostimulation of PMNs is Not Sufficient to Evoke PMN Burst Activity.

(A) Anatomical coordinates of retrogradely traced PMNs, which occupy a discrete position in the ventral horn of cervical spinal cord levels C3-5 at post-natal day 10 (321 neurons in 4 animals). (B) *ChAT^{Cre};R26R^{ChR2}* mice exhibit expression of

ChR2-EYFP in ChAT+ motor neurons (ventral horn) and cholinergic interneurons (arrows). CTB-555 labeled PMNs express both ChAT and ChR2-EYFP (see also, Figure S4). Scale bar = 100 μm.

(C) After removal of the medulla by transection at C1 and blockade of fast inhibitory synaptic transmission, 200 ms photostimulation of ChAT+ PMNs resulted in PMN unit activity for the duration of the stimulus. In contrast, 200 ms photostimulation of Vglut2+ neurons resulted in PMN burst activity lasting several seconds.

(D) 200 ms photostimulation of Vglut2+ neurons resulted in a significantly longer PMN response when compared with direct photostimulation of ChAT+ PMNs (4 mice per genotype, n = 22 responses for $ChAT^{Cre};R26R^{ChR2}$ and n = 223 responses for $Vglut2^{Cre};R26R^{ChR2}$, $^{***}P = 1.0 \times 10^{-14}$, U = 4906, Mann-Whitney U test).

(E) Direct photostimulation of ChAT+ PMNs resulted in unit activity for the duration of the stimulus: 200 ms, 500 ms, 1000 ms, 2000 ms, 4000 ms. Ca^{2+} washout—which disrupts synaptic vesicle release from presynaptic terminals—demonstrates that unit response is caused by direct photostimulation of PMNs rather than cholinergic interneurons.

(F) PMN response was directly proportional to photostimulus duration in $ChAT^{Cre};R26R^{ChR2}$ spinal cord preparations bathed in PTX/STRYCH (top, n = 3 mice) or in Ca^{2+}-free aCSF (bottom, n = 3 mice), approaching a relationship of identity for both conditions (m = 1.006).

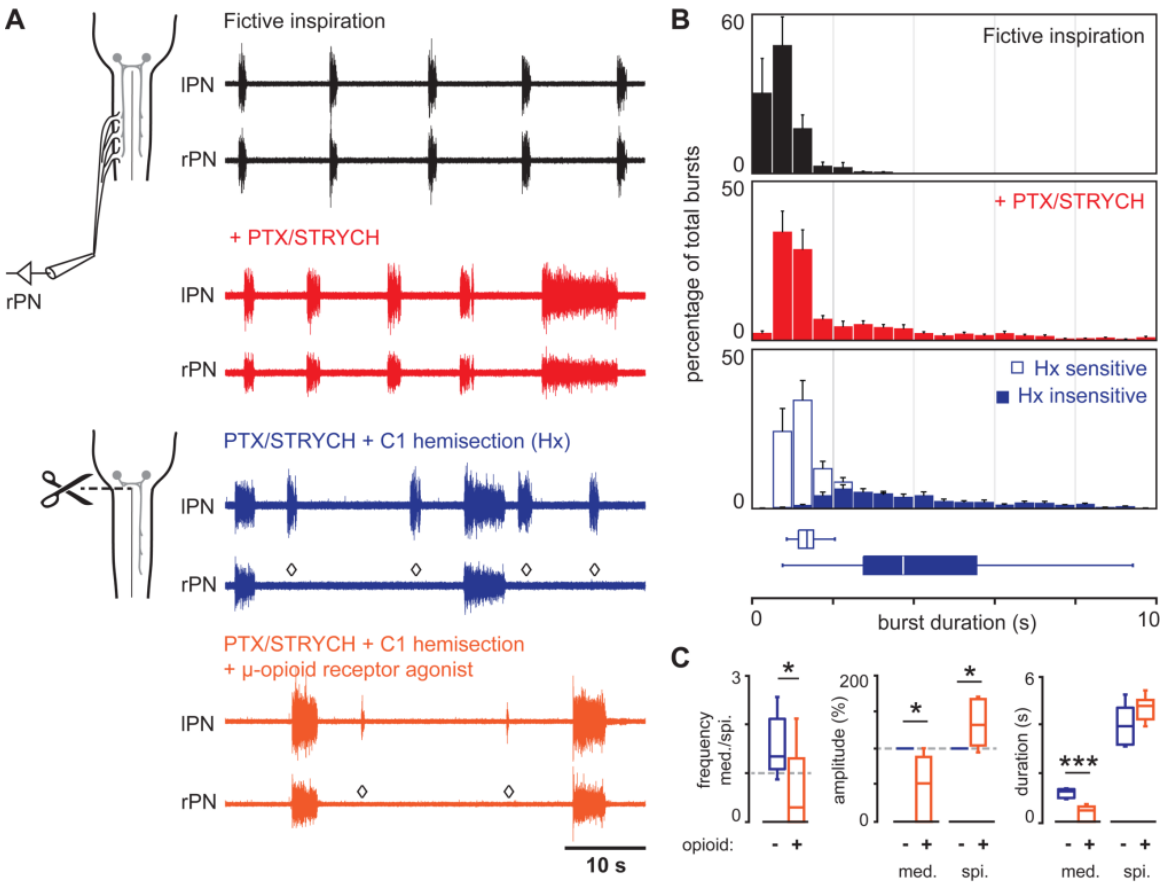

Figure 2.8: Spinal Cord Derived PMN Bursting is Independent of *Bona Fide* Inspiration.

(A) In spinomedullary preparations, blockade of fast inhibitory synaptic transmission evoked two distinct modes of PMN bursting—high frequency/short duration as well as low frequency/long duration (red traces). C1 hemisection (right side, rPN) eliminated high frequency/short duration bursts, whereas low frequency/long duration bursts were retained on both the lesioned and intact sides (blue, *n* = 8). Application of the μ-opioid receptor agonist DAMGO selectively depressed the amplitude and duration of medullary—but not spinal

cord—derived PMN bursts (orange). ◊ indicates absence of medullary derived PMN burst on the side ipsilateral to C1 hemisection.

(B) Dual modes of PMN bursting visualized in burst duration histograms (n = 8). Fictive inspiratory bursts (black) are concentrated in the range of 0-2.5 s. PTX/STRYCH application (red) causes a shift in the distribution: While a majority of bursts are 0-2.5 s in duration, a second population of longer duration bursts emerges with significantly longer duration. C1 hemisection distinguishes medullary derived PMN bursts of high frequency/short duration (open bars) from spinal cord derived PMN bursts of low frequency/long duration (shaded bars), as shorter bursts are lost on the hemisected side.

(C) Left panel: Application of the μ-opioid receptor agonist DAMGO caused medullary derived bursts to become less frequent than spinal cord derived bursts (n = 7 mice, *P = 0.038, t_{12} = 2.3, two-tailed t-test). Middle panel: the opioid agonist selectively depressed the amplitude of medullary (med.)—but not spinal cord (spi.)—derived PMN bursts (n = 7 mice, *P = 0.0202 and U = 41 for med., *P = 0.0204 and U = 41 for spi., Mann-Whitney U test). Right panel: the opioid agonist selectively shortened medullary—but not spinal cord—derived PMN bursts (n = 7 mice, ***P = 3.6 x 10^{-5} for med. and t_{12} = 6.4, P = 0.0783 and t_{12} = 1.9 for spi., two-tailed t-test).

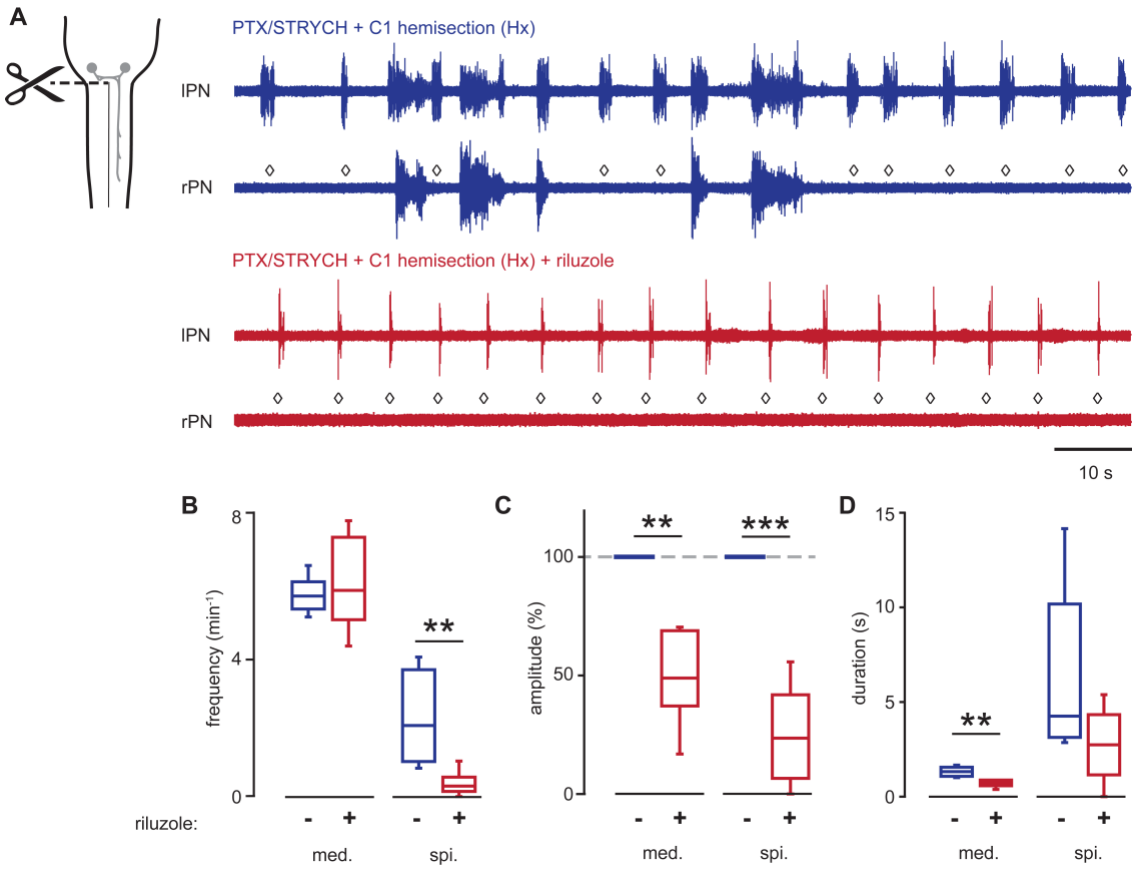

Figure 2.9: Spinal Cord Derived Bursts are Dependent on Persistent Sodium Current (I_{NaP}).

(A) A right C1 hemisection (blue traces) eliminated medullary derived bursts from the right phrenic nerve (◊, bottom trace). The remaining right PMN bursts were synchronous with the longer duration bursts on the intact side, and thus represent spinal cord derived bursts. Riluzole addition (10 μM, blocks I_{NaP} nonselectively, red traces) largely blocked spinal cord derived PMN bursts from both sides (rPN/lPN) without affecting the frequency of medullary derived bursts (lPN). ◊ indicates absence of medullary derived PMN burst on the side ipsilateral (rPN) to C1 hemisection.

(B) Selective depression of spinal cord (spi.) derived burst frequency in the presence of riluzole (n = 8; P = 0.4073 and t_{14} = 0.9 for med., two-tailed t-test; **P = 0.0022 and U = 61.5 for spi., Mann-Whitney U test).

(C) Riluzole application reduced the amplitude of medullary (n = 8, **P = 0.0084 and U = 56, Mann-Whitney U test) derived bursts but to a lesser extent than the spinal cord derived bursts (n = 8, ***P = 0.00041 and U = 64, Mann-Whitney U test).

(D) Riluzole application reduced the duration of medullary derived bursts (med.; n = 8; **P = 0.0038 and t_{14} = 3.5 for med., two-tailed t-test; P = 0.0829 and U = 49 for spi., Mann-Whitney U test).

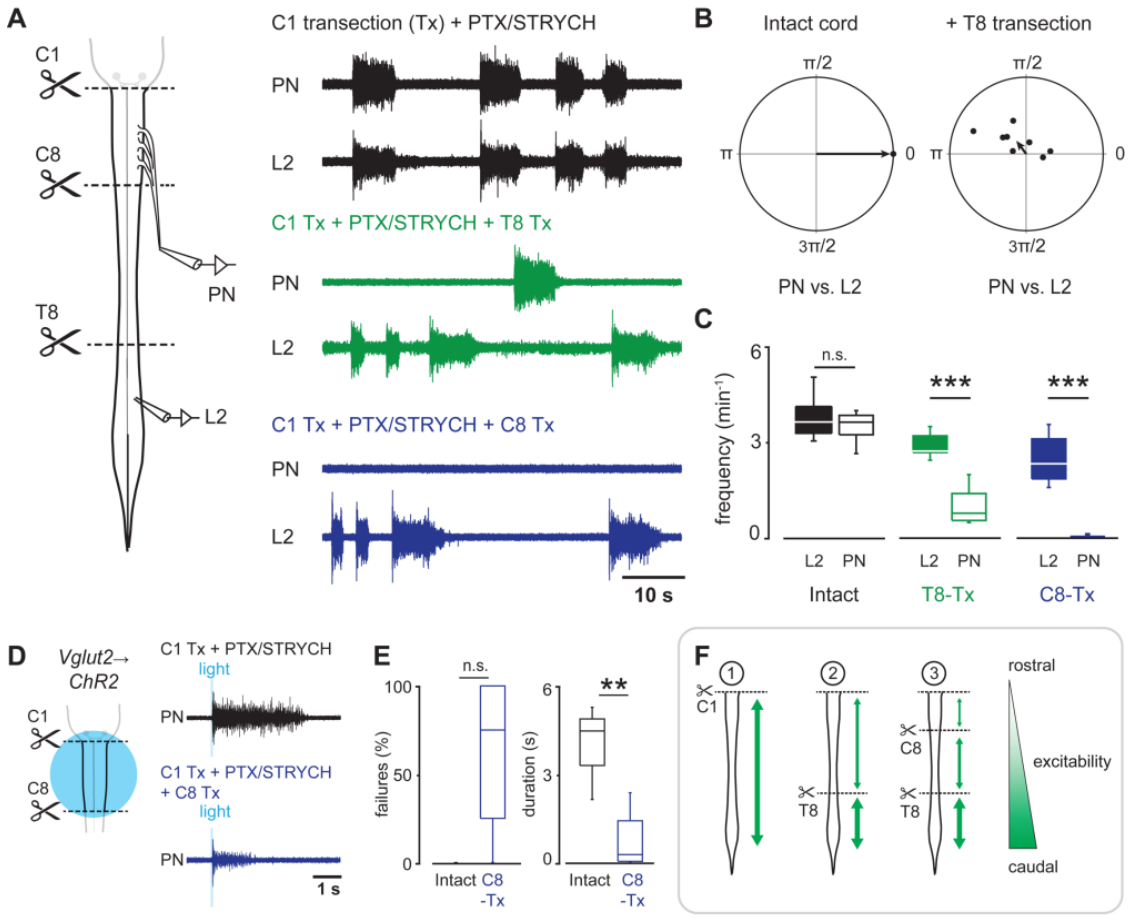

Figure 2.10: Spinal Cord Derived PMN Bursts Originate in the Thoraco-Lumbar Cord.

(A) In spinal cord preparations, blockade of fast inhibitory synaptic transmission initiated PMN bursting that was tightly coupled with L2 bursting. T8 transection disrupted PN/L2 coupling, and C8 transection eliminated PMN bursting initiated by blockade of inhibitory synaptic transmission. (B) Phase diagrams demonstrate tight PN/L2 coupling after blockade of fast inhibitory synaptic transmission. Coupling was disrupted by T8 spinal cord transection.

(C) PN burst frequency vs. L2 burst frequency. Sequential rostral spinal cord transections demonstrate that spontaneous PMN bursts originate in the thoraco-lumbar cord. PN burst frequency is significantly reduced relative to L2 after T8 transection (n = 8 mice; P = 0.0704 and t_{14} = 0.4 for intact cord, two-tailed t-test; ***P = 0.00093 and U = 64 for T8-Tx, Mann-Whitney U test), and virtually eliminated after C8 transection (n = 8 mice, ***P = 0.00055 and U = 64, Mann-Whitney U test).

(D) Although spontaneous PMN bursting is eliminated after C8 transection, small PMN bursts can still be evoked by ChR2 stimulation of Vglut2+ neurons in the cervical spinal cord.

(E) Bursts evoked by photostimulation of Vglut2+ neurons after C8 transection exhibited a higher failure rate (n = 4 mice, P = 0.067, U = 12, Mann-Whitney U test; n = 4 mice exhibited no failures when the spinal cord was intact, and n = 2 of 4 mice failed at a rate of 100% after C8 transection). *Vglut2*^{Cre}*;R26R*^{ChR2}-evoked response duration was much shorter after C8 transection compared with the intact spinal cord (n = 4 mice, **P = 0.0092, $F_{1,5.8}$ = 14.7, Welch's ANOVA).

(F) Summary of findings. In the intact disinhibited spinal cord (1), low frequency/long duration bursts propagate within the rostrocaudal extent of the cord. After T8 transection (2), long duration bursts propagate independently within the C1-T8 and T9-sacral segments. Long duration bursts are generated at a higher frequency within the T9-sacral segment. After C8 transection, spontaneous long duration bursts are largely eliminated from the cervical cord but can still be evoked by photostimulation of Vglut2+ neurons. These findings

indicate that spinal cord glutamatergic networks exhibit a gradient of excitability which is highest in the lumbar cord and lowest in the cervical cord. The rostrocaudal extent of burst propagation is indicated by green arrows, and the thickness of the green arrows represents excitability.

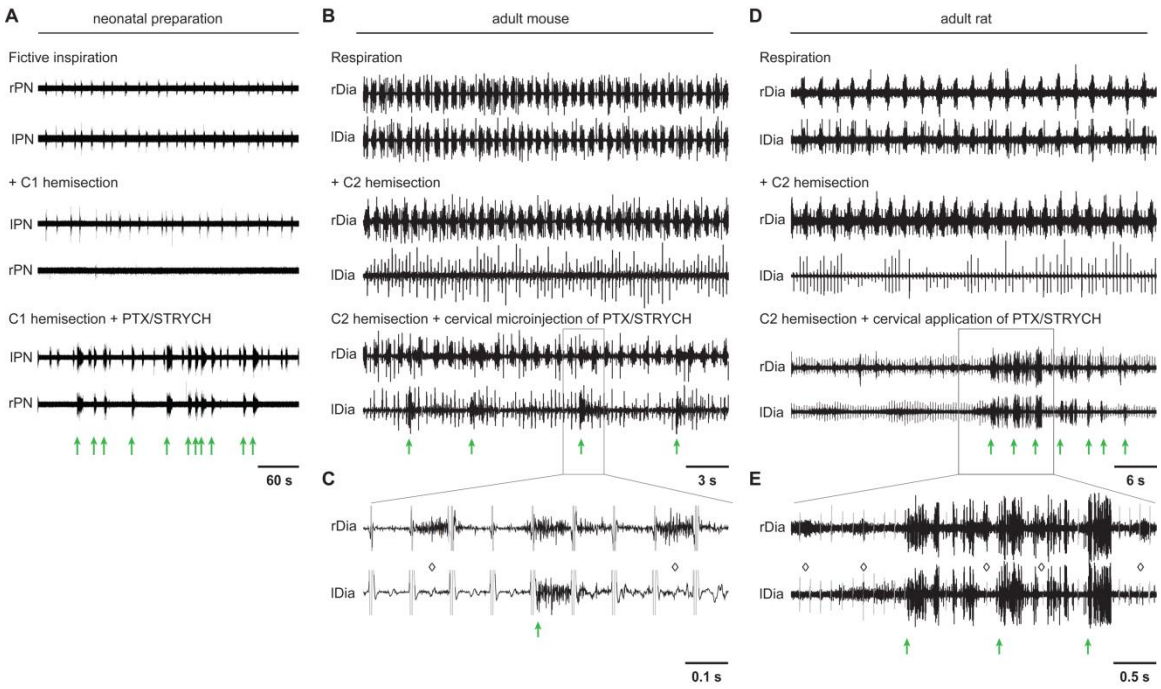

Figure 2.11: Spinal Cord Derived PMN Bursting can be Evoked After Adult Spinal Cord Injury.

(A) In the *ex vivo* preparation from neonatal mice, left C1 hemisection eliminates fictive inspiration on the side ipsilateral to lesion, and application of PTX/STRYCH initiates spinal cord derived burst activity from the dennervated phrenic motor pool (green arrows distinguish spinal cord derived bursts from bursts of medullary origin). PTX/STRYCH evoked bursting is thus dissociable from fictive inspiration (see also, Figure 2.4A).

(B) In the adult mouse, left C2 hemisection eliminates left diaphragm activity (EKG artifact is still visible). Cervical microinjection (C3-5, 3 sites, see Experimental Procedures) of PTX/STRYCH restores some PMN bursting in the paralyzed hemidiaphragm (n = 3). Green arrows indicate spinal cord derived PMN bursts.

(C) Inset from (B), EKG artifact highlighted in gray. Black portion of trace represents EMG. Diamonds indicate medullary-derived respiratory bursts which fail to initiate PMN bursting on the side ipsilateral to the lesion.

(D) In the adult rat, left C2 hemisection eliminates left diaphragm activity (EKG artifact is still visible. Intrathecal injection of PTX/STRYCH at the cervical level restored some PMN bursting in the paralyzed hemidiaphragm in 3 of 4 rats.

(E) Inset from (D), EKG artifact highlighted in gray. Diamonds indicate medullary-derived respiratory bursts which fail to initiate PMN bursting on the side ipsilateral to the lesion. In several instances, long spinal cord derived bursts were clearly spaced in between medullary derived inspiratory bursts.

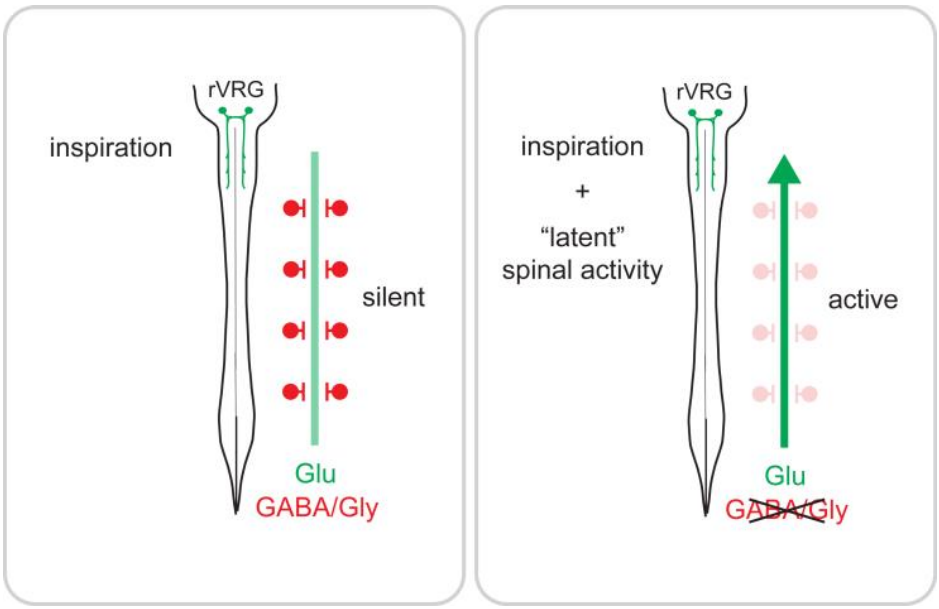

Figure 2.12: Summary of Findings.

Two independent premotor networks control PMN activity post-natally: a descending, bulbospinal inspiratory network under control of the preBötC, and a second "latent" network which exhibits spontaneous activity after suppression of GABA/glycinergic synaptic transmission.

Chapter 3: Phasic Inhibition as a Mechanism for Generation of Rapid Respiratory Rhythms

Abstract

Central neural networks operate continuously throughout life to control respiration, yet mechanisms regulating ventilatory frequency are poorly understood. Inspiration is generated by the preBötzinger complex of the ventrolateral medulla, where it is thought that excitation increases inspiratory frequency and inhibition causes apnea. To test this model, we used an *in situ* optogenetic approach to stimulate select populations of hindbrain neurons and characterize how they modulate frequency. Unexpectedly, we found that inhibition was required for increases in frequency caused by stimulation of Phox2b-lineage, putative CO_2-chemosensitive neurons. As a mechanistic explanation for inhibition-dependent increases in frequency, we found that phasic stimulation of inhibitory neurons can increase inspiratory frequency via post-inhibitory rebound. We present evidence that Phox2b-mediated increases in frequency are caused by rebound excitation following an inhibitory synaptic volley relayed by expiration. Thus, although it is widely thought that inhibition between inspiration and expiration simply prevents activity in the antagonistic phase, we instead propose a model whereby inhibitory coupling via post-inhibitory rebound excitation actually generates fast modes of inspiration.

Introduction

Mammals constantly adapt their respiratory rate to meet both homeostatic and behavioral needs (Dutschmann and Dick, 2012). Several distinct populations of hindbrain neurons modulate inspiratory frequency (Mulkey et al., 2004; Rose et al., 2009), which is ultimately defined by the preBötC, a medullary nucleus required for generation of inspiratory bursts (Cregg et al., 2017a; Jones and Dutschmann, 2016; Ramirez et al., 1998; Smith et al., 1991; Tan et al., 2008). The preBötC encompasses a heterogeneous population of neurons (Abdala et al., 2015; Morgado-Valle et al., 2010), of which a kernel of excitatory neurons gives rise to inspiratory bursts (Janczewski et al., 2013). A subset of these excitatory neurons are derived from Dbx1+ progenitors (Cui et al., 2016; Kottick and Del Negro, 2015).

The simplest model posits that inspiratory frequency (*f*, see Table 3.1 for definition of terms) is determined by a balance of excitatory and inhibitory synaptic inputs to the preBötC, where excitation increases inspiratory rate and inhibition induces apnea. This model is supported by data demonstrating that stimulation of the preBötC *in vivo* increases inspiratory rate (Alsahafi et al., 2015), selective stimulation of Dbx1+ neurons in medullary slices or *in vivo* evokes inspiratory bursting (Cui et al., 2016; Kottick and Del Negro, 2015), and stimulation of GlyT2+ inhibitory neurons in the preBötC induces apnea (Sherman et al., 2015). Thus, this “mixed input” model is widely used as a basis for understanding physiological changes in *f* (Guyenet and Bayliss, 2015; Marchenko et al., 2016).

We tested assumptions of this model in pontomedullary spinal cord preparations from neonatal mice. These preparations are especially advantageous for studying *f* because *in situ* conditions can be tightly controlled, allowing for direct comparison of *f* between experiments. Using this approach, we unexpectedly found that inhibition is required for sustaining increases in *f* caused by optogenetic stimulation of putative CO_2-chemosensitive neurons. Inhibition-dependent increases in *f* appeared to depend on a mechanism of post-inhibitory rebound following expiration. Thus, although it is widely thought that excitatory neurons generate inspiratory rhythm and inhibitory neurons only coordinate opposing activity between inspiration/expiration, these data instead lead us to propose a model in which fast inspiratory rhythms can be generated as a result of reciprocal inhibition.

Results

Excitation Increases Inspiratory Frequency

Inspiration can be assayed in neonatal hindbrain-spinal cord preparations by recording from the phrenic nerve (Figure 3.1A), which solely innervates the diaphragm. Although preparations retaining the pons do not exhibit spontaneous inspiration, fictive inspiration can be initiated by cutting off the pons at the level of cranial nerve VI (Figure 3.1A). Suppression of inspiratory bursting in pontomedullary preparations is thought to be caused by pontine inhibition of the preBötC (Hilaire et al., 1997). We found that blocking inhibition by bath application of PTX/STRYCH (i.e. disinhibition) completely accounted for

increases in *f* observed upon removal of the pons (Figure 3.1A,B). Importantly, complete inhibitory blockade does not alter sensitivity to opioids (Cregg et al., 2017a; Gray et al., 1999), indicating that the fundamental mode of preBötC-generated inspiratory bursts is not changed by application of PTX/STRYCH. From these results we conclude that inhibition suppresses *f*, and disinhibition (i.e. PTX/STRYCH application) can return *f* to a baseline frequency of 4-7 min^{-1} (Figure 3.1B, see Table 3.2 for a summary of results).

We next asked whether optogenetic stimulation of large groups of hindbrain glutamatergic neurons would be sufficient to increase *f*. In $Vglut2^{Cre}$;$R26R^{ChR2}$ preparations (where Vglut2+ neurons express ChR2-EYFP), photostimulation of Vglut2+ neurons after bath application of PTX/STRYCH led to a dramatic increase in *f* (Figure 3.1C,D). Even though photostimulation was continuous, phrenic motor neurons exhibited discrete bursting with almost no unit activity during interburst intervals (Figure 3.1C), indicating that PMN burst activity in response to photostimulation is generated by an excitatory rhythmogenic substrate rather than downstream premotor nuclei or motor neurons themselves (Cregg et al., 2017a). Importantly, the effective population of Vglut2+ neurons stimulated was large, encompassing disparate populations of ventrally-positioned excitatory neurons likely interacting with glutamatergic preBötC neurons via mono- or oligo-synaptic connections (Figure 3.2A; Figure 3.2 also contains anatomical characterization of each Cre allele used herein). Thus, after application of PTX/STRYCH, continuous photostimulation of excitatory preBötC

neurons and/or upstream excitatory populations causes rhythmic inspiratory bursting at high frequencies.

What mechanisms suppress burst initiation during interburst intervals? Photostimulation was maintained continuously, yet preBötC circuits were resistant to initiating a subsequent burst; *Vglut2*^{Cre};*R26R*^{ChR2} preparations treated with PTX/STRYCH exhibited a minimum interburst interval (IBI_{min}) of 2.42 ± 0.33 s (+ pons) and 1.69 ± 0.24 s (- pons, Figure 3.1C). Recently, Kottick and Del Negro identified a post-burst refractory period during which stimulation of excitatory Dbx1+ preBötC neurons could not initiate a subsequent inspiratory burst (Kottick and Del Negro, 2015). Presumably this refractory period is defined by time constants of activity-dependent outward currents (e.g. I_{pump}, $I_{Na\text{-}K}$, $I_{K\text{-}ATP}$) and/or biophysical constraints associated with synaptic dynamics (Guerrier et al., 2015; Kottick and Del Negro, 2015; Rubin et al., 2009). Importantly, this refractory period imposes a boundary condition that defines maximum inspiratory frequency; f_{max} is the inverse of IBI_{min}. We found that f_{max} under conditions of excitation/disinhibition was 24.8 min^{-1} in pontomedullary preparations and 35.5 min^{-1} in medullary preparations, comparable values to that of preBötC slices (9). Together, these data are consistent with a model in which inhibition decreases *f* (Figure 3.1F), disinhibition (i.e. PTX/STRYCH application) relieves inhibition and returns *f* to baseline frequency (Figure 3.1G), and excitation increases *f* (Figure 3.1H).

Inhibition is Implicated in Phox2b and Atoh1 Modulation of Frequency

To validate this model (Figure 3.1E-H), we sought to stimulate select subsets of excitatory hindbrain neurons and characterize how they modulate *f*. Our results from Figure 3.1 indicate that PTX/STRYCH application can discriminate between different modes of f modulation: *inhibition* is a decrease in *f* that is PTX/STRYCH sensitive, *disinhibition* is masked by application of PTX/STRYCH (i.e. blockade of inhibition is disinhibitory), and *excitation* is an increase in *f* that is PTX/STRYCH insensitive (see Table 3.2).

We first stimulated excitatory Phox2b-lineage neurons (Figure 3.3A), a contingent of which increase *f* as part of the central chemoreceptive response to elevated CO_2 (Abbott et al., 2009; Amiel et al., 2003; Dubreuil et al., 2008). The mechanism underlying Phox2b-mediated increases in *f* is not well understood, but is thought to result from excitation/disinhibition of the preBötC (Guyenet and Bayliss, 2015). Photostimulation of excitatory Phox2b-lineage neurons resulted in a dramatic increase in *f* (Figure 3.3A,D). Surprisingly, we found that PTX/STRYCH application completely abolished Phox2b-mediated increases in *f* (Figure 3.3B,D). It is likely that broad Phox2b-lineage photostimulation preferably engaged Phox2b+ CO_2 chemosensitive neurons because the inspiratory response to hypercapnia was also sensitive to PTX/STRYCH (Figure 3.4A,B). Importantly, PTX/STRYCH application did not cause the network to enter a state in which it could no longer be excited because stimulation of Vglut2+ neurons under these conditions still caused a robust inspiratory response (Figure 3.1C). These results indicate that *excitation* does not explain Phox2b-mediated increases in *f*.

The inspiratory response to stimulation of Phox2b-lineage neurons (Figure 3.3A) exhibited several unique properties compared with *excitation* caused by photostimulation of Vglut2+ neurons (Figure 3.1C). First, stimulation of Phox2b-lineage neurons evoked an f_{max} of a remarkable 68.6 min^{-1}. This f_{max} was much faster than that observed during global excitation of Vglut2+ neurons in the absence of inhibition (Figure 3.5A), suggesting that inhibition is critical for very fast modes of inspiration. Second, whereas *excitation* resulted in amplitude depression upon subsequent bursts (Figures 3.1C and 3.5B), *Phox2b*^{Cre};*R26R*^{ChR2} mediated increases in *f* did not (Figures 3.3A and 3.5B), suggesting that inhibitory neurons are also involved in sustaining burst amplitude at high frequencies. Finally, whereas *excitation* directly evoked inspiratory bursting within 50-150 ms of the photostimulus (Figure 3.5C), stimulation of Phox2b-lineage neurons initiated inspiration at a considerable delay (367 ± 30 ms; Figure 3.5C). Consistent with previous data (Holloway et al., 2015), we found that *Phox2b*^{Cre};*R26R*^{ChR2} mediated increases in *f* were independent of catecholamines (Figure 3.5D). Phox2b-mediated increases in *f* also required an intact pons (Figure 3.5E), suggesting that known ascending Phox2b-lineage axonal projections to the pontine Kölliker-Fuse nucleus may be important (Bochorishvili et al., 2012; Guyenet and Bayliss, 2015). Although the mechanism underlying Phox2b-mediated increases in *f* is not yet clear, these data indicate that inhibitory neurons are actively involved.

To further investigate our working model of *f* control (Figure 3.1E-H), we examined whether stimulation of excitatory Atoh1-lineage neurons would

modulate *f*. Atoh1-lineage neurons are required for proper respiratory function; *Atoh1*$^{-/-}$ mice die at birth due to respiratory failure (Huang et al., 2012; Maricich et al., 2009; Rose et al., 2009; Ruffault et al., 2015; Tupal et al., 2014). We stimulated hindbrain Atoh1-lineage neurons in the absence of spontaneous motor output (+ pons). Interestingly, this stimulation paradigm resulted in a transient increase in *f* only upon termination of the photostimulus (Figure 3.3E; $t_{1/2}$ ~18 s). Because this Atoh1 response was out of phase with the photostimulus (Figure 3.3E), we reasoned that inhibitory neurons were again likely to be involved. Consistent with this hypothesis, Atoh1-mediated increases in *f* were blocked by bath application of PTX/STRYCH (Figure 3.3F). We sought to determine whether stimulation of Atoh1-lineage neurons would suppress fictive inspiration; however, we found that Atoh1-mediated changes in *f* also required an intact pons (Figure 3.6A). Therefore, we examined whether stimulation of Atoh1-lineage neurons would suppress substance P initiated inspiratory bursting in preparations retaining the pons (Figure 3.6B). Substance P facilitates inspiratory bursting by neurokinin-1 receptor-dependent activation of Nalcn, a sodium leak channel (Yeh et al., 2017). Indeed, we found that photostimulation of Atoh1-lineage neurons suppressed substance P initiated inspiration (Figure 3.6B), demonstrating that excitatory Atoh1-lineage neurons engage the preBötC through inhibition (Figure 3.1F). Importantly, these results indicate that inhibitory neurons contribute to circuit dynamics that can promote initiation of inspiratory bursts.

Phasic Inhibition Increases Inspiratory Frequency

We directly investigated inhibitory mechanisms which contribute to increases in *f*. In *Vgat*^{Cre};*R26R*^{ChR2} medullary preparations (- pons), we found that continuous photostimulation of GABA/glycinergic neurons immediately induced apnea (Figure 3.7A). Indeed, prolonged photostimulation of medullary Vgat+ neurons almost completely arrested inspiration for the duration of the stimulus (120 s; Figure 3.7A). We observed a transient increase in *f* upon termination of the photostimulus (Figure 3.7A; $t_{1/2}$ ~4s). This increase in *f* is reminiscent of "reset" observed in response to stimulation of preBötC GlyT2+ neurons in awake mice, where inspiration resumes with consistent latency after photostimulation (Sherman et al., 2015).

To examine the nature of this mechanism, we reasoned that stimulation of inhibitory neurons in a silent preparation (+ pons) would differentiate between "reset" and "rebound". This is an important distinction to make because "reset" implies that inhibitory neurons simply dictate when the preBötC cannot initiate a burst, whereas "rebound" indicates that inhibition actually drives preBötC bursting. In pontomedullary preparations, we found that a 60 s stimulus resulted in a pronounced rebound response (Figure 3.7B; $t_{1/2}$ ~23 s). Furthermore, *phasic inhibition* induced sustained increases in *f* (Figure 3.7C), indicating that inhibition does not simply pattern the activity of an ongoing rhythm, but can drive inspiration at a high frequency. Rebound inspiratory bursts were observed from both phrenic and hypoglossal motor neurons (Figure 3.7D), which are controlled by different pre-motor nuclei. This data indicates that rebound bursts arise at the

level of the preBötC rather than downstream premotor nuclei or at the level of motor neurons themselves. The probability of observing a rebound inspiratory burst was directly proportional to the photostimulus duration (Figure 3.7E), indicating that the characteristics of an inhibitory synaptic volley predict the post-synaptic inspiratory response. Finally, rebound inspiratory bursts were blocked by application of PTX/STRYCH (Figure 3.7F). We conclude that, in addition to excitation (Figure 3.1H), *phasic inhibition* is a mechanism that increases *f* (Figure 3.7G).

Phox2b-Lineage Neurons Initiate Expiration

Our results indicate that neither excitation nor disinhibition can account for Phox2b-mediated increases in *f* (Figure 3.3B,D), therefore, we examined whether Phox2b-lineage neurons might increase *f* through *phasic inhibition*. Although Phox2b+, CO_2 chemosensitive neurons do not exhibit phasic activity themselves (Mulkey et al., 2004), they are situated within the parafacial (pF) nucleus close to a group of excitatory neurons which exhibits phasic oscillatory activity associated with expiration (known as the pF oscillator) (Huckstepp et al., 2016, 2015; Pagliardini et al., 2011; Thoby-Brisson et al., 2009). Though mechanisms of inspiratory/expiratory coupling are not well understood (Huckstepp et al., 2016), it is widely thought that inhibition is responsible for anti-phasic inspiratory/expiratory patterning because purely excitatory networks usually exhibit synchrony (Anderson et al., 2016; Cregg et al., 2017a; Talpalar et

al., 2011). Thus, in the context Phox2b-lineage photostimulation, expiration might actually initiate inspiration through *phasic inhibition*.

Whereas neonatal preparations do not normally exhibit active expiration (Figure 3.9A), we found—strikingly—that stimulation of Phox2b-lineage neurons evoked alternating expiratory/inspiratory activity (Figure 3.8A). Indeed, photostimulation of Phox2b-lineage neurons immediately evoked expiratory bursting from the L1 ventral root (Figure 3.8A,B; L1 latency = 113 ± 11 ms), which was only then followed by an inspiratory response (Figure 3.8A,B; PN latency = 389 ± 20 ms). The latency of expiration was consistent with a direct excitatory response (Figure 3.8B; compare with PN excitation, Figure 3.5C). Furthermore, we found that 50 ms Phox2b-lineage photostimulation was sufficient to cause an inspiratory burst several hundreds of milliseconds later (Figure 3.8D), a response which was blocked by application of PTX/STRYCH (Figure 3.8D, see also Figure 3.3B).

In n = 4 of 10 preparations in which we obtained particularly clear signal from the L1 ventral root, we observed full triphasic rhythms consisting of expiratory, inspiratory, and post-inspiratory bursting (Figure 3.8E). These data indicate that Phox2b-mediated increases in f do not represent sniffing behavior, which consists solely of inspiratory/post-inspiratory bursting (an elimination of the expiratory phase) (Lawson et al., 1991; Pérez de Los Cobos Pallares et al., 2016). Moreover, because pontomedullary preparations do not exhibit any spontaneous activity from the PN or L1 ventral root (see Figure 3.8A,E before photostimulus), these data indicate that stimulation of Phox2b-lineage neurons

evokes all 3 phases of respiration—expiration, inspiration, and post-inspiration (Figure 3.8E), suggesting a mode of unitary oscillation (Figure 3.8F*,* Mode 2).

We used high-speed video to further examine how the inspiratory rhythms we observed control the muscular apparatus. During fictive inspiration (- pons) we observed upward (inspiratory) ribcage movements (Figure 3.9A). We found that after initial upward deflection, the ribcage returned downward to its original position long after the termination of phrenic inspiratory bursts (Figure 3.9A), suggesting that expiration in these conditions is passive. In stark contrast, photostimulation of Phox2b-lineage neurons initially caused *downward* (expiratory) ribcage movements which were quickly succeeded by upward deflection of the ribcage (Figure 3.9B). The ribcage then returned to its original position upon termination of phrenic inspiratory bursts (Figure 3.9B).

Discussion

This study demonstrates that inhibition is critical for certain physiologic modes of increased inspiratory frequency. The mechanism of inhibition-dependent increases in *f* is independent of previously proposed models which depend on *disinhibition* (Marchenko et al., 2016); we found that *disinhibition* is not a mechanism which increases *f* above baseline frequency. Instead, the mechanism of inhibition-dependent increases in *f* appears to involve post-inhibitory rebound excitation. Photostimulation of Phox2b-lineage, putative CO_2 chemosensitive neurons evoked alternating expiratory/inspiratory activity, and resultant increases in inspiratory frequency were completely abolished by application of

PTX/STRYCH. These data lead us to propose a model in which rhythmic inspiratory bursting can be generated by the medulla in two functionally distinct modes: Excitatory circuits alone are sufficient for generation of rhythm—but a second mode of rhythm generation involving reciprocal inhibition between inspiration/expiration/post-inspiration acts in parallel to achieve homeostatic and behavioral needs.

An Inhibitory Mechanism of Rhythm Generation

How do inhibitory neurons contribute to generation of inspiratory rhythms? In the simplest model, two inhibitory neurons with reciprocal connectivity exhibit antiphasic patterning, that is, one neuron fires while the other is inhibited. Adding rebound kinetics to this system causes the output of each neuron to become rhythmic (Perkel and Mulloney, 1974; Skinner et al., 1994). In this reduced form, rhythm generation (rhythmic output of each neuron) and pattern formation (antiphasic output of each neuron) are one and the same. We propose that this type of rhythm generation is responsible for *Phox2b*^{Cre};*R26R*^{ChR2} mediated increases in f_R. Thus, under certain circumstances, respiratory rhythm generation and pattern formation may be network features that are inherently yoked. A similar type of rhythm generation has been extensively characterized in left/right swimming in the *Xenopus* tadpole (Li and Moult, 2012; Moult et al., 2013).

Modularity in Respiratory Control

During eupnea, inspiratory and expiratory burst frequency can be manipulated independently with μ-opioid receptor directed perturbations (Janczewski and Feldman, 2006). This data suggests that the respiratory system is modular, such that one phase does not drive a subsequent phase (e.g., expiration does not cause inspiration). Modular design could allow for considerable behavioral flexibility in vocalization, sigh, etc. In this case, reciprocal inhibitory coupling would simply restrict the initiation of a burst in an antagonistic phase (Figure 3.8*F*, Mode 1).

It was recently proposed, however, that in some situations expiration might actually excite inspiration, and *vice versa* (Huckstepp et al., 2016). Our data suggest that there is indeed a "switch", such that under certain circumstances expiration actually initiates inspiration through *phasic inhibition*. This type of inhibitory coupling between inspiration/expiration is fundamentally different from antagonistic motor patterning observed during eupnea (Janczewski and Feldman, 2006). Presumably, if an inhibitory synaptic volley relayed by expiration initiates inspiration, then the shape of the (present) inspiratory burst will be defined, in part, by characteristics of that (previous) inhibitory synaptic volley. This type of rhythm is deterministic, implying that rapid respiratory rates exhibit stereotyped motor patterns (Figure 3.8*F*, Mode 2). The concept of deterministic rhythms might help to explain long-lasting effects on *f* after a given stimulus. For example, we found that increases in *f* following a long inhibitory photostimulus persisted for several seconds (half-life of $t_{1/2}$ ~23 s). In another

example, photostimulation of Phox2b+ neurons in adult rats caused long-lasting ($t_{1/2}$ ~11 s) effects on *f in vivo* (Abbott et al., 2009).

Although it is unclear what underlies a “switch” between modes, the strength of inhibitory synaptic coupling is likely to contribute. In *Xenopus* tadpoles, a right/left swimming rhythm is thought to depend on post-inhibitory rebound during reciprocal inhibition between sides (Moult et al., 2013). Here, the strength of inhibition (defined by the amplitude of IPSPs in dINs) dictated the probability of observing a rebound burst (Moult et al., 2013). We also found evidence that the “strength” of an inhibitory stimulus (defined by photostimulus duration) dictates the probability of observing a rebound inspiratory burst. Importantly, rebound bursts are, by definition, increases in *f* in comparison with inhibitory synaptic volleys that do not evoke rebound. This suggests that inspiratory rhythms driven by post-inhibitory rebound (Mode 2) operate at a higher frequency. Indeed, in *Xenopus* tadpoles, weakening phasic inhibition without changing background excitation slows down left/right swimming rhythms (Li and Moult, 2012). Thus it is possible that there are frequency-dependent modes of inspiratory rhythm generation (i.e. Mode 1 – low frequency, Mode 2 – high frequency); however, the range of frequencies over which each mode operates is entirely unclear—these ranges may exhibit extensive overlap. Interestingly, we found evidence that Mode 1 and Mode 2 do segregate at least at very high frequencies: Phox2b-lineage photostimulation evoked inspiratory frequencies which far exceeded those which could be evoked by stimulation of Vglut2+ neurons after inhibitory blockade.

Mechanism of Rebound Excitation

What mechanism governs post-inhibitory rebound excitation? One possibility is that rebound excitation is mediated by hyperpolarization activated cation current (I_h) carried by HCN channels (Thoby-Brisson et al., 2000). In preBötC slices, application of Cs^{2+} or ZD7288 blocks only a portion of I_h observed in inspiratory preBötC neurons (Thoby-Brisson et al., 2000), suggesting that HCN-independent mechanisms also contribute. Inward current from T- and L-type calcium channels is known to activate upon hyperpolarization in certain contexts (Engbers et al., 2011; Wang et al., 2011). Rebound bursts might also be independent of hyperpolarization activated inward currents altogether: In one example, Purkinje cells of the cerebellar cortex can synchronize fast-spiking target neurons in the deep cerebellar nuclei via inhibition (Person and Raman, 2011). It is possible that an inhibitory synaptic volley relayed by expiration could synchronize subthreshold activity within the preBötC in a similar manner. Although neurons of the preBötC do not exhibit a high intrinsic firing rate, synchronization of just a few neurons is thought to be sufficient to evoke a population-wide burst (Kam et al., 2013). Understanding rebound mechanisms will likely be difficult without better identification of the underlying anatomical substrate(s) involved. Importantly, our results do not shed light on the anatomical location of inhibitory neurons involved in the responses generated by stimulation of Phox2b-lineage, Atoh1-lineage, and Vgat+ neurons—which may ultimately exert their effects on the preBötC through any number of different relay

configurations which we simplify as *inhibition*, *disinhibition*, *excitation*, or *phasic inhibition* (Table 3.2).

Acknowledgments

Kevin A. Chu, Thomas E. Dick, Lynn T. Landmesser, and Jerry Silver contributed as co-authors to Chapter 3. We thank JingQiang You for technical assistance. This work was supported by National Science Foundation Grant DGE-0951783 (to J.M.C.), NIH Grant U01EB21960 (to T.E.D.), NIH Grant NS074199 (to L.T.L.), and NIH Grant NS025713 (to J.S.).

Methods

Animals

All animal procedures were approved by the Case Western Reserve University Institutional Animal Care and Use Committee (IACUC). The following mice were obtained from Jackson Laboratories: *Vglut2*^{Cre} (stock #016963), *Phox2b*^{Cre} (#016223), *Atoh1*^{Cre} (#011104), *Vgat*^{Cre} (#016962), *R26R*$^{ChR2\text{-}EYFP}$ (#012569), *R26R*^{LacZ} (#012429), and *Tau*$^{lsl\text{-}LacZ}$ (#021162). Mice were maintained on a mixed background. *Vglut2*^{Cre}, *Phox2b*^{Cre}, *Atoh1*^{Cre}, or *Vgat*^{Cre} mice were crossed to *R26R*$^{ChR2\text{-}EYFP}$, *R26R*^{LacZ}, or *Tau*$^{lsl\text{-}LacZ}$ reporter mice, and heterozygous alleles were used for experiments. Animals were assigned to groups based on genotype, and experiments were performed with prior knowledge of genotype. Wild type C57BL/6J mice (stock #000664) were used in experiments which did not require genetic perturbations. We used P2-4 male and female mice for all experiments herein.

Dissection

Mice were anesthetized, decapitated at the level of the midbrain, and eviscerated. Rapid dissection was carried out in room temperature oxygenated Ringers solution (23-26 °C, 95% O_2/5% CO_2, pH = 7.4), composed of 128 mM NaCl, 4 mM KCl, 21 mM $NaHCO_3$, 0.5 mM NaH_2PO_4, 2 mM $CaCl_2$, 1 mM $MgCl_2$, and 30 mM D-glucose. The central nervous system was exposed ventrally, and phrenic nerves were dissected free from connective tissue. In a subset of

experiments, fictive inspiration was initiated by transection at the pontomedullary boundary just rostral to the anterior inferior cerebellar artery (see Fig. S1*E*,*F*). Additionally, in experiments utilizing PTX/STRYCH, we sectioned caudally at C8 (Cregg et al., 2017a).

Electrophysiology and Photostimulation

Recording was carried out under continuous perfusion of control aCSF (same composition as above) or 80% O_2/20% CO_2-equilibrated aCSF to simulate respiratory acidosis. Suction electrodes were attached to the phrenic nerve, hypoglossal nerve, and/or the L1 ventral root. Signal was filtered from 30 Hz to 1 kHz using Grass amplifiers, amplified 10,000x, and sampled using a Digidata 1440A (Molecular Devices) at a rate of 50 kHz. A Polychrome V halogen lamp was used for photostimulation, and blue light was directed at the hindbrain using a fiberoptic light guide (wavelength 473 nm, 15 nm bandwidth, Till Photonics). The spatial extent of light illumination for each experiment is represented in accompanying illustrations. Light intensity was measured with a photodiode (Cat# S120C, Thorlabs) coupled to a power meter (Cat# PM100D, Thorlabs). The light intensity used herein was ~0.20 mW/mm^2. This low level of continuous blue light maintained responses throughout the duration of the photostimulus (Figures 3.1, 3.3, 3.7, 3.8; see also Cregg et al., 2017), indicating that continuous photostimulation did not cause conduction block or tissue damage. We did not observe any electrophysiological response to photostimulation in monoallelic Cre- or *R26R*$^{ChR2\text{-}EYFP}$ strains, which indicates that Cre-mediated recombination

of the *Rosa26* locus is required for ChR2-EYFP expression and that photostimulation does not cause ChR2-independent effects. We used the following drugs: picrotoxin (PTX, $GABA_AR$ antagonist, 10 μM, Sigma), strychnine hydrochloride (STRYCH, GlyR antagonist, 0.3 μM, Sigma), prazosin hydrochloride (PRAZ, α_1-AR antagonist, 25 μM, Sigma), propranolol (PROP, β-AR antagonist, 25 μM, Sigma), and substance P acetate salt hydrate (substance P, neurokinin 1 receptor agonist, 1 μM, Sigma).

Analysis

Data was recorded using AxoScope software (Molecular Devices) and analyzed in Spike2 (Cambridge Electronic Design). Signal was processed to remove DC drift, and integrated traces are presented as rectified and smoothed (0.1-0.2 s) electroneurographs. For individual traces, we quantified burst event time and duration with respect to light onset. Raster plots were constructed in R (R Project). Individual trials were aligned by light onset, and individual bursts are represented by black rectangles. Gray boxes group together technical replicates from a single biological replicate. Instantaneous frequency (*f*) was calculated continuously every 0.1 s over 24 trials (bin = 5 s). Half-life ($t_{1/2}$) of rebound effects were estimated by exponential regression fitting of *f*. Rebound bursts were defined as those occurring within 3 s of an inhibitory stimulus. Based on data from pontomedullary preparations (Fig. 1*A*,*B*), we estimate the false-positive rate to be <0.2% for aCSF, and 30-35% after application of PTX/STRYCH. Phase relationships between PN and L1 were determined using circular plot analysis

(Kjaerulff and Kiehn, 1996), where each point represents the average vector magnitude/direction for a single biological replicate and the arrow represents the group-averaged magnitude/direction (0 is synchronous and π is asynchronous, 1 cycle = 2π rad = 360°).

Statistics

Statistical analysis was performed in JMP version 11 (SAS). Power analysis was used to determine minimum sample size. We used Shapiro-Wilk to test for normality. For data which did not exhibit a normal distribution, we used a Mann-Whitney U test followed by Bonferroni correction for multiple comparisons. For data exhibiting a normal distribution, we used Brown-Forsythe to test for equivalent variance. For cases of equivalent variance, a t-test was used for single comparisons, and a one-way ANOVA followed by Tukey-Kramer HSD *post hoc* was used for multiple comparisons. A Welch ANOVA was used in cases of unequal variance, followed by Bonferroni correction for multiple comparisons. $P < 0.05$ was considered to be statistically significant, where $*P < 0.05$, $**P < 0.01$, $***P < 0.001$. Data is presented as mean ± standard error mean, $n = 8$ biological replicates for each group unless stated otherwise. In box and whisker plots, whiskers represent the range excluding outliers.

X-Gal Staining and Imaging

Post-dissection, tissue was fixed for 30 minutes in 4% paraformaldehyde and subsequently washed in PBS. On a subset of samples ($n = 8$ per genotype)

we performed whole mount x-gal staining for 2 hours at 37 ^{o}C, which allowed x-gal substrate to react with LacZ-expressing cells positioned within 152 ± 13 µm (*n* = 3) of the tissue surface. The remaining samples (*n* = 8 per genotype) were sectioned at 20 µm with a cryostat, and x-gal stained overnight at 37 °C. We captured brightfield wholemount images using a stereomicroscope (Zeiss). Sections were imaged using a Leitz Orthoplan 2 upright brightfield microscope.

High-Speed Video

A Retiga EXi camera (QImaging) attached to a Navitar Zoom 7000 lens was used to capture high speed video of ribcage movements (10-50 frames per second, f.p.s.). Images were acquired using QCapture Pro 6 (QImaging) and Micromanager 1.4 (Micromanager) software. Ribcage movements were quantified in ImageJ, using the outermost point of a single rib for x-y measurements.

Table 3.1: Definition of Terms Related to Chapter 3.

Term	Variable	Units	Definition
Inspiratory Frequency	f	min^{-1}	instantaneous phrenic burst frequency measured relative to light onset and across trials, bin = 5 s
Average Inspiratory Frequency	$\bar{f}$	min^{-1}	average phrenic burst frequency over a given time interval
Change in Average Inspiratory Frequency	$\Delta\bar{f}$	min^{-1}	change in average frequency relative to a pre-stimulus baseline normalized to 0
Minimum Interburst Interval	IBI_{min}	s	time between the first two bursts observed in response to photostimulation
Maximum Inspiratory Frequency	f_{max}	min^{-1}	inverse of IBI_{min}
Latency		ms	time between onset of photostimulation and unit/burst response in raw trace

Table 3.2. Summary of Results Related to Chapter 3.

Genotype / Treatment	**+/- Pons**	$\bar{f}$ **(min^{-1})**	↑ or ↓ relative to baseline	**PTX/ STRYCH sensitive**	**Interpretation**
WT	-	4.94 ± 0.30	baseline	No	Baseline
WT	+	0.08 ± 0.05	↓	Yes	Inhibition
Vglut2^{Cre};R26R^{ChR2}	+	14.29 ± 0.76	↑	No	Excitation
Vglut2^{Cre};R26R^{ChR2}	-	13.25 ± 0.63	↑	No	Excitation
Phox2b^{Cre};R26R^{ChR2}	+	16.13 ± 1.45	↑	Yes	Phasic Inhibition
WT + CO_2	+	11.78 ± 0.77	↑	Yes	Phasic Inhibition
Atoh1^{Cre};R26R^{ChR2} + Substance P	+	1.10 ± 0.82	↓	Yes	Inhibition
Vgat^{Cre};R26R^{ChR2} continuous light	-	0.31 ± 0.15	↓	Yes	Inhibition
Vgat^{Cre};R26R^{ChR2} pulsed light	+	9.54 ± 0.17	↑	Yes	Phasic Inhibition

Inhibition is a decrease in *f* which is PTX/STRYCH sensitive. *Disinhibition* (i.e. PTX/STRYCH application) only relieves inhibition, returning *f* to baseline; disinhibition cannot increase *f* above baseline. *Excitation* is an increase in *f* which is insensitive to application of PTX/STRYCH. *Phasic Inhibition* is an increase in f which is PTX/STRYCH sensitive. Data are mean ± s.e.m.

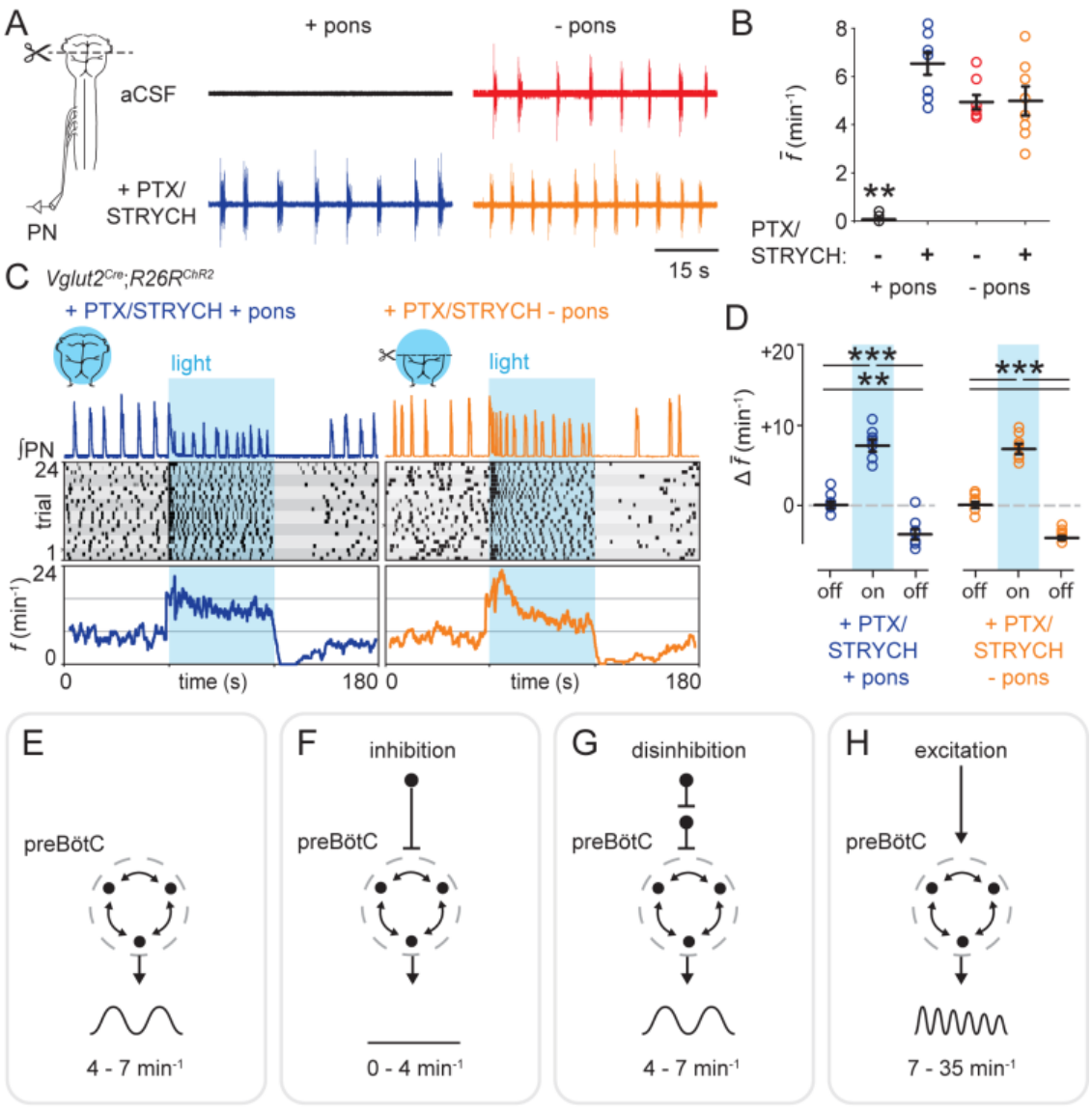

Figure 3.1: Excitation Increases Inspiratory Frequency.

(A) *Top left*, pontomedullary preparations do not exhibit spontaneous inspiration. *Top right*, transection at the pontomedullary boundary initiates fictive inspiration. *Bottom left*, PTX/STRYCH application to pontomedullary preparations also initiates fictive inspiration. *Bottom right*, fictive inspiration initiated via transection at the pontomedullary boundary is not affected by application of PTX/STRYCH.

(B) Quantification of average *f*. ***P* < 0.01 aCSF + pons vs. all other conditions.

(C) *Top*, after application of PTX/STRYCH, stimulation of excitatory neurons resulted in high frequency inspiratory bursting (f_{max} + pons = 24.8 min^{-1}; f_{max} - pons = 35.5 min^{-1}). *Middle*, raster plots were constructed from 8 biological replicates (highlighted by gray boxes), with 3 technical replicates each. *Bottom*, *f* averaged over 24 trials relative to light onset.

(D) Change in average *f* during and after light stimulation relative to baseline (off). PTX/STRYCH + pons: Baseline vs. photostimulation, ****P* = $1.3x10^{-5}$. Photostimulation vs. after, ****P* = $1.0x10^{-7}$. Baseline vs. after, ***P* = 0.0012. PTX/STRYCH - pons: Baseline vs. photostimulation, ****P* = $3.2x10^{-6}$. Photostimulation vs. after, ****P* = $1.5x10^{-7}$. Before vs. after, ****P* = $2.1x10^{-6}$. Welch's ANOVA with Bonferroni correction. *n* = 8 for each condition. Data are mean ± s.e.m.

(E-H) *Top* and *Middle*, illustration of tested hypothesis and preBötC. *Bottom*, summary of finding.

(E) Baseline *f*.

(F) Inhibition decreases *f* (see panels A,B).

(G) Disinhibition can return *f* to baseline frequency, but does not increase *f* above baseline (see panels A,B).

(H) Excitation increases f (see panels C,D).

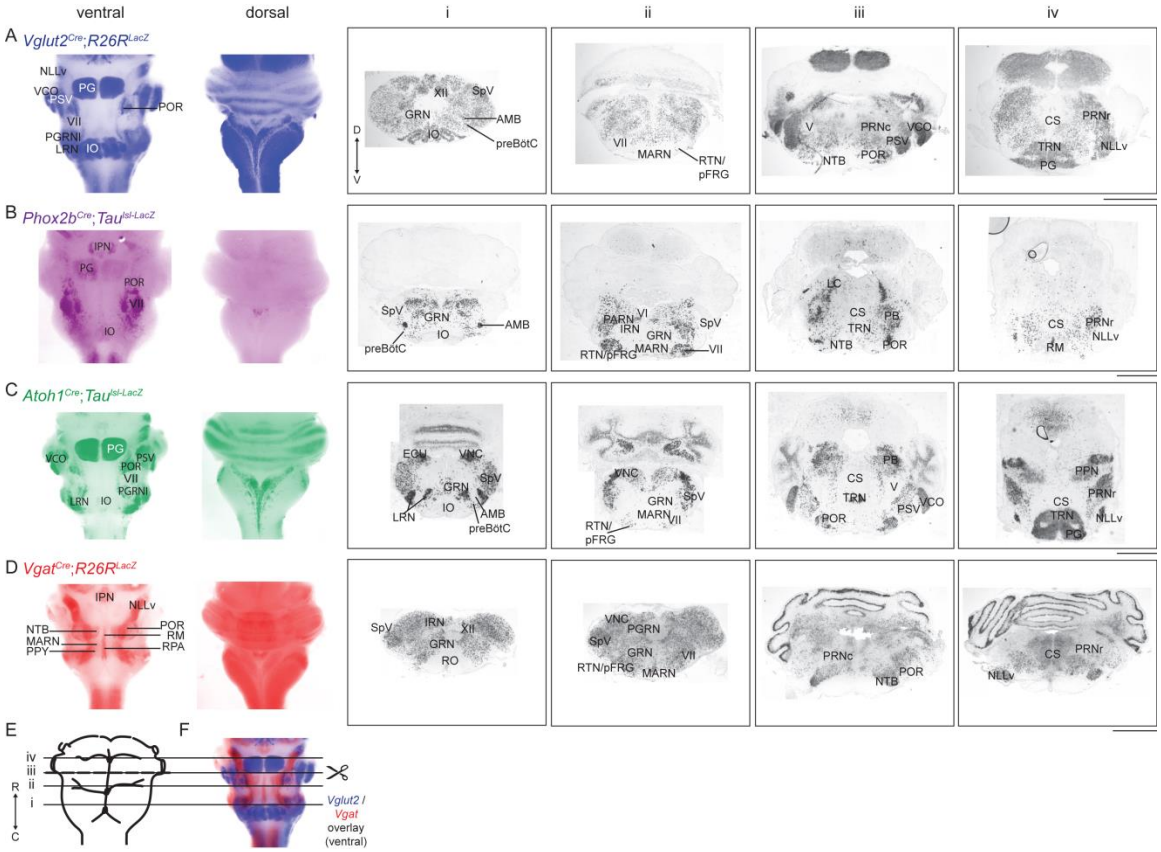

Figure 3.2: Characterization of Cre-Recombinase Alleles.

(A) X-gal staining for LacZ expression in *Vglut2*^{Cre}*;R26R*^{LacZ} mice. *Left*, wholemount staining. Hindbrain pseudocolored blue. *Right*, selected sections from four coronal planes (see schematic at bottom).

(B-D) X-gal staining for LacZ expression in *Phox2b*^{Cre}*;Tau*$^{lsl\text{-}LacZ}$, *Atoh1*^{Cre}*;Tau*$^{lsl\text{-}LacZ}$, and *Vgat*^{Cre}*;R26R*^{LacZ} mice, respectively. Wholemount images are pseudocolored purple, green, and red, respectively. LacZ expression closely matches Cre-recombinase expression patterns characterized for these alleles previously (Matei et al., 2005; Scott et al., 2011; Vong et al., 2011).

(E) Illustration of the hindbrain in relationship to brainstem vasculature, and the approximate level of transverse coronal sections in (A-D). For experiments initiating fictive inspiration, the pons was removed by transection at level iii.
(F) A wholemount overlay demonstrates that brainstem nuclei enriched for Vglut2+ neurons are generally less enriched for Vgat+ neurons and *vice versa*, indicating that these genes mark terminally differentiated, non-overlapping populations of excitatory and inhibitory neurons, respectively (Vong et al., 2011). Scale bars = 1 mm. Arrows indicate rostral (R), caudal (C), dorsal (D), and ventral (V) directions.

Abbreviations (alphabetical): AMB, nucleus ambiguous; CS, superior central nucleus raphé; ECU, external cuneate nucleus; GRN, gigantocellular reticular nucleus; IO, inferior olivary complex; IPN, interpeduncular nucleus; IRN, intermediate reticular nucleus; LC, locus coeruleus; LRN, lateral reticular nucleus; MARN, magnocellular reticular nucleus; NLLv, nucleus of the lateral lemniscus, ventral part; NTB, nucleus of the trapezoid body; PARN, parvicellular reticular nucleus; PB, parabrachial nucleus; PG, pontine grey; PGRNl, paragigantocellular reticular nucleus, lateral; POR, superior olivary complex, periolivary region; PPN, pedunculopontine nucleus; PPY, parapyramidal nucleus; PRNc, pontine reticular nucleus, caudal; preBötC, preBötzinger complex; PRNr, pontine reticular nucleus, rostral; PSV, principal sensory nucleus of the trigeminal; RM, nucleus raphé magnus; RO, nucleus raphé obscurus; RPA, nucleus raphé pallidus; RTN/pFRG, retrotrapezoid nucleus/parafacial

respiratory group; SpV, spinal nucleus of the trigeminal; TRN, tegmental reticular nucleus; V, motor nucleus of trigeminal; VCO, ventral cochlear nucleus; VI, abducens nucleus; VII, facial motor nucleus; VNC, vestibular nuclei; XII, hypoglossal motor nucleus.

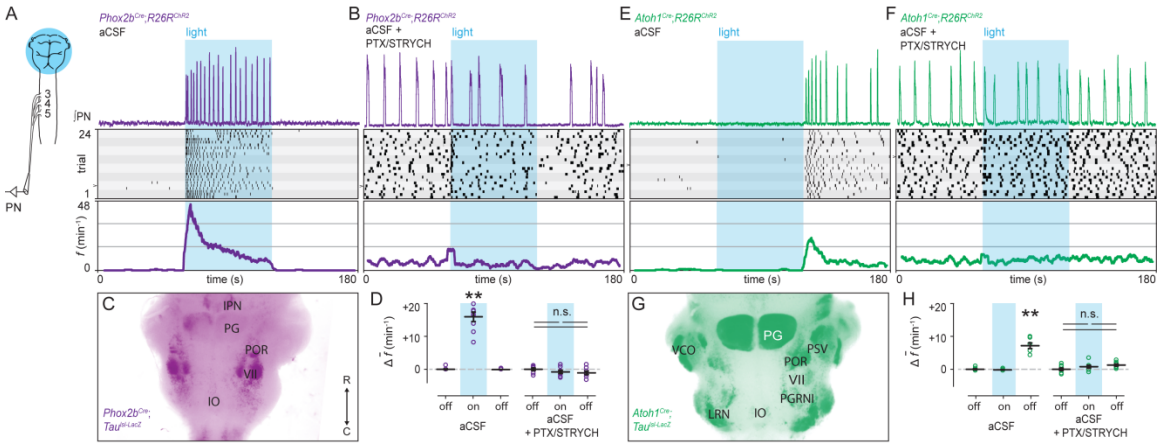

Figure 3.3: Inhibition is Implicated in Phox2b and Atoh1 Modulation of Inspiratory Frequency.

(A) Stimulation of Phox2b-lineage neurons dramatically increased *f* (f_{max} = 68.6 min^{-1}).

(B) Phox2b-mediated increases in *f* were blocked by bath application of PTX/STRYCH.

(C) Anatomical identification of ventral Phox2b-lineage neurons likely stimulated in the brainstem. Arrow indicates rostral and caudal directions.

(D) Change in average *f* during and after light stimulation relative to baseline. Baseline vs. photostimulation, $^{**}P$ = 0.002. Photostimulation vs. after, $^{**}P$ = 0.002. Mann-Whitney U test with Bonferroni correction. PTX/STRYCH blocked the effect of photostimulation (Mann-Whitney U test).

(E) Stimulation of Atoh1-lineage neurons resulted in a transient increase in *f* after the termination of the photostimulus.

(F) Atoh1-mediated increases in *f* were blocked by application of PTX/STRYCH.

(G) Position of ventral Atoh1-lineage neurons likely stimulated in the brainstem.

(H) Change in average *f* during and after light stimulation relative to baseline. Baseline vs. after, ***P* = 0.002. Photostimulation vs. after, ***P* = 0.002. Mann-Whitney U test with Bonferroni correction. PTX/STRYCH blocked the effect of photostimulation (one-way ANOVA). *n* = 8 for each condition, data are mean ± s.e.m.

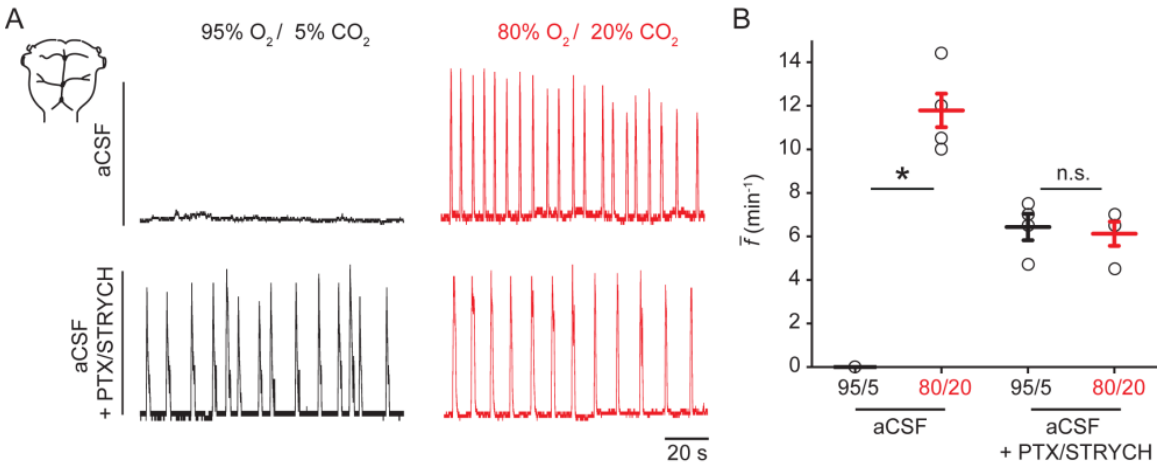

Figure 3.4: The Inspiratory Response to Hypercapnia is Dependent on Inhibitory Synaptic Transmission.

(A) Phrenic nerve recordings from pontomedullary preparations. *Top left*, no spontaneous inspiratory bursting is observed under normocapnic (95% O_2 / 5% CO_2) conditions. *Top right*, hypercapnic aCSF (80% O_2 / 20% CO_2) causes rapid inspiratory bursting. *Bottom left*, after application of PTX/STRYCH, pontomedullary preparations exhibit a baseline frequency of 4-7 min^{-1}. *Bottom right*, PTX/STRYCH application blocks hypercapnia-induced increases in *f*.

(B) Quantification of average *f* in response to hypercapnia. PTX/STRYCH application blocks hypercapnia-induced increases in *f*. **P* = 0.04. Mann-Whitney U test with Bonferroni correction. *n* = 5 for aCSF, *n* = 4 for aCSF + PTX/STRYCH. Data are mean ± s.e.m.

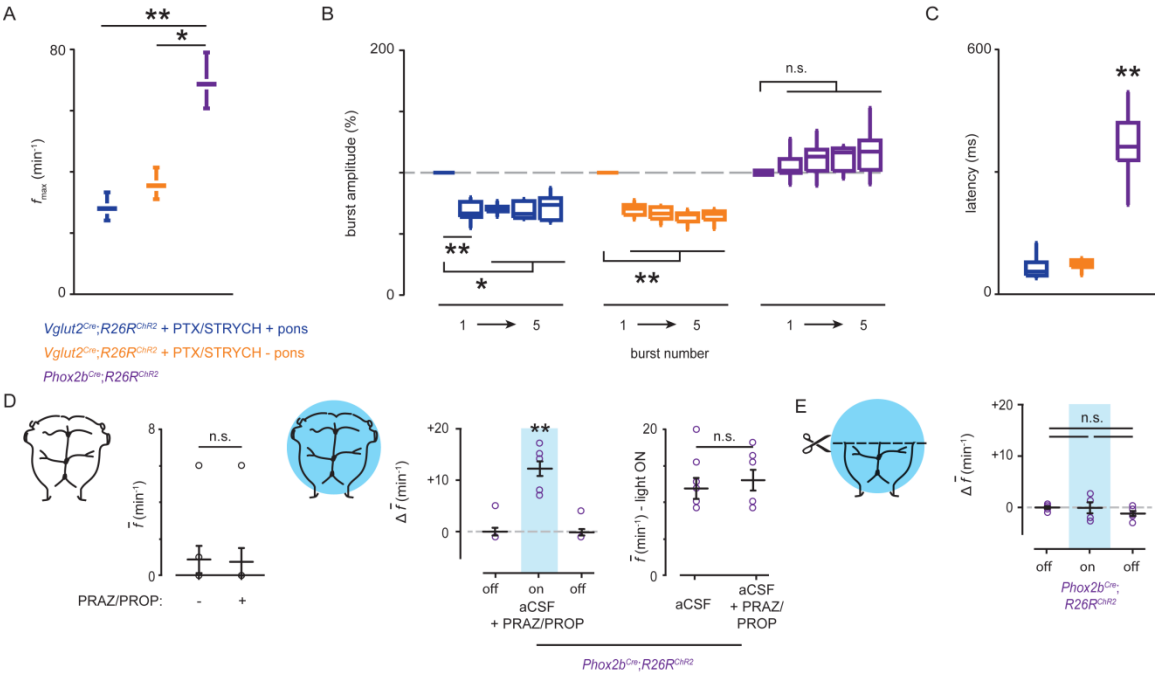

Figure 3.5: *Phox2b*^{Cre};*R26R*^{ChR2} Mediated Increases in *f* Compared with *Vglut2*^{Cre};*R26R*^{ChR2} + PTX/STRYCH Induced *Excitation*.

(A) f_{max} in response to stimulation of Phox2b+ neurons was much faster than f_{max} during stimulation of Vglut2+ neurons in the absence of inhibition. *Phox2b* vs. *Vglut2* + PTX/STRYCH + pons, ***P* = 0.005. *Phox2b* vs. *Vglut2* + PTX/STRYCH - pons, **P* = 0.04. Mann-Whitney U test with Bonferroni correction. *n* = 8 for each condition, error bars represent s.e.m.

(B) Stimulation of Vglut2+ neurons in the presence of PTX/STRYCH resulted in smaller inspiratory burst amplitude for successive bursts. *Vglut2* + PTX/STRYCH + pons, burst #1 vs. #2-5: **P* <0.05 and ***P* <0.01. *Vglut2* + PTX/STRYCH - pons, burst #1 vs. #2-5, ***P* = 0.004. Mann-Whitney U test with Bonferroni correction. Stimulation of Phox2b+ neurons (purple) did not result in depression of burst amplitude upon successive bursts (no significance, Mann-Whitney U

test). *n* = 8 for each condition, whiskers represent range. Bursts are numbered beginning with the first burst observed in response to the photostimulus.

(C) Whereas the response latency following stimulation of Vglut2+ neurons exhibited minimal delay (~100 ms), stimulation of Phox2b+ neurons evoked an inspiratory burst at a significant delay (367 ± 30 ms). *Phox2b* vs. *Vglut2* + PTX/STRYCH + pons, ***P* = 0.003. *Phox2b* vs. *Vglut2* + PTX/STRYCH - pons, ***P* = 0.003. Mann-Whitney U test with Bonferroni correction. *n* = 8 for each condition, whiskers represent range.

(D) *Phox2b*^{Cre}*;R26R*^{ChR2} mediated increases in *f* were insensitive to application of α_1- and β-adrenergic receptor antagonists (+ PRAZ/PROP). *Left*, application of PRAZ/PROP had no effect on baseline *f* in pontomedullary preparations (no significance, Mann-Whitney U test). *Middle*, baseline vs. photostimulation, ***P* = 0.002. Photostimulation vs. after light, ***P* = 0.002. Mann-Whitney U test with Bonferroni correction. *Right*, no significance, Mann-Whitney U test. *n* = 8 for each condition. Data are mean ± s.e.m.

(E) *Phox2b*^{Cre}*;R26R*^{ChR2} mediated increases in *f* required an intact pons (no significance, Welch's ANOVA). *n* = 6 mice. Data are mean ± s.e.m.

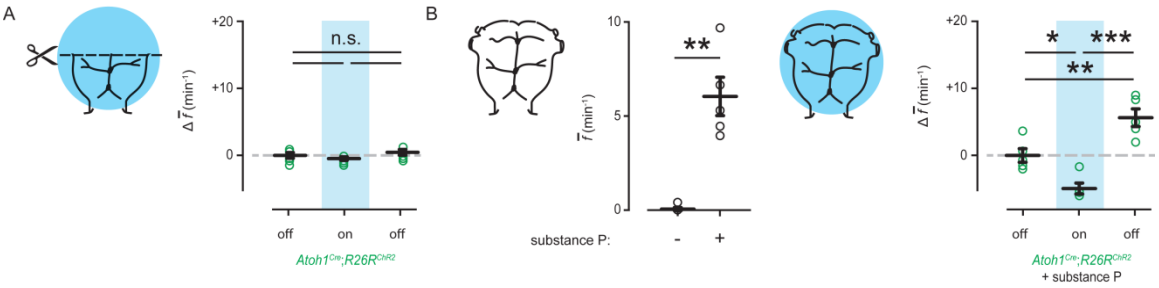

Figure 3.6: *Atoh1*^{Cre}*;R26R*^{ChR2} Suppression of Substance P Initiated Inspiratory Bursting.

(A) *Atoh1*^{Cre}*;R26R*^{ChR2} response required an intact pons (compare with Fig. 2*E*,*H*, no significance, one-way ANOVA). *n* = 5 mice.

(B) In pontomedullary preparations, stimulation of Atoh1+ neurons suppressed substance P evoked bursting. **P* = 0.017 baseline vs. photostimulation, ****P* = 4.1×10^{-5} photostimulation vs. after light, ***P* = 0.007 baseline vs. after light, one-way ANOVA and *post hoc* Tukey-Kramer HSD. *n* = 5 mice. Data are mean ± s.e.m.

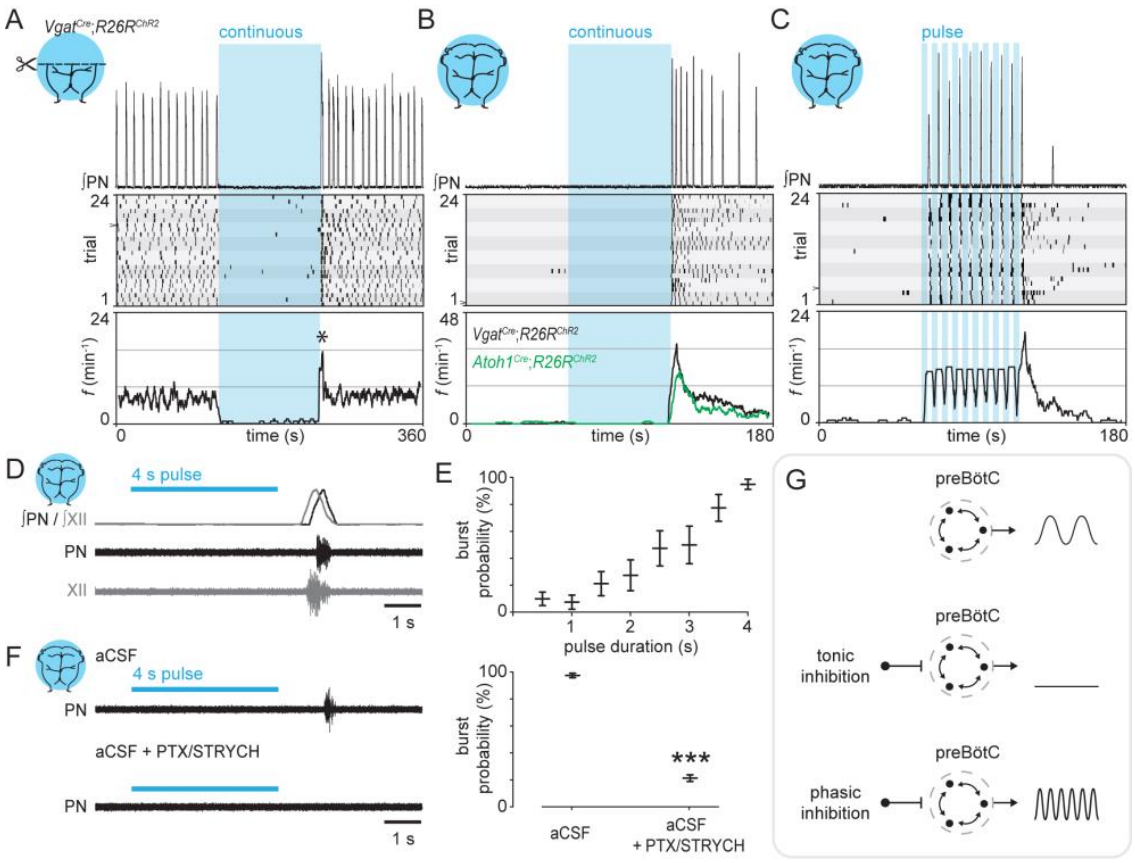

Figure 3.7: *Phasic Inhibition* can Drive Increases in Inspiratory Frequency.

(A) Photostimulation of Vgat+ neurons during fictive inspiration suppressed burst initiation for the duration of the photostimulus. *Bottom*, analysis of *f* indicated a reset-like response upon light off (asterisk, half-life of $t_{1/2}$ ~4s).

(B) In a silent preparation, stimulation of Vgat+ neurons evoked inspiratory bursting via a rebound-like mechanism (half life of $t_{1/2}$ ~23 s).

(C) Phasic inhibition evoked inspiratory bursting at high frequencies.

(D) Rebound bursts recruit phrenic and hypoglossal motor neurons (*n* = 5), indicating that rebound bursts arise from the preBötC.

(E) The probability of observing a rebound burst in response to stimulation of inhibitory neurons was directly proportional to the photostimulus duration. *n* = 8, data are mean ± s.e.m.

(F) PTX/STRYCH application blocked rebound inspiratory bursts. ***$P = 5.5 \times 10^{-4}$. Mann-Whitney U test. *n* = 8, data are mean ± s.e.m.

(G) Whereas tonic inhibition suppresses inspiratory burst initiation, *phasic inhibition* can actually increase *f* via post-inhibitory rebound.

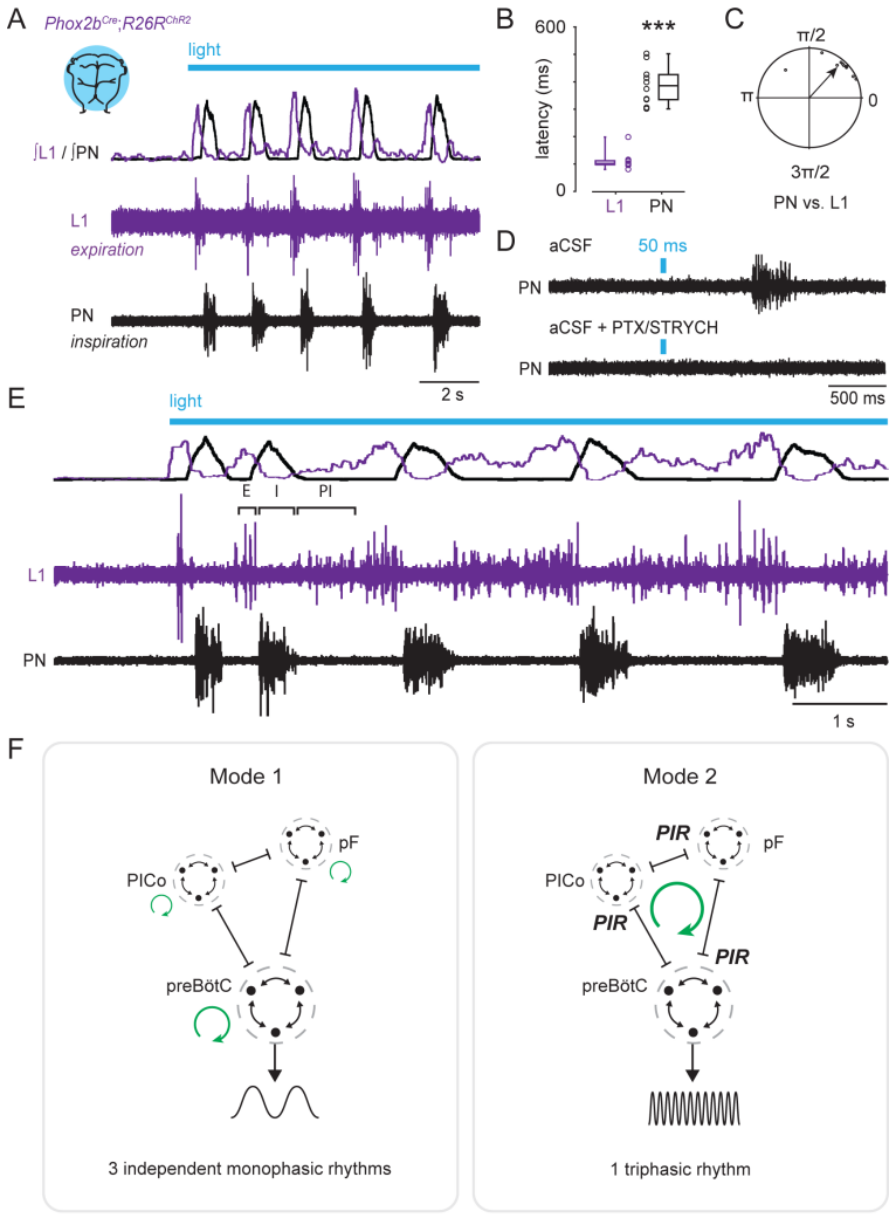

Figure 3.8: Phox2b-Lineage Neurons Evoke Expiration, Inspiration, and Post-Inspiration.

(A) Stimulation of Phox2b-lineage neurons evoked phasic expiratory (L1) motor activity preceding inspiratory bursts.

(B) Latency to first response. *n* = 10 preparations, ***P = 0.0002, Mann-Whitney U test.

(C) Coupling between PN and L1 exhibited a phase separation of 0.85 ± 0.17 rad (49 ± 10°; *n* = 10).

(D) 50 ms *Phox2b*^{Cre};*R26R*^{ChR2} photostimulation was sufficient to cause an inspiratory burst several hundreds of milliseconds later. This inspiratory response was blocked by application of PTX/STRYCH (see also Fig. 2*B*).

(E) Stimulation of Phox2b-lineage neurons evoked all 3 phases of respiration—expiration (E), inspiration (I), and post-inspiration (PI), forming a continuous triphasic rhythm.

(F) Illustration of proposed coupling between E, I, and PI. In Mode 1, inhibition does not couple E/I/PI and instead causes antiphasic patterning (Janczewski and Feldman, 2006). Here, rhythmic oscillations in motor output are the consequence of excitatory mechanisms. In Mode 2, inhibition causes post-inhibitory rebound, which acts to couple E, I, and PI. Here, unitary rhythmic oscillation is produced as a consequence of inhibitory synaptic coupling. pF, parafacial oscillator (E); preBötC (I); PICo, post-inspiratory complex (PI); PIR, post-inhibitory rebound excitation.

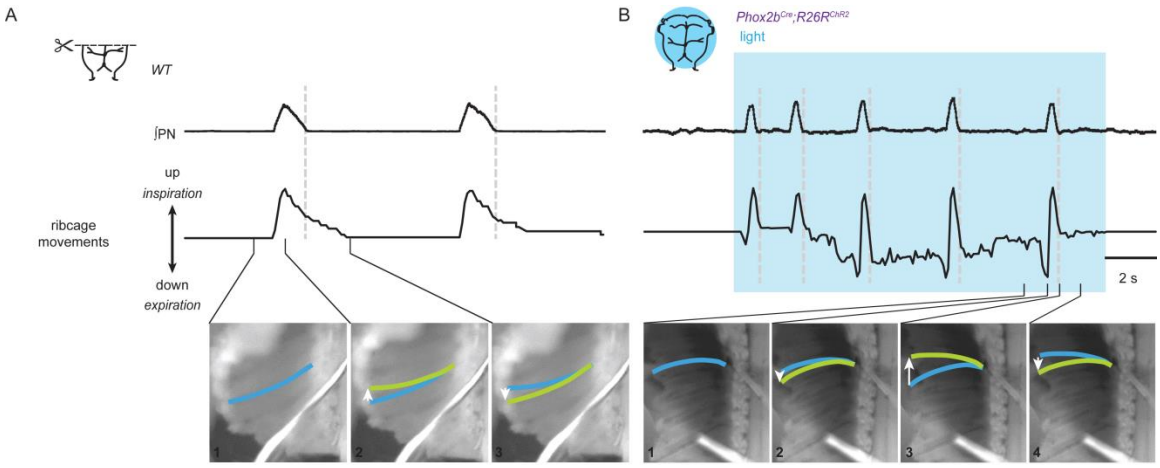

Figure 3.9: High Speed Video Demonstrates Two Distinct Modes of Inspiration.

(A) *Top*, during fictive inspiration, phrenic bursts exhibited a low frequency and long duration. *Bottom*, simultaneous quantification of ribcage movement indicated no active expiratory (downward) movement during fictive inspiration, and in contrast, the ribcage exhibited passive recoil, returning to its original position long after termination of the inspiratory burst.

(B) *Top*, stimulation of Phox2b+ neurons caused high frequency inspiratory bursts. *Bottom*, simultaneous quantification of ribcage movement indicated an active expiratory (downward) phase which was quickly followed by an upward ribcage deflection. The ribcage then returned to its original position upon termination of phrenic inspiratory bursts. Blue line indicates the original position of a single rib from previous image, and a green line indicates current (final) position of the rib.

Chapter 4: Discussion

In this work I have presented two surprising discoveries regarding the neural control of respiration: First, I found that two distinct premotor substrates can generate phrenic motor bursts—the preBötC, which generates *bona fide* inspiration (Jones and Dutschmann, 2016; Ramirez et al., 1998; Smith et al., 1990), as well as a "latent" spinal network which can generate spontaneous phrenic motor bursts after inhibitory blockade. Second, I found that inhibition is required for certain physiological modes of increased inspiratory frequency. In this chapter I will discuss the significance of these findings in the context of previous work, as well as technical limitations of our experimental approach and future experimental directions.

Two Distinct Premotor Networks Generate Phrenic Motor Bursts

In lumbar spinal cord circuits which generate locomotor rhythms, inhibitory blockade causes spontaneous, synchronous bursting across associated ventral (motor) roots (Bracci et al., 1996; Talpalar et al., 2011); excitatory premotor networks which normally exhibit antagonistic right/left and flexor/extensor patterns exhibit synchronous bursting (Bracci et al., 1996). This coincident bursting is due to recurrent excitatory interactions; deletion of *Vglut2* blocks synchronous activity caused by recurrent excitation (Talpalar et al., 2011). Although this synchronous burst activity does not resemble normal locomotion, it is thought to represent underlying rhythmogenic action of discrete populations of

excitatory neurons—which form the basis for mammalian locomotion (Hagglund et al., 2013; Hägglund et al., 2010; Kiehn, 2016).

We found that bursts generated by excitatory neurons within the lumbar or thoracic cord following blockade of inhibitory synaptic transmission also evoke burst activity of phrenic motor neurons. Unexpectedly, pharmacologic and spinal hemisection/transection experiments demonstrated that these bursts were dissociable from bursts of activity which are generated by the preBötC (Cregg et al., 2017a). Furthermore, direct stimulation of phrenic motor neurons after blockade of inhibitory synaptic transmission was not sufficient to evoke burst activity. The simplest interpretation of these results is 1) bursts of phrenic motor activity arise at the premotor level, and 2) two distinct premotor networks can initiate phrenic motor bursts.

We found that bursts generated by excitatory neurons within the spinal cord did not exhibit functional interaction at the premotor level with bursts generated by the preBötC, and instead this burst activity impinged on phrenic motor neurons themselves. We interpret these results to indicate that these two distinct burst-generating substrates do not exhibit anatomical connectivity at the premotor level: If excitatory transmission relayed to the spinal cord via the rVRG exhibited connectivity with excitatory burst-generating networks of the cord, presumably it would initiate an ectopic spinal cord derived burst. Similarly, if a spinal cord derived network exhibited ascending connectivity with the preBötC, then this activity would presumably initiate an ectopic inspiratory burst. This however, was not the case; inspiratory bursts did not initiate ectopic spinal cord

derived bursts, and spinal cord derived bursts did not initiate ectopic inspiratory bursts.

There is one alternative interpretation here which is worthwhile to note because it pertains to discussion of purely excitatory networks at-large, and may be particularly relevant to discussions of hindbrain networks herein: It is possible that there are “weak” excitatory connections between the rVRG and an expansive excitatory network within the spinal cord, such that comparatively smaller burst activity which is relayed to the cord via the rVRG is “buffered” by a comparatively larger network within the cord. Thus, such inspiratory burst activity might manifest within excitatory networks of the cord, but due to “buffering”, this activity may be insufficient to evoke a network-wide burst which recruits activity of motor neurons too. Such “buffering” within recurrent excitatory networks has been described specifically in the case of the preBötC (Kam et al., 2013). Here, activation of one single neuron is not sufficient to evoke a population wide burst (Kam et al., 2013).

Nonetheless, Kam and colleagues found that stimulation of only 4-9 neurons could evoke a population-wide burst of ~1000 neurons (Kam et al., 2013). Indeed, in another system, stimulation of single cortical pyramidal cells is sufficient to evoke whisking movements (Brecht et al., 2004), which are controlled by rhythmogenic networks of the medulla (McElvain et al., 2017). Thus, we think that if excitatory connections between the rVRG and an expansive excitatory network within the cord exist, then they are exceedingly sparse.

These considerations suggest that excitatory premotor networks which generate phrenic motor bursts (i.e. preBötC and spinal cord) are functionally independent, which begs the question of what physiological role an excitatory spinal network plays if it does not generate inspiration. Although it is tempting to speculate that spinal cord derived bursts are associated with a specific behavioral function post-natally (e.g. gasping)—and we cannot discount this hypothesis—we did not uncover evidence of this in our studies. Instead, in our preliminary work (which is not published herein), we examined whether spinal premotor networks might be involved in other aspects of phrenic motor neuron physiology. Specifically, given the similarities between propagating bursts within the disinhibited cord and those which occur during embryogenesis (Hanson and Landmesser, 2003; Myers et al., 2005), as well as the known roles that propagating embryonic burst activity plays in development of motor systems (Kastanenka and Landmesser, 2010, 2013; Myers et al., 2005), we examined whether premotor networks might be involved in the maturation of phrenic motor neurons during development.

As reviewed in Chapter 1 (Development of Respiratory Circuits), early embryonic networks of the spinal cord exhibit spontaneous propagating burst activity which is generated by cholinergic and GABA/glycinergic (but not glutamatergic) excitatory synaptic transmission (Hanson and Landmesser, 2003). At this stage (E12-E14), phrenic motor axons enter the diaphragm and intramuscular branching is largely complete by E13.5 (Brandon et al., 2003; Misgeld et al., 2002). Intramuscular branching patterns are dependent on activity

of phrenic motor neurons themselves; *ChAT*$^{-/-}$ mice exhibit hyperinnervation of the diaphragm.

In our ongoing work (which is not published herein), we assessed whether GABA/glycinergic or glutamatergic premotor networks are required for appropriate diaphragm innervation. We characterized intramuscular nerve branching in the diaphragm after germline knockout of *Vgat* or *Vglut2*, which are required for GABA/glycinergic and glutamatergic synaptic transmission, respectively (Talpalar et al., 2011; Wallen-Mackenzie et al., 2006; Wojcik et al., 2006). In contrast to *ChAT*$^{-/-}$ diaphragms which exhibit dramatic hyperinnervation, the basic branching pattern in the *Vglut2*$^{-/-}$ diaphragm was very similar to the WT pattern. This was not unexpected since glutamate antagonists do not greatly affect the frequency of spontaneous spinal cord derived bursts between E12.5 and E13.5 (Hanson and Landmesser, 2003; Momose-Sato et al., 2012a, 2012b). Nonetheless, while *Vgat*$^{-/-}$ and *Vgat*$^{-/-}$;*Vglut2*$^{-/-}$ diaphragms did not exhibit the extreme changes in innervation, more subtle changes in branching pattern were evident, including a decrease in intramuscular branching at the level of tertiary and quaternary branches. Indeed, a reduction in intramuscular nerve branching has been documented in *Vgat*$^{-/-}$ mice previously (Fogarty et al., 2015).

Interestingly, generation of early embryonic waves of activity requires persistent sodium current (Wang et al., 2009b), as we found for spinal cord derived PMN bursts in the disinhibited postnatal spinal cord. Furthermore, though large scale waves propagating within the spinal cord are lost when GABA/glycine become inhibitory around E14, propagating burst activity can be restored by

blocking GABA transmission with bicuculline (Momose-Sato and Sato, 2013). These data suggest that early embryonic waves of activity, which are similar to those which are observed in the disinhibited spinal cord, can drive PMN bursting and that this activity coordinates the basic pattern of diaphragm innervation.

Our data revealed that spinal cord derived PMN bursting, although normally silent postnatally, can be initiated in both adult mice and adult rats by application of PTX/STRYCH to the cervical spinal cord (Cregg et al., 2017a). Indeed, other investigators have observed PMN activity after application of $GABA_AR$/GlyR inhibitors to the cervical cord (Ghali and Marchenko, 2016; Zimmer and Goshgarian, 2007), although mechanisms underlying this activity were never investigated.

Is it possible that spinal derived PMN burst activity manifests in the adult animal under certain physiologic conditions? Interestingly, we have observed spinal derived PMN activity in the context of various manipulations aimed at restoring function to denervated PMNs after high cervical spinal cord lesion (Alilain et al., 2008, 2011), although the origin of this activity was never examined. In unpublished work from our laboratory we have characterized long-lasting waves of diaphragm activity which can appear in chronically injured rats (submitted, P.M. Warren and J. Silver). Given that such “spastic” activity has also been observed in human patients with high cervical spinal cord injury (Silver and Lehr, 1981), we think that spinal cord derived PMN burst activity can arise in some physiologic situations of increased network excitability. Interestingly, recent data has implicated recurrent excitatory networks in the generation of spasticity

(Bellardita et al., 2017). Here, excitatory networks appear to play a dominant role in the initiation of spastic events (Bellardita et al., 2017), although excitability and aberrant plateau potentials within motor neurons also contribute (Adams and Hicks, 2005; Bellardita et al., 2017; Bennett et al., 2001; Li et al., 2003). Thus, dysregulation of excitatory networks within the spinal cord could underlie aberrant PMN activity in pathological situations of increased network excitability such as SCI.

Inhibitory Modes of Respiratory Rhythm Generation

In the 1980s, it was hypothesized that respiratory rhythm was a network phenomenon where rhythm is generated by sequential phase transitions between expiration, inspiration, and post-inspiration (von Euler, 1983; Richter, 1982). Several seminal discoveries since that time have changed the way we think about rhythmogenic networks of the medulla. First, the discovery that inhibition is not required for rhythmogenesis *per se* led to several new hypotheses regarding generation of respiratory rhythm (Feldman and Smith, 1989; Rekling and Feldman, 1998). Second, discovery that discrete populations of excitatory neurons served as the basis for bursts of activity (Koshiya and Smith, 1999; Smith et al., 1991), and that some of these neurons exhibit pacemaker properties (Johnson et al., 1994), led to the view that specific premotor burst modules control activity of groups of motor neurons (Hagglund et al., 2013; Hägglund et al., 2010). Bursts of activity generated by groups of

excitatory neurons within the preBötC can be both self-generating and self-terminating, and thus, inhibitory neurons are dispensable for generation of respiratory rhythm both *in vitro* and *in vivo* (Feldman and Smith, 1989; Janczewski et al., 2013; Smith et al., 1991). Therefore, to summarize many years of work by several outstanding laboratories and investigators within the field, current thought would posit that excitatory neurons generate respiratory rhythm and inhibitory neurons modulate respiratory pattern (Janczewski et al., 2013; Sherman et al., 2015).

Nonetheless, our data complement these previous findings by demonstrating that distinct modes of inhibitory rhythm generation may act in parallel to achieve both homeostatic and behavioral needs. In this section we discuss how our results lend support to this hypothesis, predictions of this hypothesis, as well as caveats and alternative interpretations of this data.

Favored Hypothesis

Using the *en bloc* preparation to investigate how central neural networks control respiratory frequency, we unexpectedly found that certain modes of increased inspiratory frequency require inhibitory synaptic transmission; stimulation of Phox2b-lineage, putative CO_2 chemosensitive neurons resulted in dramatic increases in frequency, and these increases in frequency were abolished by application of $GABA_A$/GlyR antagonists. Furthermore, hypercapnia-induced increases in frequency were blocked by application of $GABA_A$/GlyR antagonists. These data indicate that inhibition may actively participate in

increasing frequency. As a mechanistic basis for inhibition induced increases in frequency, we found that stimulation of inhibitory neurons can increase frequency via a mechanism of post-inhibitory rebound excitation; inhibition-dependent increases in frequency were independent of mechanisms associated with disinhibition. We found further evidence that Phox2b-mediated increases in frequency were caused by rebound excitation. Thus, we propose a model whereby discrete excitatory oscillators can generate rhythm, but inhibitory coupling via post-inhibitory rebound excitation acts as a parallel mechanism for generation of respiratory rhythms across a broad frequency spectrum (Cregg et al., 2017b; Skinner et al., 1994).

To understand how inhibitory neurons can generate rhythm, it is useful to think of a *purely inhibitory* network consisting of just two inhibitory neurons with reciprocal connectivity (Perkel and Mulloney, 1974). In this simple case, neuron A fires while neuron B is inhibited—neurons A and B fire out of phase. When neuron A stops firing, neuron B does not start firing automatically. Instead, the dynamics of action potential firing within neuron B are largely independent of neuron A, except that these neurons will not fire at the same time. Adding rebound kinetics to this system, however, dramatically changes the dynamics: Here, when neuron A stops firing, neuron B starts firing due to rebound excitation. Likewise, when neuron B stops firing, neuron A starts firing due to rebound excitation. In this simple system, generation of rhythm (the rhythmic firing of each neuron) and pattern (the antiphasic firing of each neuron) are inherently yoked (Perkel and Mulloney, 1974; Skinner et al., 1994).

Such modes of inhibitory coupling are, indeed, physiologic. In *Xenopus* tadpoles, reciprocal inhibitory coupling is thought to be responsible for left/right swimming rhythms (Li and Moult, 2012; Moult et al., 2013). Here, the strength of inhibition (defined by the amplitude of IPSPs in dINs) dictated the probability of observing a rebound burst (Moult et al., 2013), and weakening phasic inhibition without changing background excitation slowed down left/right swimming rhythms (Li and Moult, 2012).

We propose that a similar mechanism of inhibitory coupling underlies Phox2b-mediated increases in inspiratory frequency (Cregg et al., 2017b). Here, Phox2b-lineage neurons don't increase inspiratory frequency via excitation of the preBötC, as has been predicted (Bochorishvili et al., 2012; Guyenet and Bayliss, 2015). Instead, Phox2b-lineage neurons increase frequency via *phasic inhibition*. This hypothesis, which is well supported by our data, represents a radically different way of understanding respiration in that the mechanism underlying change in respiratory frequency is exactly opposite of what has been predicted (Gray et al., 1999). Indeed, this hypothesis requires that inhibitory mechanisms of respiratory rhythm generation exist, which is controversial (Janczewski et al., 2013; Marchenko et al., 2016; Sherman et al., 2015).

Importantly, however, our data indicate that there may be two distinct modes of rhythm generation—Mode 1, which is purely excitatory, and Mode 2 which depends on inhibitory synaptic coupling between inspiration/expiration. As we have discussed previously (Cregg et al., 2017b), these modes are different in several ways and may act over distinct frequency ranges. One prediction of our

hypothesis which is not intuitive, however, is that there is a mechanism of preBötC recruitment which can cause forward progression in a triphasic respiratory cycle. Here, recruitment of the preBötC would cause initiation of a subsequent post-inspiratory burst. Thus, I suggest that recruitment of spontaneous preBötC bursts and those recruited via phasic inhibition may be fundamentally different.

In principle, neurons embedded within a purely excitatory network can only do one thing—excite each other (Buzsáki, 2006). This wiring configuration results in a one-way trajectory of excitatory synaptic events, ending in a population-level burst (Kam et al., 2013). Interestingly, the shape of spontaneous preBötC-generated inspiratory bursts is very similar to those evoked ectopically via glutamate uncaging (Kam et al., 2013). These data suggest that simple excitation of the preBötC always induces population burst activity of similar trajectory—recurrent excitation causes increasing recruitment of more and more excitatory neurons which results in burst activity, followed by self-termination of burst activity via activity-dependent outward currents. In light of our results, I hypothesize that *phasic inhibition* can allow for dramatic alterations of this trajectory as follows: Rebound excitation following the release of an inhibitory synaptic volley in a large fraction of excitatory neurons would allow for non-linear recruitment of the preBötC. In essence, the mode of recruitment for *phasic inhibition* would likely be very different than spontaneous bursts, and potentially differently from those recruited via *excitation*. This is a straightforward hypothesis to test within transverse medullary preBötC slices, as recent data has

demonstrated that hyperpolarization of Dbx1-lineage neurons can cause what appear to be rebound bursts (Koizumi et al., 2016).

Caveats and Alternative Interpretations

It is important to note that our experiments were performed in *en bloc* preparations derived from neonatal mice. It has long been thought that the *en bloc* preparation represents a reduced system when compared with awake adult animals (Okada et al., 1993; St John, 2009). Indeed, the *en bloc* preparation contains no vagal mechanosensory feedback, which is known to play a significant role in the modulation of respiratory rhythms which are generated centrally (Janczewski et al., 2013). Furthermore, a certain amount of respiratory network maturation is known to occur postnatally (Huckstepp et al., 2016). Despite these considerations, *frequency* should still have a mechanistic explanation regardless of the state. Therefore, I argue that mechanisms underlying the control of *frequency* in a reduced state are also likely to exist at least at some level in more intact preparations.

We found that application of $GABA_AR$/GlyR antagonists decoupled the effects of $Phox2b^{Cre};R26R^{ChR2}$ stimulation from effects on inspiratory burst frequency. This was a very surprising finding to us because it suggested that inhibitory neurons are actively involved in increasing inspiratory frequency. These results could not be attributed to hyperexcitability of the preBötC, because stimulation of Vglut2+ neurons after inhibitory blockade still caused a robust response. Nonetheless, there is at least one important alternative consideration

which merits discussion. Similar to “buffering” considerations mentioned above (Chapter 4, Two Distinct Premotor Networks Generate Phrenic Motor Bursts), it is possible—and likely—that there are Phox2b-lineage neurons which do exhibit at least some mono- or oligo-synaptic excitatory connections with the preBötC (Bochorishvili et al., 2012). Here, a small number of Phox2b-lineage excitatory connections might evoke subthreshold activity within the preBötC, but no effect on inspiratory frequency would be observed because the excitatory action of Phox2b+ neurons is “buffered” by a comparatively larger excitatory network recruited following the blockade of inhibition. Indeed, Anderson and colleagues have found that blockade of inhibition causes the preBötC and PICo to burst in synchrony due to an “unmasking” of (a presumably small number of) excitatory connections between the preBötC and PICo (Anderson and Ramirez, 2017; Anderson et al., 2016). This data indicates that blockade of inhibitory synaptic transmission causes the “kernel” of excitatory neurons which generates inspiratory rhythm to become much larger.

These considerations raise the possibility that inhibition may allow the preBötC to be much more responsive to incoming excitatory volleys initiated by Phox2b-lineage neurons, and that blockade of inhibition abolishes Phox2b-mediated increases in frequency due to “buffering”. I find that this hypothesis is unlikely for several reasons. First, if the pF, preBötC, and PICo (which generate expiration, inspiration, and post-inspiration, respectively) do indeed begin to oscillate in synchrony after blockade of inhibition due to “unmasking” of (presumably weak and non-specific) excitatory connections between the three, it

is hard to explain a lack of change in frequency following inhibitory blockade because we show that stimulation of Phox2b-lineage neurons simultaneously evoke changes in frequency for all 3 phases. If there were significant excitatory connections between Phox2b-lineage neurons and the pF, preBötC, and PICo, we should have observed at least some change in frequency. Thus, we suggest that any existent excitatory connections between Phox2b-lineage neurons and the preBötC are only weak and non-specific. Second, we were able to demonstrate that stimulation of Phox2b-lineage neurons always evokes expiration first. If Phox2b-lineage neurons increase frequency of all three phases via *excitation*, it is hard to explain why there is specific recruitment of expiration first and then subsequent orderly recruitment of inspiration and post-inspiration, with the frequency of each phase of respiration being equivalent. Finally—and this is the most important point—the fact that the dramatic Phox2b-lineage effects on frequency were blocked by inhibition indicates that inhibition is critical for high frequencies even if the underlying mechanism is not fully understood.

Owing to considerations which were not discussed within our original manuscript, we were not able to demonstrate that stimulation of Phox2b-lineage neurons following blockade of inhibitory synaptic transmission could evoke rhythmic expiratory bursting within the L1 ventral root (thus decoupling inspiration and expiration). Presumably Phox2b-lineage neurons do have a significant number of highly specific excitatory connections with the pF since we observed a direct expiratory response within ~100 ms of photostimulation. As we demonstrate in Chapter 2, however, application of PTX/STRYCH causes

synchronous bursting across all motor pools situated within the spinal cord, and that this bursting can be abolished within the phrenic motor pool following C8 transection. Thus, in all of our experiments in which we blocked inhibitory synaptic transmission, we performed a C8 transection to distinguish between PMN bursts originating within the cord and those which were derived from the preBötC. Although split bath experiments—where spinal cord and hindbrain compartments are perfused separately—might have allowed us to overcome this technical limitation, we actually found in several trials that PTX/STRYCH readily diffused within the parenchyma. I suspect that this diffusion (which was not detectable using dyes administered to a single compartment) might be attributed to the DMSO solvent used to dissolve PTX.

It is important to note that the *Phox2b*^{Cre} allele which we used in our studies actually marks a number of different populations of hindbrain neurons, including catecholaminergic C1 neurons, facial motor neurons, and neurons of the pFRG/RTN (as well as others). Importantly, we demonstrate that the effects of *Phox2b*^{ChR2}*;R26R*^{ChR2} photostimulation were independent of catecholamines, that is, they were not abolished by application of the α_1- and β-adrenergic antagonists prazosin and propranolol, respectively. We also have shown in within this body of work that bursts of inspiratory activity arise at the premotor level, which indicates that stimulation of Phox2b-lineage motor neurons is not likely to contribute to the effects we observe (Cregg et al., 2017a). Furthermore, consistent with the idea that stimulation of Phox2b-lineage neurons preferably engages CO_2 chemoreceptive neurons of the pFRG, we found that blockade of

inhibitory synaptic transmission completely abolished increases in frequency caused by hypercapnic aCSF (aCSF which is bubbled in elevated CO_2). Stimulation of Phox2b-lineage neurons also faithfully recapitulated the response observed upon stimulation of Phox2b-lineage pFRG neurons *in vivo*—a dramatic increase in frequency which also recruited expiratory bursting (Abbott et al., 2011), suggesting that we are engaging this same population of Phox2b-lineage, CO_2 chemosensitive neurons. Most importantly, however, the effects we observe are interesting despite considerations of which specific anatomical substrates contribute to them; stimulation of Phox2b-lineage neurons results in a dramatic increase in frequency which simultaneously evokes all 3 phases of respiration, and this effect is completely blocked by application of $GABA_AR$/GlyR inhibitors—this observation is highly unique.

Finally, although we found that several modes of increased frequency required inhibitory neurons, including increases in frequency caused by CO_2 as well as stimulation of Phox2b-lineage, Atoh1-lineage, and Vgat+ neurons, our experiments lack the spatial resolution necessary to determine where putative (and critical) inhibitory synapses are located. This problem is not necessarily unique to our system, and it is one of the reasons why it has been difficult to understand the role of inhibition in respiration more generally (Janczewski et al., 2013; Marchenko et al., 2016; Sherman et al., 2015). I discuss experimental approaches which may help to understand underlying inhibitory substrates in greater anatomical detail below (see Chapter 4, Understanding Inhibition and Future Outlook).

Unexpectedly, we found that changes in inspiratory frequency induced by stimulation of Phox2b-lineage and Atoh1-lineage neurons required an intact pons (Cregg et al., 2017b). This observation was somewhat surprising given that rhythmogenic circuits which generate expiration, inspiration, and post-inspiration are all contained within the medulla (Anderson and Ramirez, 2017; Anderson et al., 2016; Huckstepp et al., 2016, 2015; Janczewski and Feldman, 2006; Mellen et al., 2003; Onimaru et al., 2003; Pagliardini et al., 2011; Smith et al., 1991; Thoby-Brisson et al., 2009). Nonetheless, these data compliment several previous observations.

First, in 2016, Jones and Dutschmann demonstrated that an intact pons is required for sequential expiratory, inspiratory, and post-inspiratory phase transitions (Jones and Dutschmann, 2016). Here, in *in situ* preparations lacking the pons, Jones and Dutschmann found that motor output associated with expiration, inspiration, and post-inspiration actually occurs in synchrony rather than in sequential phases. Sequential phase transitions were only observed in *in situ* preparations which retained the pons (Jones and Dutschmann, 2016). Our results suggest that expiratory/inspiratory phase transitions are important for Phox2b-mediated increases in frequency. Thus, as predicted from the work of Jones and Dutschmann, it should not be surprising that medullary preparations (which lack the pons) do not exhibit increases in frequency during stimulation of

Phox2b-lineage neurons. Indeed, although the causative population of Phox2b-lineage, CO_2 chemosensitive neurons resides in the pFRG (which is fully contained within the medulla), Phoxb-lineage neurons also exhibit known ascending axonal projections to the pontine Kölliker-Fuse nucleus (Bochorishvili et al., 2012; Guyenet and Bayliss, 2015).

Second, although medullary populations of Atoh1-lineage neurons are thought to contribute to neonatal lethality in *Atoh1* null mice (Huang et al., 2012; Rose et al., 2009; Ruffault et al., 2015), full penetrance of the *Atoh1* null phenotype is only observed in animals which also exhibit deletion of *Atoh1* in tissues rostral to the rhombomere 3/4 boundary (Huang et al., 2012; Maricich et al., 2009), which includes most of the pons (Gray, 2008, 2013). Indeed, in characterization of the $Atoh1^{Cre}$ allele used in our studies, we found that more rostral dorsolateral pontine structures involved in respiratory control, including the parabrachial nucleus and the Kölliker-Fuse, are derived from the Atoh1-lineage (data not shown). Interestingly, in striking similarity to preparations which lack the pons (Jones and Dutschmann, 2016), Tupal and colleagues found that *Atoh1* null mice exhibit a lack of phase-delay between expiration, inspiration, and post-inspiration (Tupal et al., 2014).

Our data do not allow us to make any specific conclusions regarding the contributions of medullary versus pontine Atoh1-lineage neural populations to the responses we observe, but our data do provide several important pieces to the puzzle of the role of Atoh1-lineage neurons in respiratory control. Specifically, we found that post-inhibitory rebound following stimulation of Atoh1-lineage neurons

may be a mechanistic basis for observations that Atoh1-lineage neurons are both critical for normal respiratory frequency at birth and essential for phase-delay between expiration, inspiration, and post-inspiration (Tupal et al., 2014); stimulation of Atoh1-lineage neurons increases frequency via post-inhibitory rebound excitation and this increase in frequency is offset from the action of Atoh1-lineage neurons themselves (i.e. Atoh1-mediated inspiratory responses are out of phase with the photostimulus). Furthermore, our observation that Atoh1-lineage responses are abolished following removal of the pons is consistent with aforementioned data indicating a critical role for pontine structures in controlling expiratory, inspiratory, and post-inspiratory phase transitions (Jones and Dutschmann, 2016).

Much previous work has underscored the importance of the pons in modulation and control of respiration (Dutschmann and Dick, 2012). In contrast to previous results indicating that the pons may be involved in the modulation of rhythms which are generated by the medulla (Dutschmann and Herbert, 2006), our data actually place pontine structures within a core rhythmogenic hindbrain network. Although it is clear that each phase of respiration is generated by a specific population of neurons within the medulla (Anderson and Ramirez, 2017), our data suggest that it is actually the inhibitory interaction between these phases which contributes to rhythmogenesis. Thus, given data indicating a critical role for the pons in the control of these phase transitions (Jones and Dutschmann, 2016), I posit that pontine structures may be critical for generation of certain respiratory rhythms.

The dorsolateral pons is thought to regulate upper airway patency (Dutschmann and Dick, 2012). Thus, the pons may act in "gating" transitions between inspiration and expiration (Dutschmann and Herbert, 2006; Mörschel and Dutschmann, 2009), perhaps to accommodate other behaviors mediated by the upper airway, including swallowing and vocalization. Presumably, this so-called "gate" could act in two distinct ways—first by acting outside core rhythmogenic circuitry as an inspiratory off-switch (Dutschmann and Herbert, 2006; Richter, 1982), or second, amongst core rhythmogenic circuitry as part of the transition from inspiration to expiration. Given my hypothesis that inspiratory rhythms can in some cases be deterministic (Cregg et al., 2017b), it would be important to gate these rhythms such that inspiration does not cause aspiration of the lungs. Thus, although excitatory circuits within the medulla generate distinct phases of respiration (Anderson and Ramirez, 2017), it is possible that an internal copy circuit acts in parallel to gate respiration with distinct behaviors associated with the upper airway (Azim et al., 2014).

Defining Respiratory Frequency

Respiratory frequency (*f*) is defined by inspiration. Models attempting to explain respiratory frequency can therefore be simplified by ignoring a number of hindbrain structures which contribute to respiratory rhythmogenesis, and focusing instead on transition states of the preBötC alone. In this framework, it is widely thought that inspiratory frequency is defined by a balance of excitatory and

inhibitory synaptic input to the preBötC (Gray et al., 1999; Guyenet and Bayliss, 2015; Marchenko et al., 2016). This simplified model, however, does not account for how inspiratory burst pattern affects *f* (Janczewski et al., 2013). Interestingly, bilateral injection of the preBötC with GABA/glycine receptor antagonists significantly reduces *f*. These changes are partially attributed to a lengthening of inspiratory burst duration due to lack of inhibition (Cui et al., 2016; Janczewski et al., 2013). Thus, both inspiratory rhythm- and pattern-generating mechanisms contribute to changes in *f* by the following relationship:

$$f = \frac{1}{\text{cycle length}} = \frac{1}{T_I + T_{IBI}}$$

where rhythm-generating mechanisms are responsible for determining burst timing (interburst interval, T_{IBI}) and pattern-generating mechanisms regulate burst duration (T_I).

During the quiescent phase (T_{IBI}), excitation can initiate an inspiratory burst (Alsahafi et al., 2015; Cui et al., 2016; Kottick and Del Negro, 2015), whereas inhibition causes a delay until the next spontaneous inspiratory burst (Sherman et al., 2015). Within the framework we establish in the equation above, our data contributes to an understanding of how *f* is controlled by demonstrating that inhibition during T_{IBI} can actually increase *f* (Cregg et al., 2017b); inhibition can evoke ectopic bursts during the quiescent phase via a mechanism of post-inhibitory rebound excitation. Indeed, there is good evidence that inhibition within the preBötC itself, in this case due to hyperpolarization of Dbx1-lineage neurons,

can actually promote the generation of inspiratory bursts (Koizumi et al., 2016). Furthermore, hyperpolarization-activated inward currents have been described in so-called Type 1 inspiratory neurons of the preBötC (Thoby-Brisson et al., 2000). Thus, both inhibition and excitation can increase frequency during T_{IBI}.

During bursting (T_I), the story is more complicated. First, inhibition is likely to terminate bursts—although I am unaware of any direct data demonstrating this point. Excitation can, however, also terminate inspiratory bursts via activity-dependent outward currents (Del Negro et al., 2005). Therefore, because two distinct mechanisms *can likely* terminate inspiratory bursts, it remains unknown what mechanism *does* terminate inspiratory bursting *in vivo* (Dick et al., 2015). The idea that only a single mechanism *does* terminate inspiratory bursts *in vivo* during eupnea, however, could be a bit misleading. Indeed, in classic dynamical systems literature (Izhikevich, 2010; Skinner et al., 1994), it is both intrinsic and synaptic release and escape mechanisms that can contribute to oscillations within *purely inhibitory* neural networks. Given this literature, it is likely that more than one mechanism terminates inspiratory bursting at the same time.

If inhibition and excitation can both terminate inspiratory bursting, this would mean that inhibition and excitation both increase *f* during T_I by shortening the length of inspiratory bursts. Nonetheless, there is also data indicating that a lack of inhibition can decrease *f* due to enhanced excitation during T_I. Thus, the role of excitation during T_I is a bit confusing—excitation can terminate bursts via activity-dependent outward currents (e.g. I_{pump}, $I_{Na\text{-}K}$, $I_{K\text{-}ATP}$), but a lack of inhibition (resulting in increased excitation) can also lengthen bursts (Feldman and Smith,

1989). Here, however, the mechanism underlying increased excitation following inhibitory blockade likely is the result of an effective increase in the number of neurons recruited by inspiratory bursts (Anderson et al., 2016; Bracci et al., 1996; Cregg et al., 2017a; Talpalar et al., 2011).

In 2016, Cui and colleagues purportedly identified distinct rhythm and pattern generating “microcircuits” within the preBötC (Cui et al., 2016). I disagree with these authors’ definition of “microcircuits”—which was presumably the entire preBötC (I think this term should be reserved for more specific motifs, such as feed-forward inhibition, etc.). Nonetheless, the authors generated some interesting data indicating that modulation of inspiratory output via photoactivation of somatostatin-positive neurons could augment inspiratory burst duration (Cui et al., 2016). The emerging picture is that GPCR modulation of preBötC activity can significantly prolong inspiratory burst duration (Li et al., 2016)—perhaps contributing to the sigh behavior *in vivo* (Lieske et al., 2000; Ramirez, 2014; Tryba et al., 2006). This prolongation of inspiratory burst duration (T_I) ultimately decreases inspiratory burst frequency (Li et al., 2016).

These data together indicate that there is a complex relationship in how inhibition and excitation regulate *f*, and this depends on the phase (i.e. T_I versus T_{IBI}) in which inhibition/excitation are integrated by the preBötC. My point in discussing these considerations is to demonstrate that even in a well-defined network—which has been studied in slice preparations for ~25 years—understanding frequency is problematic. Thus, network models which purport to understand frequency seem premature. Ultimately though, understanding

respiration—a behavior which exhibits coordination of motor neurons across the entire extent of the hindbrain and spinal cord—will require network models that integrate component (e.g. preBötC) models of respiration.

Future Outlook

Use of reduced preparations has led to some of the most formidable discoveries in respiratory control (Feldman and Smith, 1989; Del Negro et al., 2002b; Onimaru et al., 2003; Smith et al., 1991). While there has always been debate as to whether discoveries made in reduced systems can be generalized to the awake adult animal (Richter and Smith, 2014; St John, 2009), several of the discoveries which were originally made in reduced preparations have later proven to hold true in adult animals (Feldman and Smith, 1989; Huckstepp et al., 2015; Janczewski et al., 2013; Onimaru et al., 2003; Ramirez et al., 1998; Sherman et al., 2015; Smith et al., 1991). Arguments that discoveries made in reduced systems may not be relevant to more intact systems have led to the idea that deconstruction of neural networks should (perhaps always) be performed in the adult animal (Huckstepp et al., 2016). I argue, however, that the recent trend toward studying respiration primarily in adult animals has been somewhat counterproductive. Rather complex questions can and have been addressed within a more intact system, but at the end, we are left guessing at what underlying mechanisms contribute to given experimental observations (Huckstepp et al., 2016; Marchenko et al., 2016).

Use of intact adult preparations has often been rationalized on the basis that slice or medullary *en bloc* preparations do not exhibit triphasic respiratory rhythms (Richter and Smith, 2014; Smith et al., 1990; St John, 2009). Indeed, although hypoglossal inspiratory motor neurons are usually recruited prior to phrenic motor neurons *in vivo* (Leiter and St. John, 2004), hypoglossal and phrenic motor neurons exhibit aberrant synchronous recruitment in medullary spinal cord preparations (Smith et al., 1990). In our experiments, we unexpectedly found that photostimulation of Phox2b-lineage, putative CO_2 chemoreceptive neurons can evoke full triphasic rhythms consisting of expiration, inspiration, and post-inspiration. We further found that inspiratory bursts recruited by post-inhibitory rebound, as well as those recruited by stimulation of Phox2b-lineage neurons, exhibit hypoglossal motor neuron recruitment *prior to* recruitment of phrenic motor neurons. In both of these situations in which we observed eupneic-like motor patterns *in vitro*, the pons was kept intact. These data are consistent with recent data indicating that the pons is critical for phase transitions between expiration, inspiration, and post-inspiration (Jones and Dutschmann, 2016; Mörschel and Dutschmann, 2009).

I think that this data should provide new impetus for studying respiration in the neonatal *en bloc* preparation. The *en bloc* preparation has many unique advantages compared with studying respiration *in vivo* or even compared with *in situ* preparations derived from adult rodents. First, the *en bloc* preparation is highly accessible for recording, imaging, and optogenetic/electrical stimulation experiments. Because *en bloc* preparations are derived from the P0-5 nervous

system of neonatal mice, the small size of these preparations combined with increased optical clarity due to a lack of myelin makes them especially suited for imaging studies (Onimaru et al., 2003; Thoby-Brisson et al., 2009). Second, these tools for engaging and measuring neural networks are readily complemented by pharmacological approaches. Third, the *en bloc* preparation is easy to use and highly reproducible, making it easy to compare data from many animals across experiments. Finally, the dynamics of respiration are slower when compared with respiration *in vivo*, making it easier to manipulate this activity and/or capture it using optical approaches. In this case, the contribution of T_{IBI} to *f* is negligible and rhythmogenic (T_I-associated) mechanisms are the primary mechanisms underlying *f* (Cregg et al., 2017b).

Nonetheless, within this body of work, we also ran into several technical limitations which would need to be addressed for the *en bloc* preparation to be useful for addressing the questions we raise herein. Within this section, I outline technological developments which would greatly facilitate use of the *en bloc* preparation for "discovery mode", that is, for quickly defining hypotheses about the generation of respiratory rhythms which can subsequently be tested in adult models (which are experimentally less tractable).

Using the *en bloc* preparation, physiological patterns of motor output are only observed in preparations retaining the pons. Interestingly, however, these preparations actually do not exhibit spontaneous activity (at least in preparations ≥P2, P0 and P1 preparations likely do exhibit some spontaneous activity). Thus, to access respiratory physiology within the *en bloc* preparation, a mechanism for

initiating respiration—which is accepted as being physiologic—would need to be established. Although some have used Substance P to increase frequency in these preparations (Gray et al., 1999; Huang et al., 2012), NK1R (the Substance P GPCR receptor) actually desensitizes relatively quickly (~5-10 min) (Huang et al., 2012).

In our studies we have used a channelrhodopsin-2 strategy for initiating respiration with blue light. Specifically, we used a *Phox2b*^{Cre} allele—which appears to preferentially recruit CO_2 chemosensitive neurons of the pFRG—to turn respiration on. This approach has received some criticism because it likely also recruits C1 neurons, facial motor neurons, as well as other Phox2b-lineage populations too. Recently it was found that expression of TASK-2 and GPR4 selectively mark neurons of the pFRG and act as part of the molecular components responsible for detection of CO_2. Thus, generation of a *TASK-2*^{Cre} and/or *GPR4*^{Cre} allele might enable more specific engagement of this circuitry. In our ongoing work, we have generated a *TASK-2*^{Cre} allele using CRISPR/Cas9 to facilitate knockin of Cre to the *TASK-2* ATG start site. Although we hypothesized that this would allow Cre expression in terminally differentiated populations of CO_2 chemosensitive neurons (Gestreau et al., 2010), we actually found that this allele turns on in an early progenitor state such that expression from a Cre-reporter allele is exhibited in all tissues that we have explored to date (e.g. CNS, muscle). Given that GPCRs can exhibit highly stereotyped expression patterns (Mombaerts et al., 1996), it is possible that a *GPR4*^{Cre} allele would allow Cre expression specific to terminally differentiated neurons within the pFRG.

Nonetheless, our observation that photostimulation of Phox2b-lineage neurons evokes a highly specific and stereotyped respiratory motor output, with expiratory motor activity recruited within ~100 ms of the photostimulus followed by inspiration at a latency of ~350 ms, might enable us to use this same approach for access to respiratory circuitry in unparalleled ways. If we could combine photostimulation approaches with recording and optical imaging approaches, we may be able to reconstruct how triphasic respiratory rhythms are generated centrally—linking recording data from expiratory, inspiratory, and post-inspiratory motor outputs with imaging data from discrete populations of CNS neurons. Red-shifted channelrhodopsin alleles might be combined with tissue-specific calcium reporter alleles allowing simultaneous stimulation and electrical/optical recording experiments (Chen et al., 2013; Lin et al., 2013). Although this seems at first like a farfetched idea, the alleles actually already exist: A *Phox2b*^{Flpo}*;R26R*^{Ksvo} approach for stimulating Phox2b-lineage neurons using red light could be combined with *Vglut2*^{Cre}*;R26R*^{GCamp6} or *Vgat*^{Cre}*;R26R*^{GCamp6} for simultaneous imaging of activity within glutamatergic or GABA/glycinergic neurons, respectively. Activity within discrete hindbrain populations (such as Atoh1-lineage) could then be imaged and reconstructed temporally based on the onset of photostimulation and relative to motor outputs.

Put simply, I envision the first “map” of core circuits which generate respiratory rhythm within the hindbrain. Based on our data, this map would encompass at least 3 discrete populations of excitatory neurons within the ventral medulla (including the pF, preBötC, and PICo), inhibitory neurons which regulate

their phasing, and may also extend dorsally to include structures of the dorsolateral pons (Dutschmann and Dick, 2012). Imaging such large and disparate populations of hindbrain neurons is only now becoming possible. Recently, Sofroniew and colleagues demonstrated use of a two-photon mesoscope which can image a 5 mm diameter field at a depth of 1 mm and at a rate of 1 Hz (Sofroniew et al., 2016), and indeed, smaller volumes can be sampled even more quickly. Using an approach like this would, in theory, be sufficient for visualization of the “map” I describe. With a map of core circuits which generate respiratory rhythm within the hindbrain—and an understanding of the excitatory and inhibitory dynamics which underlie rhythmogenesis—questions concerning how dysfunction in neural circuitry relates to different disease states will become more tractable.

References

Abbott, S.B.G., Stornetta, R.L., Fortuna, M.G., Depuy, S.D., West, G.H., Harris, T.E., and Guyenet, P.G. (2009). Photostimulation of retrotrapezoid nucleus Phox2b-expressing neurons in vivo produces long-lasting activation of breathing in rats. J. Neurosci. *29*, 5806–5819.

Abbott, S.B.G., Stornetta, R.L., Coates, M.B., and Guyenet, P.G. (2011). Phox2b-expressing neurons of the parafacial region regulate breathing rate, inspiration, and expiration in conscious rats. J. Neurosci. *31*, 16410–16422.

Abdala, A.P., Paton, J.F.R., and Smith, J.C. (2015). Defining inhibitory neurone function in respiratory circuits: opportunities with optogenetics? J. Physiol. *593*, 3033–3046.

Abdala, A.P., Toward, M.A., Dutschmann, M., Bissonnette, J.M., and Paton, J.F.R. (2016). Deficiency of GABAergic synaptic inhibition in the Kölliker-Fuse area underlies respiratory dysrhythmia in a mouse model of Rett syndrome. J. Physiol. *594*, 223–237.

Abdala, A.P.L., Dutschmann, M., Bissonnette, J.M., and Paton, J.F.R. (2010). Correction of respiratory disorders in a mouse model of Rett syndrome. Proc. Natl. Acad. Sci. *107*, 18208–18213.

Adams, M., and Hicks, A. (2005). Spasticity after spinal cord injury. Spinal Cord *43*, 577–586.

Akazawa, C., Ishibashi, M., Shimizu, C., Nakanishi, S., and Kageyama, R. (1995). A mammalian helix-loop-helix factor structurally related to the product of Drosophila proneural gene atonal is a positive transcriptional regulator expressed in the developing nervous system. J. Biol. Chem. *270*, 8730–8738.

Alilain, W., and Silver, J. (2009). Shedding light on restoring respiratory function after spinal cord injury. Front. Mol. Neurosci. *2*, 18.

Alilain, W.J., Li, X., Horn, K.P., Dhingra, R., Dick, T.E., Herlitze, S., and Silver, J. (2008). Light-induced rescue of breathing after spinal cord injury. J. Neurosci. *28*, 11862–11870.

Alilain, W.J., Horn, K.P., Hu, H., Dick, T.E., and Silver, J. (2011). Functional regeneration of respiratory pathways after spinal cord injury. Nature *475*, 196–200.

Alsahafi, Z., Dickson, C.T., and Pagliardini, S. (2015). Optogenetic excitation of preBötzinger complex neurons potently drives inspiratory activity in vivo. J. Physiol. *593*, 3673–3692.

Amiel, J., Laudier, B., Attié-Bitach, T., Trang, H., de Pontual, L., Gener, B., Trochet, D., Etchevers, H., Ray, P., Simonneau, M., et al. (2003). Polyalanine expansion and frameshift mutations of the paired-like homeobox gene PHOX2B in congenital central hypoventilation syndrome. Nat. Genet. *33*, 459–461.

An, M.C., Lin, W., Yang, J., Dominguez, B., Padgett, D., Sugiura, Y., Aryal, P., Gould, T.W., Oppenheim, R.W., Hester, M.E., et al. (2010). Acetylcholine negatively regulates development of the neuromuscular junction through distinct cellular mechanisms. Proc. Natl. Acad. Sci. U. S. A. *107*, 10702–10707.

Anderson, T.M., and Ramirez, J.M. (2017). Respiratory rhythm generation: triple oscillator hypothesis. F1000Research *6*, 139.

Anderson, T.M., Garcia, A.J., Baertsch, N.A., Pollak, J., Bloom, J.C., Wei, A.D., Rai, K.G., and Ramirez, J.M. (2016). A novel excitatory network for the control of breathing. Nature *536*, 76–80.

Asada, H., Kawamura, Y., Maruyama, K., Kume, H., Ding, R.G., Kanbara, N., Kuzume, H., Sanbo, M., Yagi, T., and Obata, K. (1997). Cleft palate and decreased brain gamma-aminobutyric acid in mice lacking the 67-kDa isoform of glutamic acid decarboxylase. Proc. Natl. Acad. Sci. U. S. A. *94*, 6496–6499.

Azim, E., Jiang, J., Alstermark, B., and Jessell, T.M. (2014). Skilled reaching relies on a V2a propriospinal internal copy circuit. Nature *508*, 357–363.

Bagnall, M.W., and McLean, D.L. (2014). Modular organization of axial microcircuits in zebrafish. Science *343*, 197–200.

Barber, R.P., Phelps, P.E., Houser, C.R., Crawford, G.D., Salvaterra, P.M., and Vaughn, J.E. (1984). The morphology and distribution of neurons containing choline acetyltransferase in the adult rat spinal cord: An immunocytochemical study. J. Comp. Neurol. *229*, 329–346.

Bayliss, D.A., Talley, E.M., Sirois, J.E., and Lei, Q. (2001). TASK-1 is a highly modulated pH-sensitive “leak” K(+) channel expressed in brainstem respiratory neurons. Respir. Physiol. *129*, 159–174.

Bayliss, D.A., Barhanin, J., Gestreau, C., and Guyenet, P.G. (2015). The role of pH-sensitive TASK channels in central respiratory chemoreception. Pflügers Arch. - Eur. J. Physiol. *467*, 917–929.

Bellardita, C., Caggiano, V., Leiras, R., Caldeira, V., Fuchs, A., Bouvier, J., Löw, P., and Kiehn, O. (2017). Spatiotemporal correlation of spinal network dynamics underlying spasms in chronic spinalized mice. Elife *6*, e23011.

Ben-Arie, N., McCall, A.E., Berkman, S., Eichele, G., Bellen, H.J., and Zoghbi, H.Y. (1996). Evolutionary conservation of sequence and expression of the bHLH protein Atonal suggests a conserved role in neurogenesis. Hum. Mol. Genet. *5*, 1207–1216.

Ben-Arie, N., Bellen, H.J., Armstrong, D.L., McCall, A.E., Gordadze, P.R., Guo, Q., Matzuk, M.M., and Zoghbi, H.Y. (1997). Math1 is essential for genesis of cerebellar granule neurons. Nature *390*, 169–172.

Benarroch, E.E. (2007). Brainstem respiratory control: substrates of respiratory failure of multiple system atrophy. Mov. Disord. *22*, 155–161.

Bennett, D.J., Li, Y., Harvey, P.J., and Gorassini, M. (2001). Evidence for plateau potentials in tail motoneurons of awake chronic spinal rats with spasticity. J. Neurophysiol. *86*, 1972–1982.

Blanchi, B., Kelly, L.M., Viemari, J.C., Lafon, I., Burnet, H., Bévengut, M., Tillmanns, S., Daniel, L., Graf, T., Hilaire, G., et al. (2003). MafB deficiency causes defective respiratory rhythmogenesis and fatal central apnea at birth. Nat. Neurosci. *6*, 1091–1100.

Bochorishvili, G., Stornetta, R.L., Coates, M.B., and Guyenet, P.G. (2012). Pre-Bötzinger complex receives glutamatergic innervation from galaninergic and other retrotrapezoid nucleus neurons. J. Comp. Neurol. *520*, 1047–1061.

Borday, C., Coutinho, A., Germon, I., Champagnat, J., and Fortin, G. (2006). Pre-/post-otic rhombomeric interactions control the emergence of a fetal-like respiratory rhythm in the mouse embryo. J. Neurobiol. *66*, 1285–1301.

Bouvier, J., Thoby-Brisson, M., Renier, N., Dubreuil, V., Ericson, J., Champagnat, J., Pierani, A., Chédotal, A., and Fortin, G. (2010). Hindbrain interneurons and axon guidance signaling critical for breathing. Nat. Neurosci. *13*, 1066–1074.

Bracci, E., Ballerini, L., and Nistri, A. (1996). Localization of rhythmogenic networks responsible for spontaneous bursts induced by strychnine and bicuculline in the rat isolated spinal cord. J. Neurosci. *16*, 7063–7076.

Brandon, E.P., Lin, W., D'Amour, K.A., Pizzo, D.P., Dominguez, B., Sugiura, Y., Thode, S., Ko, C.P., Thal, L.J., Gage, F.H., et al. (2003). Aberrant patterning of neuromuscular synapses in choline acetyltransferase-deficient mice. J. Neurosci. *23*, 539–549.

Brecht, M., Schneider, M., Sakmann, B., and Margrie, T.W. (2004). Whisker movements evoked by stimulation of single pyramidal cells in rat motor cortex. Nature *427*, 704–710.

Brockhaus, J., Ballanyi, K., Smith, J.C., and Richter, D.W. (1993). Microenvironment of respiratory neurons in the in vitro brainstem-spinal cord of neonatal rats. J. Physiol. *462*, 421–445.

Brown, T.G. (1911). The intrinsic factors in the act of progression in the mammal. Proc. R. Soc. London. Ser. B, Contain. Pap. a Biol. Character 308–319.

Brown, T.G. (1914). On the nature of the fundamental activity of the nervous centres; together with an analysis of the conditioning of rhythmic activity in progression, and a theory of the evolution of function in the nervous system. J. Physiol. *48*, 18–46.

Brown-Séquard, C.E. (1860). Course of lectures on the physiology and pathology of the central nervous system : delivered at the Royal College of Surgeons of England in May, 1858 (Philadelphia: Collins).

Brunet, J.F., and Pattyn, A. (2002). Phox2 genes - from patterning to connectivity. Curr. Opin. Genet. Dev. *12*, 435–440.

Brust, R.D., Corcoran, A.E., Richerson, G.B., Nattie, E., and Dymecki, S.M. (2014). Functional and developmental identification of a molecular subtype of brain serotonergic neuron specialized to regulate breathing dynamics. Cell Rep. *9*, 2152–2165.

Buttry, J.L., and Goshgarian, H.G. (2014). Injection of WGA-Alexa 488 into the ipsilateral hemidiaphragm of acutely and chronically C2 hemisected rats reveals activity-dependent synaptic plasticity in the respiratory motor pathways. Exp. Neurol. *261*, 440–450.

Buzsáki, G. (2006). Rhythms of the brain (Oxford University Press).

Caldeira, V., Dougherty, K.J., Borgius, L., and Kiehn, O. (2017). Spinal Hb9::Cre-derived excitatory interneurons contribute to rhythm generation in the mouse. Sci. Rep. *7*, 41369.

Chang, R.B., Strochlic, D.E., Williams, E.K., Umans, B.D., and Liberles, S.D. (2015). Vagal sensory neuron subtypes that differentially control breathing. Cell *161*, 622–633.

Chatonnet, F., Wrobel, L.J., Mézières, V., Pasqualetti, M., Ducret, S., Taillebourg, E., Charnay, P., Rijli, F.M., and Champagnat, J. (2007). Distinct roles of Hoxa2 and Krox20 in the development of rhythmic neural networks controlling inspiratory depth, respiratory frequency, and jaw opening. Neural Dev. *2*, 19.

Chen, T.W., Wardill, T.J., Sun, Y., Pulver, S.R., Renninger, S.L., Baohan, A., Schreiter, E.R., Kerr, R.A., Orger, M.B., Jayaraman, V., et al. (2013). Ultrasensitive fluorescent proteins for imaging neuronal activity. Nature *499*, 295–300.

Coglianese, C.J., Peiss, C.N., and Wurster, R.D. (1977). Rhythmic phrenic nerve activity and respiratory activity in spinal dogs. Respir. Physiol. *29*, 247–254.

Cohen, M.I. (1979). Neurogenesis of respiratory rhythm in the mammal. Physiol. Rev. *59*, 1105–1173.

Corcoran, A.E., Hodges, M.R., Wu, Y., Wang, W., Wylie, C.J., Deneris, E.S., and Richerson, G.B. (2009). Medullary serotonin neurons and central CO2 chemoreception. Respir. Physiol. Neurobiol. *168*, 49–58.

Coste, B., Mathur, J., Schmidt, M., Earley, T.J., Ranade, S., Petrus, M.J., Dubin, A.E., and Patapoutian, A. (2010). Piezo1 and Piezo2 are essential components of distinct mechanically activated cation channels. Science *330*, 55–60.

Coutinho, A.P., Borday, C., Gilthorpe, J., Jungbluth, S., Champagnat, J., Lumsden, A., and Fortin, G. (2004). Induction of a parafacial rhythm generator by rhombomere 3 in the chick embryo. J. Neurosci. *24*, 9383–9390.

Cregg, J.M., Wiseman, S.L., Pietrzak-Goetze, N.M., Smith, M.R., Jaroch, D.B., Clupper, D.C., and Gilbert, R.J. (2010). A rapid, quantitative method for assessing axonal extension on biomaterial platforms. Tissue Eng. Part C Methods *16*, 167–172.

Cregg, J.M., DePaul, M.A., Filous, A.R., Lang, B.T., Tran, A., and Silver, J. (2014). Functional regeneration beyond the glial scar. Exp. Neurol. *253*, 197–207.

Cregg, J.M., Chu, K.A., Hager, L.E., Maggard, R.S.S.J., Stoltz, D.R., Edmond, M., Alilain, W.J., Philippidou, P., Landmesser, L.T., and Silver, J. (2017a). A latent propriospinal network can restore diaphragm function after high cervical spinal cord injury. Cell Rep. *21*, 654–665.

Cregg, J.M., Chu, K.A., Dick, T.E., Landmesser, L.T., and Silver, J. (2017b). Phasic inhibition as a mechanism for generation of rapid respiratory rhythms. Proc. Natl. Acad. Sci. U. S. A. doi: 10.1073/pnas.1711536114.

Cui, Y., Kam, K., Sherman, D., Janczewski, W.A., Zheng, Y., and Feldman, J.L. (2016). Defining preBötzinger complex rhythm- and pattern-generating neural microcircuits in vivo. Neuron *91*, 602–614.

Czarnecki, A., Le Corronc, H., Rigato, C., Le Bras, B., Couraud, F., Scain, A.L.,

Allain, A.E., Mouffle, C., Bullier, E., Mangin, J.M., et al. (2014). Acetylcholine controls GABA-, glutamate-, and glycine-dependent giant depolarizing potentials that govern spontaneous motoneuron activity at the onset of synaptogenesis in the mouse embryonic spinal cord. J. Neurosci. *34*, 6389–6404.

Davies, J.G., Kirkwood, P.A., and Sears, T.A. (1985). The detection of monosynaptic connexions from inspiratory bulbospinal neurones to inspiratory motoneurones in the cat. J. Physiol. *368*, 33–62.

Decima, E.E., von Euler, C., and Thoden, U. (1969). Intercostal-to-phrenic reflexes in the spinal cat. Acta Physiol. Scand. *75*, 568–579.

DePuy, S.D., Kanbar, R., Coates, M.B., Stornetta, R.L., and Guyenet, P.G. (2011). Control of breathing by raphe obscurus serotonergic neurons in mice. J. Neurosci. *31*, 1981–1990.

Dick, T.E., Dutschmann, M., Feldman, J.L., Fong, A.Y., Hülsmann, S., Morris, K.M., Ramirez, J.M., Smith, J.C., and Respiratory Neurobiology Consortium (2015). Facts and challenges in respiratory neurobiology. Respir. Physiol. Neurobiol. 10.1016/j.resp.2015.01.014.

Dobbins, E.G., and Feldman, J.L. (1994). Brainstem network controlling descending drive to phrenic motoneurons in rat. J. Comp. Neurol. *347*, 64–86.

Dougherty, K.J., Zagoraiou, L., Satoh, D., Rozani, I., Doobar, S., Arber, S., Jessell, T.M., and Kiehn, O. (2013). Locomotor rhythm generation linked to the output of spinal Shox2 excitatory interneurons. Neuron *80*, 920–933.

Dubin, A.E., Schmidt, M., Mathur, J., Petrus, M.J., Xiao, B., Coste, B., and Patapoutian, A. (2012). Inflammatory signals enhance Piezo2-mediated mechanosensitive currents. Cell Rep. *2*, 511–517.

Dubreuil, V., Ramanantsoa, N., Trochet, D., Vaubourg, V., Amiel, J., Gallego, J., Brunet, J.F., and Goridis, C. (2008). A human mutation in Phox2b causes lack of CO2 chemosensitivity, fatal central apnea, and specific loss of parafacial neurons. Proc. Natl. Acad. Sci. U. S. A. *105*, 1067–1072.

Dubreuil, V., Thoby-Brisson, M., Rallu, M., Persson, K., Pattyn, A., Birchmeier, C., Brunet, J.F., Fortin, G., and Goridis, C. (2009). Defective respiratory rhythmogenesis and loss of central chemosensitivity in Phox2b mutants targeting retrotrapezoid nucleus neurons. J. Neurosci. *29*, 14836–14846.

Duffin, J., and van Alphen, J. (1995). Bilateral connections from ventral group inspiratory neurons to phrenic motoneurons in the rat determined by cross-correlation. Brain Res. *694*, 55–60.

Dutschmann, M., and Dick, T.E. (2012). Pontine mechanisms of respiratory control. Compr. Physiol. *2*, 2443–2469.

Dutschmann, M., and Herbert, H. (2006). The Kölliker-Fuse nucleus gates the postinspiratory phase of the respiratory cycle to control inspiratory off-switch and upper airway resistance in rat. Eur. J. Neurosci. *24*, 1071–1084.

Dutschmann, M., Bautista, T.G., Mörschel, M., and Dick, T.E. (2014). Learning to breathe: Habituation of Hering–Breuer inflation reflex emerges with postnatal brainstem maturation. Respir. Physiol. Neurobiol. *195*, 44–49.

Ellenberger, H.H., and Feldman, J.L. (1988). Monosynaptic transmission of respiratory drive to phrenic motoneurons from brainstem bulbospinal neurons in rats. J. Comp. Neurol. *269*, 47–57.

Ellenberger, H.H., Feldman, J.L., and Goshgarian, H.G. (1990). Ventral respiratory group projections to phrenic motoneurons: electron microscopic evidence for monosynaptic connections. J. Comp. Neurol. *302*, 707–714.

Engbers, J.D.T., Anderson, D., Tadayonnejad, R., Mehaffey, W.H., Molineux, M.L., and Turner, R.W. (2011). Distinct roles for I(T) and I(H) in controlling the frequency and timing of rebound spike responses. J. Physiol. *589*, 5391–5413.

von Euler, C. (1983). On the central pattern generator for the basic breathing rhythmicity. J. Appl. Physiol. *55*, 1647–1659.

Ezure, K. (1990). Synaptic connections between medullary respiratory neurons and considerations on the genesis of respiratory rhythm. Prog. Neurobiol. *35*, 429–450.

Feldman, J.L., and Kam, K. (2015). Facing the challenge of mammalian neural microcircuits: taking a few breaths may help. J. Physiol. *593*, 3–23.

Feldman, J.L., and Del Negro, C.A. (2006). Looking for inspiration: new perspectives on respiratory rhythm. Nat. Rev. Neurosci. *7*, 232–242.

Feldman, J.L., and Smith, J.C. (1989). Cellular mechanisms underlying modulation of breathing pattern in mammals. Ann. N. Y. Acad. Sci. *563*, 114–130.

Feldman, J.L., Smith, J.C., Ellenberger, H.H., Connelly, C.A., Liu, G.S., Greer, J.J., Lindsay, A.D., and Otto, M.R. (1990). Neurogenesis of respiratory rhythm and pattern: emerging concepts. Am. J. Physiol. *259*, 879–886.

Feldman, J.L., Kam, K., and Janczewski, W.A. (2009). Practice makes perfect, even for breathing. Nat. Neurosci. *12*, 961–963.

Flourakis, M., Kula-Eversole, E., Hutchison, A.L., Han, T.H., Aranda, K., Moose, D.L., White, K.P., Dinner, A.R., Lear, B.C., Ren, D., et al. (2015). A conserved bicycle model for circadian clock control of membrane excitability. Cell *162*, 836–848.

Flourens, M. (1858). Nouveau details sur le noeud vital. Compt Rend Acad Sci *47*, 803–806.

Fogarty, M.J., Yanagawa, Y., Obata, K., Bellingham, M.C., and Noakes, P.G. (2015). Genetic absence of the vesicular inhibitory amino acid transporter differentially regulates respiratory and locomotor motor neuron development. Brain Struct. Funct. *220*, 525–540.

Fortin, G., Jungbluth, S., Lumsden, A., and Champagnat, J. (1999). Segmental specification of GABAergic inhibition during development of hindbrain neural networks. Nat. Neurosci. *2*, 873–877.

Fremeau, R.T., Voglmaier, S., Seal, R.P., and Edwards, R.H. (2004). VGLUTs define subsets of excitatory neurons and suggest novel roles for glutamate. Trends Neurosci. *27*, 98–103.

Garcia, A.J., Koschnitzky, J.E., and Ramirez, J.M. (2013). The physiological determinants of Sudden Infant Death Syndrome. Respir. Physiol. Neurobiol. *189*, 288–300.

Gardner, R.T., Wang, L., Lang, B.T., Cregg, J.M., Dunbar, C.L., Woodward, W.R., Silver, J., Ripplinger, C.M., and Habecker, B.A. (2015). Targeting protein tyrosine phosphatase σ after myocardial infarction restores cardiac sympathetic innervation and prevents arrhythmias. Nat. Commun. *6*.

Gaultier, C., Amiel, J., Dauger, S., Trang, H., Lyonnet, S., Gallego, J., and Simonneau, M. (2004). Genetics and early disturbances of breathing control: the genetics of childhood disease and development: a series of review articles. Pediatr. Res. *55*, 729–733.

Gestreau, C., Heitzmann, D., Thomas, J., Dubreuil, V., Bandulik, S., Reichold, M., Bendahhou, S., Pierson, P., Sterner, C., Peyronnet-Roux, J., et al. (2010). Task2 potassium channels set central respiratory CO2 and O2 sensitivity. Proc. Natl. Acad. Sci. *107*, 2325–2330.

Ghali, M.Z. (2017). The crossed phrenic phenomenon. Neural Regen. Res. *12*, 845.

Ghali, M.G.Z., and Marchenko, V. (2016). Patterns of phrenic nerve discharge after complete high cervical spinal cord injury in the decerebrate rat. J.

Neurotrauma *33*, 1115–1127.

Gomeza, J., Hülsmann, S., Ohno, K., Eulenburg, V., Szöke, K., Richter, D., and Betz, H. (2003a). Inactivation of the glycine transporter 1 gene discloses vital role of glial glycine uptake in glycinergic inhibition. Neuron *40*, 785–796.

Gomeza, J., Ohno, K., Hülsmann, S., Armsen, W., Eulenburg, V., Richter, D.W., Laube, B., and Betz, H. (2003b). Deletion of the mouse glycine transporter 2 results in a hyperekplexia phenotype and postnatal lethality. Neuron *40*, 797–806.

Gray, P.A. (2008). Transcription factors and the genetic organization of brain stem respiratory neurons. J. Appl. Physiol. *104*, 1513–1521.

Gray, P.A. (2013). Transcription factors define the neuroanatomical organization of the medullary reticular formation. Front. Neuroanat. *7*, 7.

Gray, P.A., Rekling, J.C., Bocchiaro, C.M., and Feldman, J.L. (1999). Modulation of respiratory frequency by peptidergic input to rhythmogenic neurons in the preBötzinger complex. Science *286*, 1566–1568.

Gray, P.A., Janczewski, W.A., Mellen, N., McCrimmon, D.R., and Feldman, J.L. (2001). Normal breathing requires preBötzinger complex neurokinin-1 receptor-expressing neurons. Nat. Neurosci. *4*, 927–930.

Gray, P.A., Hayes, J.A., Ling, G.Y., Llona, I., Tupal, S., Picardo, M.C.D., Ross, S.E., Hirata, T., Corbin, J.G., Eugenin, J., et al. (2010). Developmental origin of preBotzinger complex respiratory neurons. J. Neurosci. *30*, 14883–14895.

Greer, J.J., and Martin-Caraballo, M. (2017). Developmental plasticity of phrenic motoneuron and diaphragm properties with the inception of inspiratory drive transmission in utero. Exp. Neurol. *287*, 137–143.

Greer, J.J., Funk, G.D., and Ballanyi, K. (2006). Preparing for the first breath: prenatal maturation of respiratory neural control. J. Physiol. *570*, 437–444.

Grillner, S. (2006). Biological pattern generation: the cellular and computational logic of networks in motion. Neuron *52*, 751–766.

Grossmann, K.S., Giraudin, A., Britz, O., Zhang, J., and Goulding, M. (2010). Genetic dissection of rhythmic motor networks in mice. Prog. Brain Res. *187*, 19–37.

Guerrier, C., Hayes, J.A., Fortin, G., and Holcman, D. (2015). Robust network oscillations during mammalian respiratory rhythm generation driven by synaptic dynamics. Proc. Natl. Acad. Sci. U. S. A. *112*, 9728–9733.

Guertin, P.A. (2012). Central pattern generator for locomotion: anatomical, physiological, and pathophysiological considerations. Front. Neurol. *3*, 183.

Guyenet, P.G., and Bayliss, D.A. (2015). Neural control of breathing and CO2 homeostasis. Neuron *87*, 946–961.

Guyenet, P.G., Stornetta, R.L., and Bayliss, D.A. (2010). Central respiratory chemoreception. J. Comp. Neurol. *518*, 3883–3906.

Guyenet, P.G., Bayliss, D.A., Stornetta, R.L., Ludwig, M.G., Kumar, N.N., Shi, Y., Burke, P.G.R., Kanbar, R., Basting, T.M., Holloway, B.B., et al. (2016). Proton detection and breathing regulation by the retrotrapezoid nucleus. J. Physiol. *594*, 1529–1551.

Hagglund, M., Dougherty, K.J., Borgius, L., Itohara, S., Iwasato, T., and Kiehn, O. (2013). Optogenetic dissection reveals multiple rhythmogenic modules underlying locomotion. Proc. Natl. Acad. Sci. *110*, 11589–11594.

Hägglund, M., Borgius, L., Dougherty, K.J., and Kiehn, O. (2010). Activation of groups of excitatory neurons in the mammalian spinal cord or hindbrain evokes locomotion. Nat. Neurosci. *13*, 246–252.

Hanson, M.G., and Landmesser, L.T. (2003). Characterization of the circuits that generate spontaneous episodes of activity in the early embryonic mouse spinal cord. J. Neurosci. *23*, 587–600.

Harvey, R.J., and Yee, B.K. (2013). Glycine transporters as novel therapeutic targets in schizophrenia, alcohol dependence and pain. Nat. Rev. Drug Discov. *12*, 866–885.

Hayes, J.A., and Del Negro, C.A. (2007). Neurokinin receptor-expressing pre-botzinger complex neurons in neonatal mice studied in vitro. J. Neurophysiol. *97*, 4215–4224.

Hayes, J.A., Wang, X., and Del Negro, C.A. (2012). Cumulative lesioning of respiratory interneurons disrupts and precludes motor rhythms in vitro. Proc. Natl. Acad. Sci. *109*, 8286–8291.

Hayes, J.A., Kottick, A., Picardo, M.C.D., Halleran, A.D., Smith, R.D., Smith, G.D., Saha, M.S., and Del Negro, C.A. (2017). Transcriptome of neonatal preBötzinger complex neurones in Dbx1 reporter mice. Sci. Rep. *7*, 8669.

Hilaire, G., Bou, C., and Monteau, R. (1997). Rostral ventrolateral medulla and respiratory rhythmogenesis in mice. Neurosci. Lett. *224*, 13–16.

Hilton, B.J., Lang, B.T., and Cregg, J.M. (2012). Keratan sulfate proteoglycans in plasticity and recovery after spinal cord injury. J. Neurosci. *32*.

Hodges, M.R., Tattersall, G.J., Harris, M.B., McEvoy, S.D., Richerson, D.N., Deneris, E.S., Johnson, R.L., Chen, Z.F., and Richerson, G.B. (2008). Defects in breathing and thermoregulation in mice with near-complete absence of central serotonin neurons. J. Neurosci. *28*, 2495–2505.

Holloway, B.B., Viar, K.E., Stornetta, R.L., and Guyenet, P.G. (2015). The retrotrapezoid nucleus stimulates breathing by releasing glutamate in adult conscious mice. Eur. J. Neurosci. *42*, 2271–2282.

Huang, R., Baca, S.M., Worrell, J.W., Liu, X., Seo, Y., Leiter, J.C., and Lu, D.C. (2016). Modulation of respiratory output by cervical epidural stimulation in the anesthetized mouse. J. Appl. Physiol. *121*, 1272–1281.

Huang, W.H., Tupal, S., Huang, T.W., Ward, C.S., Neul, J.L., Klisch, T.J., Gray, P.A., and Zoghbi, H.Y. (2012). Atoh1 governs the migration of postmitotic neurons that shape respiratory effectiveness at birth and chemoresponsiveness in adulthood. Neuron *75*, 799–809.

Hübner, C.A., Stein, V., Hermans-Borgmeyer, I., Meyer, T., Ballanyi, K., and Jentsch, T.J. (2001). Disruption of KCC2 reveals an essential role of K-Cl cotransport already in early synaptic inhibition. Neuron *30*, 515–524.

Huckstepp, R.T., Henderson, L.E., Cardoza, K.P., and Feldman, J.L. (2016). Interactions between respiratory oscillators in adult rats. Elife *5*, e14203.

Huckstepp, R.T.R., Cardoza, K.P., Henderson, L.E., and Feldman, J.L. (2015). Role of parafacial nuclei in control of breathing in adult rats. J. Neurosci. *35*, 1052–1067.

Hülsmann, S., Mesuret, G., Dannenberg, J., Arnoldt, M., and Niebert, M. (2016). GlyT2-dependent preservation of Mecp2-expression in inhibitory neurons improves early respiratory symptoms but does not rescue survival in a mouse model of Rett Syndrome. Front. Physiol. *7*, 385.

Hurtado, A., Cregg, J.M., Wang, H.B., Wendell, D.F., Oudega, M., Gilbert, R.J., and McDonald, J.W. (2011). Robust CNS regeneration after complete spinal cord transection using aligned poly-l-lactic acid microfibers. Biomaterials *32*.

Izhikevich, E.M. (2010). Dynamical systems in neuroscience : the geometry of excitability and bursting (MIT Press).

Jacquin, T.D., Borday, V., Schneider-Maunoury, S., Topilko, P., Ghilini, G., Kato, F., Charnay, P., and Champagnat, J. (1996). Reorganization of pontine

rhythmogenic neuronal networks in Krox-20 knockout mice. Neuron *17*, 747–758.

Janczewski, W.A., and Feldman, J.L. (2006). Distinct rhythm generators for inspiration and expiration in the juvenile rat. J. Physiol. *570*, 407–420.

Janczewski, W.A., Tashima, A., Hsu, P., Cui, Y., and Feldman, J.L. (2013). Role of inhibition in respiratory pattern generation. J. Neurosci. *33*, 5454–5465.

Jankowska, E., Jukes, M.G., Lund, S., and Lundberg, A. (1967). The effect of DOPA on the spinal cord. 5. Reciprocal organization of pathways transmitting excitatory action to alpha motoneurones of flexors and extensors. Acta Physiol. Scand. *70*, 369–388.

Jean-Xavier, C., Mentis, G.Z., O'Donovan, M.J., Cattaert, D., and Vinay, L. (2007). Dual personality of GABA/glycine-mediated depolarizations in immature spinal cord. Proc. Natl. Acad. Sci. *104*, 11477–11482.

Johnson, S.M., Smith, J.C., Funk, G.D., and Feldman, J.L. (1994). Pacemaker behavior of respiratory neurons in medullary slices from neonatal rat. J. Neurophysiol. *72*, 2598–2608.

Jonas, P., Bischofberger, J., and Sandkühler, J. (1998). Corelease of two fast neurotransmitters at a central synapse. Science *281*, 419–424.

Jones, S.E., and Dutschmann, M. (2016). Testing the hypothesis of neurodegeneracy in respiratory network function with a priori transected arterially perfused brain stem preparation of rat. J. Neurophysiol. *115*, 2593–2607.

Kaczyńska, K., and Szereda-Przestaszewska, M. (2013). Nodose ganglia-modulatory effects on respiration. Physiol. Res *62*, 227–235.

Kam, K., Worrell, J.W., Ventalon, C., Emiliani, V., and Feldman, J.L. (2013). Emergence of population bursts from simultaneous activation of small subsets of preBötzinger complex inspiratory neurons. J. Neurosci. *33*, 3332–3338.

Kang, B.J., Chang, D.A., MacKay, D.D., West, G.H., Moreira, T.S., Takakura, A.C., Gwilt, J.M., Guyenet, P.G., and Stornetta, R.L. (2007). Central nervous system distribution of the transcription factor Phox2b in the adult rat. J. Comp. Neurol. *503*, 627–641.

Kastanenka, K. V., and Landmesser, L.T. (2010). In vivo activation of channelrhodopsin-2 reveals that normal patterns of spontaneous activity are required for motoneuron guidance and maintenance of guidance molecules. J. Neurosci. *30*, 10575–10585.

Kastanenka, K. V., and Landmesser, L.T. (2013). Optogenetic-mediated

increases in in vivo spontaneous activity disrupt pool-specific but not dorsal-ventral motoneuron pathfinding. Proc. Natl. Acad. Sci. *110*, 17528–17533.

Katz, D.M., Dutschmann, M., Ramirez, J.M., and Hilaire, G. (2009). Breathing disorders in Rett syndrome: progressive neurochemical dysfunction in the respiratory network after birth. Respir. Physiol. Neurobiol. *168*, 101–108.

Kiehn, O. (2016). Decoding the organization of spinal circuits that control locomotion. Nat. Rev. Neurosci. *17*, 224–238.

Kjaerulff, O., and Kiehn, O. (1996). Distribution of networks generating and coordinating locomotor activity in the neonatal rat spinal cord in vitro: a lesion study. J. Neurosci. *16*, 5777–5794.

Koizumi, H., Mosher, B., Tariq, M.F., Zhang, R., Koshiya, N., and Smith, J.C. (2016). Voltage-dependent rhythmogenic property of respiratory pre-Bötzinger complex glutamatergic, Dbx1-derived, and somatostatin-expressing neuron populations revealed by graded optogenetic inhibition. eNeuro *3*.

Koshiya, N., and Guyenet, P.G. (1996). Tonic sympathetic chemoreflex after blockade of respiratory rhythmogenesis in the rat. J. Physiol. *491*, 859–869.

Koshiya, N., and Smith, J.C. (1999). Neuronal pacemaker for breathing visualized in vitro. Nature *400*, 360–363.

Kottick, A., and Del Negro, C.A. (2015). Synaptic depression influences inspiratory-expiratory phase transition in Dbx1 interneurons of the preBötzinger complex in neonatal mice. J. Neurosci. *35*, 11606–11611.

Kowalski, K.E., Hsieh, Y.H., Dick, T.E., and DiMarco, A.F. (2013). Diaphragm activation via high frequency spinal cord stimulation in a rodent model of spinal cord injury. Exp. Neurol. *247*, 689–693.

Kumar, N.N., Velic, A., Soliz, J., Shi, Y., Li, K., Wang, S., Weaver, J.L., Sen, J., Abbott, S.B.G., Lazarenko, R.M., et al. (2015). Regulation of breathing by CO2 requires the proton-activated receptor GPR4 in retrotrapezoid nucleus neurons. Science *348*, 1255–1260.

Landmesser, L.T., O'Donovan, M.J., and Honig, M. (1983). The response of avian hindlimb motor and sensory neurons to an altered periphery. Prog. Clin. Biol. Res. *110*, 207–216.

Lane, M.A., White, T.E., Coutts, M.A., Jones, A.L., Sandhu, M.S., Bloom, D.C., Bolser, D.C., Yates, B.J., Fuller, D.D., and Reier, P.J. (2008). Cervical prephrenic interneurons in the normal and lesioned spinal cord of the adult rat. J. Comp. Neurol. *511*, 692–709.

Lang, B.T., Cregg, J.M., Depaul, M.A., Tran, A.P., Xu, K., Dyck, S.M., Madalena, K.M., Brown, B.P., Weng, Y.L., Li, S., et al. (2015). Modulation of the proteoglycan receptor PTPσ promotes recovery after spinal cord injury. Nature *518*.

Langendorff, O. (1880). Ueber die spinalen centren der athmung. Arch. Für Physiol. 518–549.

Lanuza, G.M., Gosgnach, S., Pierani, A., Jessell, T.M., and Goulding, M. (2004). Genetic identification of spinal interneurons that coordinate left-right locomotor activity necessary for walking movements. Neuron *42*, 375–386.

Latal, A.T., Kremer, T., Gomeza, J., Eulenburg, V., and Hülsmann, S. (2010). Development of synaptic inhibition in glycine transporter 2 deficient mice. Mol. Cell. Neurosci. *44*, 342–352.

Lawson, E.E., Richter, D.W., Czyzyk-Krzeska, M.F., Bischoff, A., and Rudesill, R.C. (1991). Respiratory neuronal activity during apnea and other breathing patterns induced by laryngeal stimulation. J. Appl. Physiol. *70*, 2742–2749.

Lee, L.Y., and Yu, J. (2014). Sensory nerves in lung and airways. In Comprehensive Physiology, (Hoboken, NJ, USA: John Wiley & Sons, Inc.), pp. 287–324.

Leiter, J.C., and St. John, W.M. (2004). Phrenic, vagal and hypoglossal activities in rat: pre-inspiratory, inspiratory, expiratory components. Respir. Physiol. Neurobiol. *142*, 115–125.

Lepore, A.C., Rauck, B., Dejea, C., Pardo, A.C., Rao, M.S., Rothstein, J.D., and Maragakis, N.J. (2008). Focal transplantation–based astrocyte replacement is neuroprotective in a model of motor neuron disease. Nat. Neurosci. *11*, 1294–1301.

Li, W.C., and Moult, P.R. (2012). The control of locomotor frequency by excitation and inhibition. J. Neurosci. *32*, 6220–6230.

Li, P., Janczewski, W.A., Yackle, K., Kam, K., Pagliardini, S., Krasnow, M.A., and Feldman, J.L. (2016). The peptidergic control circuit for sighing. Nature *530*, 293–297.

Li, Y., Gorassini, M.A., and Bennett, D.J. (2003). Role of persistent sodium and calcium currents in motoneuron firing and spasticity in chronic spinal rats. J. Neurophysiol. *91*, 767–783.

Lieske, S.P., Thoby-Brisson, M., Telgkamp, P., and Ramirez, J.M. (2000).

Reconfiguration of the neural network controlling multiple breathing patterns: eupnea, sighs and gasps. Nat. Neurosci. *3*, 600–607.

Lin, J.Y., Knutsen, P.M., Muller, A., Kleinfeld, D., and Tsien, R.Y. (2013). ReaChR: a red-shifted variant of channelrhodopsin enables deep transcranial optogenetic excitation. Nat. Neurosci. *16*, 1499–1508.

Lipski, J. (1984). Is there electrical coupling between phrenic motoneurons in cats? Neurosci. Lett. *46*, 229–234.

Lipski, J., Duffin, J., Kruszewska, B., and Zhang, X. (1993). Upper cervical inspiratory neurons in the rat: an electrophysiological and morphological study. Exp. Brain Res. *95*, 477–487.

Lois, J.H., Rice, C.D., and Yates, B.J. (2009). Neural circuits controlling diaphragm function in the cat revealed by transneuronal tracing. J. Appl. Physiol. *106*, 138–152.

Long, S., and Duffin, J. (1986). The neuronal determinants of respiratory rhythm. Prog. Neurobiol. *27*, 101–182.

Lu, B., Su, Y., Das, S., Liu, J., Xia, J., and Ren, D. (2007). The neuronal channel Nalcn contributes resting sodium permeability and is required for normal respiratory rhythm. Cell *129*, 371–383.

Lu, B., Su, Y., Das, S., Wang, H., Wang, Y., Liu, J., and Ren, D. (2009). Peptide neurotransmitters activate a cation channel complex of NALCN and UNC-80. Nature *457*, 741–744.

Ludwig, M.G., Vanek, M., Guerini, D., Gasser, J.A., Jones, C.E., Junker, U., Hofstetter, H., Wolf, R.M., and Seuwen, K. (2003). Proton-sensing G-protein-coupled receptors. Nature *425*, 93–98.

Lumsden, A., and Krumlauf, R. (1996). Patterning the vertebrate neuraxis. Science *274*, 1109–1115.

Macefield, G., and Nail, B. (1987). Phrenic and external intercostal motoneuron activity during progressive asphyxia. J. Appl. Physiol. *63*, 1413–1420.

Mantilla, C.B., Zhan, W.Z., and Sieck, G.C. (2009). Retrograde labeling of phrenic motoneurons by intrapleural injection. J. Neurosci. Methods *182*, 244–249.

Marchenko, V., Koizumi, H., Mosher, B., Koshiya, N., Tariq, M.F., Bezdudnaya, T.G., Zhang, R., Molkov, Y.I., Rybak, I.A., and Smith, J.C. (2016). Perturbations of respiratory rhythm and pattern by disrupting synaptic inhibition within pre-

Bötzinger and Bötzinger complexes. eNeuro *3*.

Marder, E. (2001). Moving rhythms. Nature *410*, 755–755.

Maricich, S.M., Wellnitz, S.A., Nelson, A.M., Lesniak, D.R., Gerling, G.J., Lumpkin, E.A., and Zoghbi, H.Y. (2009). Merkel cells are essential for light-rouch responses. Science *324*, 1580–1582.

Matei, V., Pauley, S., Kaing, S., Rowitch, D., Beisel, K.W., Morris, K., Feng, F., Jones, K., Lee, J., and Fritzsch, B. (2005). Smaller inner ear sensory epithelia in Neurog1 null mice are related to earlier hair cell cycle exit. Dev. Dyn. *234*, 633–650.

McClellan, A.D. (1984). Descending control and sensory gating of “fictive” swimming and turning responses elicited in an in vitro preparation of the lamprey brainstem/spinal cord. Brain Res. *302*, 151–162.

McCrimmon, D.R., Monnier, A., Ptak, K., Zummo, G., Zhang, Z., and Alheid, G.F. (2001). Respiratory rhythm generation: preBötzinger neuron discharge patterns and persistent sodium current. Adv. Exp. Med. Biol. *499*, 147–152.

McElvain, L.E., Friedman, B., Karten, H.J., Svoboda, K., Wang, F., Deschênes, M., and Kleinfeld, D. (2017). Circuits in the rodent brainstem that control whisking in concert with other orofacial motor actions. Neuroscience 10.1016/j.neuroscience.2017.08.034.

McKay, L.C., Janczewski, W.A., and Feldman, J.L. (2005). Sleep-disordered breathing after targeted ablation of preBötzinger complex neurons. Nat. Neurosci. *8*, 1142–1144.

McLean, D.L., and Dougherty, K.J. (2015). Peeling back the layers of locomotor control in the spinal cord. Curr. Opin. Neurobiol. *33*, 63–70.

Mellen, N.M., Janczewski, W.A., Bocchiaro, C.M., and Feldman, J.L. (2003). Opioid-induced quantal slowing reveals dual networks for respiratory rhythm generation. Neuron *37*, 821–826.

Mentis, G.Z., Alvarez, F.J., Bonnot, A., Richards, D.S., Gonzalez-Forero, D., Zerda, R., and O’Donovan, M.J. (2005). Noncholinergic excitatory actions of motoneurons in the neonatal mammalian spinal cord. Proc. Natl. Acad. Sci. U. S. A. *102*, 7344–7349.

Misgeld, T., Burgess, R.W., Lewis, R.M., Cunningham, J.M., Lichtman, J.W., and Sanes, J.R. (2002). Roles of neurotransmitter in synapse formation: development of neuromuscular junctions lacking choline acetyltransferase. Neuron *36*, 635–648.

Mitchell, G.S. (2004). Back to the future: carbon dioxide chemoreceptors in the mammalian brain. Nat. Neurosci. *7*, 1288–1290.

Mombaerts, P., Wang, F., Dulac, C., Chao, S.K., Nemes, A., Mendelsohn, M., Edmondson, J., and Axel, R. (1996). Visualizing an olfactory sensory map. Cell *87*, 675–686.

Momose-Sato, Y., and Sato, K. (2013). Optical imaging of the spontaneous depolarization wave in the mouse embryo: origins and pharmacological nature. Ann. N. Y. Acad. Sci. *1279*, 60–70.

Momose-Sato, Y., Nakamori, T., and Sato, K. (2012a). Spontaneous depolarization wave in the mouse embryo: origin and large-scale propagation over the CNS identified with voltage-sensitive dye imaging. Eur. J. Neurosci. *35*, 1230–1241.

Momose-Sato, Y., Nakamori, T., and Sato, K. (2012b). Pharmacological mechanisms underlying switching from the large-scale depolarization wave to segregated activity in the mouse central nervous system. Eur. J. Neurosci. *35*, 1242–1252.

Morgado-Valle, C., Baca, S.M., and Feldman, J.L. (2010). Glycinergic pacemaker neurons in preBötzinger complex of neonatal mouse. J. Neurosci. *30*, 3634–3639.

Mörschel, M., and Dutschmann, M. (2009). Pontine respiratory activity involved in inspiratory/expiratory phase transition. Philos. Trans. R. Soc. Lond. B. Biol. Sci. *364*, 2517–2526.

Moult, P.R., Cottrell, G.A., and Li, W.C. (2013). Fast silencing reveals a lost role for reciprocal inhibition in locomotion. Neuron *77*, 129–140.

Mulkey, D.K., Stornetta, R.L., Weston, M.C., Simmons, J.R., Parker, A., Bayliss, D.A., and Guyenet, P.G. (2004). Respiratory control by ventral surface chemoreceptor neurons in rats. Nat. Neurosci. *7*, 1360–1369.

Mulkey, D.K., Talley, E.M., Stornetta, R.L., Siegel, A.R., West, G.H., Chen, X., Sen, N., Mistry, A.M., Guyenet, P.G., and Bayliss, D.A. (2007). TASK channels determine pH sensitivity in select respiratory neurons but do not contribute to central respiratory chemosensitivity. J. Neurosci. *27*, 14049–14058.

Myers, C.P., Lewcock, J.W., Hanson, M.G., Gosgnach, S., Aimone, J.B., Gage, F.H., Lee, K.F., Landmesser, L.T., and Pfaff, S.L. (2005). Cholinergic input is required during embryonic development to mediate proper assembly of spinal locomotor circuits. Neuron *46*, 37–49.

National Spinal Cord Injury Statistical Center (2016). Spinal cord injury (SCI) 2016 facts and figures at a glance. J. Spinal Cord Med. *39*, 493–494.

Del Negro, C.A., and Hayes, J.A. (2008). A “group pacemaker” mechanism for respiratory rhythm generation. J. Physiol. *586*, 2245–2246.

Del Negro, C.A., Johnson, S.M., Butera, R.J., and Smith, J.C. (2001). Models of respiratory rhythm generation in the pre-Bötzinger complex. III. Experimental tests of model predictions. J. Neurophysiol. *86*, 59–74.

Del Negro, C.A., Koshiya, N., Butera, R.J., and Smith, J.C. (2002a). Persistent sodium current, membrane properties and bursting behavior of pre-bötzinger complex inspiratory neurons in vitro. J. Neurophysiol. *88*, 2242–2250.

Del Negro, C.A., Morgado-Valle, C., and Feldman, J.L. (2002b). Respiratory rhythm: an emergent network property? Neuron *34*, 821–830.

Del Negro, C.A., Morgado-Valle, C., Hayes, J.A., Mackay, D.D., Pace, R.W., Crowder, E.A., and Feldman, J.L. (2005). Sodium and calcium current-mediated pacemaker neurons and respiratory rhythm generation. J. Neurosci. *25*, 446–453.

Del Negro, C.A., Pace, R.W., and Hayes, J.A. (2008). What role do pacemakers play in the generation of respiratory rhythm? Adv. Exp. Med. Biol. *605*, 88–93.

Del Negro, C.A., Hayes, J.A., and Rekling, J.C. (2011). Dendritic Calcium Activity Precedes Inspiratory Bursts in preBotzinger Complex Neurons. J. Neurosci. *31*, 1017–1022.

Niemi, J.P., DeFrancesco-Lisowitz, A., Cregg, J.M., Howarth, M., and Zigmond, R.E. (2016). Overexpression of the monocyte chemokine CCL2 in dorsal root ganglion neurons causes a conditioning-like increase in neurite outgrowth and does so via a STAT3 dependent mechanism. Exp. Neurol. *275*.

Nishimaru, H., Restrepo, C.E., Ryge, J., Yanagawa, Y., and Kiehn, O. (2005). Mammalian motor neurons corelease glutamate and acetylcholine at central synapses. Proc. Natl. Acad. Sci. U. S. A. *102*, 5245–5249.

Nonomura, K., Woo, S.H., Chang, R.B., Gillich, A., Qiu, Z., Francisco, A.G., Ranade, S.S., Liberles, S.D., and Patapoutian, A. (2017). Piezo2 senses airway stretch and mediates lung inflation-induced apnoea. Nature *541*, 176–181.

Okada, Y., Mückenhoff, K., Holtermann, G., Acker, H., and Scheid, P. (1993). Depth profiles of pH and PO2 in the isolated brain stem-spinal cord of the neonatal rat. Respir. Physiol. *93*, 315–326.

Oliveira, A.L.R., Hydling, F., Olsson, E., Shi, T., Edwards, R.H., Fujiyama, F., Kaneko, T., Hökfelt, T., Cullheim, S., and Meister, B. (2003). Cellular localization of three vesicular glutamate transporter mRNAs and proteins in rat spinal cord and dorsal root ganglia. Synapse *50*, 117–129.

Onimaru, H., Homma, I., Gilthorpe, J., Jungbluth, S., Champagnat, J., Lumsden, A., and Fortin, G. (2003). A novel functional neuron group for respiratory rhythm generation in the ventral medulla. J. Neurosci. *23*, 1478–1486.

Otsuka, M., and Konishi, S. (1974). Electrophysiology of mammalian spinal cord in vitro. Nature *252*, 733–734.

Pace, R.W., Mackay, D.D., Feldman, J.L., and Del Negro, C.A. (2007). Inspiratory bursts in the preBötzinger complex depend on a calcium-activated non-specific cation current linked to glutamate receptors in neonatal mice. J. Physiol. *582*, 113–125.

Pagliardini, S., Janczewski, W.A., Tan, W., Dickson, C.T., Deisseroth, K., and Feldman, J.L. (2011). Active expiration induced by excitation of ventral medulla in adult anesthetized rats. J. Neurosci. *31*, 2895–2905.

Pattyn, A., Morin, X., Cremer, H., Goridis, C., and Brunet, J.F. (1999). The homeobox gene Phox2b is essential for the development of autonomic neural crest derivatives. Nature *399*, 366–370.

Peña, F., Parkis, M.A., Tryba, A.K., and Ramirez, J.M. (2004). Differential contribution of pacemaker properties to the generation of respiratory rhythms during normoxia and hypoxia. Neuron *43*, 105–117.

Pérez de Los Cobos Pallares, F., Bautista, T.G., Stanić, D., Egger, V., and Dutschmann, M. (2016). Brainstem-mediated sniffing and respiratory modulation during odor stimulation. Respir. Physiol. Neurobiol. *233*, 17–24.

Perkel, D.H., and Mulloney, B. (1974). Motor pattern production in reciprocally inhibitory neurons exhibiting postinhibitory rebound. Science *185*, 181–183.

Person, A.L., and Raman, I.M. (2011). Purkinje neuron synchrony elicits time-locked spiking in the cerebellar nuclei. Nature *481*, 502–505.

Philippidou, P., and Dasen, J.S. (2013). Hox genes: choreographers in neural development, architects of circuit organization. Neuron *80*, 12–34.

Philippidou, P., Walsh, C.M., Aubin, J., Jeannotte, L., and Dasen, J.S. (2012). Sustained Hox5 gene activity is required for respiratory motor neuron development. Nat. Neurosci. *15*, 1636–1644.

Porter, W.T. (1895). The path of the respiratory impulse from the bulb to the phrenic nuclei. J. Physiol. *17*, 455–485.

Ptak, K., Yamanishi, T., Aungst, J., Milescu, L.S., Zhang, R., Richerson, G.B., and Smith, J.C. (2009). Raphé neurons stimulate respiratory circuit activity by multiple mechanisms via endogenously released serotonin and substance P. J. Neurosci. *29*, 3720–3737.

Rahman, J., Latal, A.T., Besser, S., Hirrlinger, J., and Hülsmann, S. (2013). Mixed miniature postsynaptic currents resulting from co-release of glycine and GABA recorded from glycinergic neurons in the neonatal respiratory network. Eur. J. Neurosci. *37*, 1229–1241.

Rahman, J., Besser, S., Schnell, C., Eulenburg, V., Hirrlinger, J., Wojcik, S.M., and Hülsmann, S. (2015). Genetic ablation of VIAAT in glycinergic neurons causes a severe respiratory phenotype and perinatal death. Brain Struct. Funct. *220*, 2835–2849.

Ramirez, J.M. (2011). The human pre-Botzinger complex identified. Brain *134*, 8–10.

Ramirez, J.M. (2014). The integrative role of the sigh in psychology, physiology, pathology, and neurobiology. In Progress in Brain Research, pp. 91–129.

Ramirez, J.M., Quellmalz, U.J., and Richter, D.W. (1996). Postnatal changes in the mammalian respiratory network as revealed by the transverse brainstem slice of mice. J. Physiol. *491*, 799–812.

Ramirez, J.M., Schwarzacher, S.W., Pierrefiche, O., Olivera, B.M., and Richter, D.W. (1998). Selective lesioning of the cat pre-Bötzinger complex in vivo eliminates breathing but not gasping. J. Physiol. *507*, 895–907.

Ramirez, J.M., Ward, C.S., and Neul, J.L. (2013a). Breathing challenges in Rett syndrome: lessons learned from humans and animal models. Respir. Physiol. Neurobiol. *189*, 280–287.

Ramirez, J.M., Garcia, A.J., Anderson, T.M., Koschnitzky, J.E., Peng, Y.J., Kumar, G.K., and Prabhakar, N.R. (2013b). Central and peripheral factors contributing to obstructive sleep apneas. Respir. Physiol. Neurobiol. *189*, 344–353.

Ranade, S.S., Woo, S.H., Dubin, A.E., Moshourab, R.A., Wetzel, C., Petrus, M., Mathur, J., Bégay, V., Coste, B., Mainquist, J., et al. (2014). Piezo2 is the major transducer of mechanical forces for touch sensation in mice. Nature *516*, 121–125.

Ray, R.S., Corcoran, A.E., Brust, R.D., Kim, J.C., Richerson, G.B., Nattie, E., and Dymecki, S.M. (2011). Impaired respiratory and body temperature control upon acute serotonergic neuron inhibition. Science *333*, 637–642.

Ray, R.S., Corcoran, A.E., Brust, R.D., Soriano, L.P., Nattie, E.E., and Dymecki, S.M. (2013). Egr2-neurons control the adult respiratory response to hypercapnia. Brain Res. *1511*, 115–125.

Rees, M.I., Harvey, K., Pearce, B.R., Chung, S.K., Duguid, I.C., Thomas, P., Beatty, S., Graham, G.E., Armstrong, L., Shiang, R., et al. (2006). Mutations in the gene encoding GlyT2 (SLC6A5) define a presynaptic component of human startle disease. Nat. Genet. *38*, 801–806.

Reinoso, M.A., Sieck, G.C., and Hubmayr, R.D. (1996). Respiratory muscle coordination in acute spinal dogs. Respir. Physiol. *104*, 29–37.

Rekling, J.C., and Feldman, J.L. (1998). PreBötzinger complex and pacemaker neurons: hypothesized site and kernel for respiratory rhythm generation. Annu. Rev. Physiol. *60*, 385–405.

Ren, J., and Greer, J.J. (2006). Modulation of respiratory rhythmogenesis by chloride-mediated conductances during the perinatal period. J. Neurosci. *26*, 3721–3730.

Revill, A.L., Vann, N.C., Akins, V.T., Kottick, A., Gray, P.A., Del Negro, C.A., and Funk, G.D. (2015). Dbx1 precursor cells are a source of inspiratory XII premotoneurons. Elife *4*.

Reyes, R., Duprat, F., Lesage, F., Fink, M., Salinas, M., Farman, N., and Lazdunski, M. (1998). Cloning and expression of a novel pH-sensitive two pore domain K+ channel from human kidney. J. Biol. Chem. *273*, 30863–30869.

Richter, D.W. (1982). Generation and maintenance of the respiratory rhythm. J. Exp. Biol. *100*, 93–107.

Richter, D.W., and Smith, J.C. (2014). Respiratory rhythm generation in vivo. Physiology *29*, 58–71.

Ritter, B., and Zhang, W. (2000). Early postnatal maturation of GABA A -mediated inhibition in the brainstem respiratory rhythm-generating network of the mouse. Eur. J. Neurosci. *12*, 2975–2984.

Rivera, C., Voipio, J., Payne, J.A., Ruusuvuori, E., Lahtinen, H., Lamsa, K., Pirvola, U., Saarma, M., and Kaila, K. (1999). The K+/Cl- co-transporter KCC2 renders GABA hyperpolarizing during neuronal maturation. Nature *397*, 251–255.

Rose, M.F., Ren, J., Ahmad, K.A., Chao, H.T., Klisch, T.J., Flora, A., Greer, J.J., and Zoghbi, H.Y. (2009). Math1 is essential for the development of hindbrain neurons critical for perinatal breathing. Neuron *64*, 341–354.

Rovainen, C.M. (1983). Generation of respiratory activity by the lamprey brain exposed to picrotoxin and strychnine, and weak synaptic inhibition in motoneurons. Neuroscience *10*, 875–882.

Rubin, J.E., Hayes, J.A., Mendenhall, J.L., and Del Negro, C.A. (2009). Calcium-activated nonspecific cation current and synaptic depression promote network-dependent burst oscillations. Proc. Natl. Acad. Sci. U. S. A. *106*, 2939–2944.

Ruffault, P.L., D'Autréaux, F., Hayes, J.A., Nomaksteinsky, M., Autran, S., Fujiyama, T., Hoshino, M., Hägglund, M., Kiehn, O., Brunet, J.F., et al. (2015). The retrotrapezoid nucleus neurons expressing Atoh1 and Phox2b are essential for the respiratory response to CO2. Elife *4*, e07051.

Russier, M., Kopysova, I.L., Ankri, N., Ferrand, N., and Debanne, D. (2002). GABA and glycine co-release optimizes functional inhibition in rat brainstem motoneurons in vitro. J. Physiol. *541*, 123–137.

Rybak, I.A., Ptak, K., Shevtsova, N.A., and McCrimmon, D.R. (2003). Sodium currents in neurons from the rostroventrolateral medulla of the rat. J. Neurophysiol. *90*, 1635–1642.

Schneider-Maunoury, S., Topilko, P., Seitandou, T., Levi, G., Cohen-Tannoudji, M., Pournin, S., Babinet, C., and Charnay, P. (1993). Disruption of Krox-20 results in alteration of rhombomeres 3 and 5 in the developing hindbrain. Cell *75*, 1199–1214.

Schwarzacher, S.W., Rüb, U., and Deller, T. (2011). Neuroanatomical characteristics of the human pre-Bötzinger complex and its involvement in neurodegenerative brainstem diseases. Brain *134*, 24–35.

Scott, M.M., Williams, K.W., Rossi, J., Lee, C.E., and Elmquist, J.K. (2011). Leptin receptor expression in hindbrain Glp-1 neurons regulates food intake and energy balance in mice. J. Clin. Invest. *121*, 2413–2421.

Sherman, D., Worrell, J.W., Cui, Y., and Feldman, J.L. (2015). Optogenetic perturbation of preBötzinger complex inhibitory neurons modulates respiratory pattern. Nat. Neurosci. *18*, 408–414.

Shevtsova, N.A., Büsselberg, D., Molkov, Y.I., Bischoff, A.M., Smith, J.C., Richter, D.W., and Rybak, I.A. (2014). Effects of glycinergic inhibition failure on respiratory rhythm and pattern generation. In Progress in Brain Research, pp.

25–38.

Shi, Y., Abe, C., Holloway, B.B., Shu, S., Kumar, N.N., Weaver, J.L., Sen, J., Perez-Reyes, E., Stornetta, R.L., Guyenet, P.G., et al. (2016). Nalcn is a “leak” sodium channel that regulates excitability of brainstem chemosensory neurons and breathing. J. Neurosci. *36*, 8174–8187.

Silver, J.R., and Lehr, R.P. (1981). Dyspnoea during generalised spasms in tetraplegic patients. J. Neurol. Neurosurg. Psychiatry *44*, 842–845.

Skinner, F.K., Kopell, N., and Marder, E. (1994). Mechanisms for oscillation and frequency control in reciprocally inhibitory model neural networks. J. Comput. Neurosci. *1*, 69–87.

Smith, J.C., and Feldman, J.L. (1987). In vitro brainstem-spinal cord preparations for study of motor systems for mammalian respiration and locomotion. J. Neurosci. Methods *21*, 321–333.

Smith, J., Ellenberger, H., Ballanyi, K., Richter, D., and Feldman, J. (1991). Pre-Botzinger complex: a brainstem region that may generate respiratory rhythm in mammals. Science *254*, 726–729.

Smith, J.C., Greer, J.J., Liu, G.S., and Feldman, J.L. (1990). Neural mechanisms generating respiratory pattern in mammalian brain stem-spinal cord in vitro. I. Spatiotemporal patterns of motor and medullary neuron activity. J. Neurophysiol. *64*, 1149–1169.

Sofroniew, N.J., Flickinger, D., King, J., and Svoboda, K. (2016). A large field of view two-photon mesoscope with subcellular resolution for in vivo imaging. Elife *5*.

St John, W.M. (1990). Neurogenesis, control, and functional significance of gasping. J. Appl. Physiol. *68*, 1305–1315.

St John, W.M. (2009). Noeud vital for breathing in the brainstem: gasping--yes, eupnoea--doubtful. Philos. Trans. R. Soc. Lond. B. Biol. Sci. *364*, 2625–2633.

Stein, V., Hermans-Borgmeyer, I., Jentsch, T.J., and Hübner, C.A. (2004). Expression of the KCl cotransporter KCC2 parallels neuronal maturation and the emergence of low intracellular chloride. J. Comp. Neurol. *468*, 57–64.

Stornetta, R.L., Rosin, D.L., Wang, H., Sevigny, C.P., Weston, M.C., and Guyenet, P.G. (2003). A group of glutamatergic interneurons expressing high levels of both neurokinin-1 receptors and somatostatin identifies the region of the pre-Bötzinger complex. J. Comp. Neurol. *455*, 499–512.

Stornetta, R.L., Moreira, T.S., Takakura, A.C., Kang, B.J., Chang, D.A., West, G.H., Brunet, J.F., Mulkey, D.K., Bayliss, D.A., and Guyenet, P.G. (2006). Expression of Phox2b by brainstem n neurons involved in chemosensory integration in the adult rat. J. Neurosci. *26*, 10305–10314.

Stuart, D.G., and Hultborn, H. (2008). Thomas Graham Brown (1882--1965), Anders Lundberg (1920-), and the neural control of stepping. Brain Res. Rev. *59*, 74–95.

Suzue, T. (1984). Respiratory rhythm generation in the in vitro brain stem-spinal cord preparation of the neonatal rat. J. Physiol. *354*, 173–183.

Suzue, T., and Jessell, T. (1980). Opiate analgesics and endorphins inhibit rat dorsal root potential in vitro. Neurosci. Lett. *16*, 161–166.

Swiatek, P.J., and Gridley, T. (1993). Perinatal lethality and defects in hindbrain development in mice homozygous for a targeted mutation of the zinc finger gene Krox20. Genes Dev. *7*, 2071–2084.

Talley, E.M., Solorzano, G., Lei, Q., Kim, D., and Bayliss, D.A. (2001). CNS distribution of members of the two-pore-domain (KCNK) potassium channel family. J. Neurosci. *21*, 7491–7505.

Talpalar, A.E., Endo, T., Löw, P., Borgius, L., Hägglund, M., Dougherty, K.J., Ryge, J., Hnasko, T.S., and Kiehn, O. (2011). Identification of minimal neuronal networks Involved in flexor-extensor alternation in the mammalian spinal cord. Neuron *71*, 1071–1084.

Tan, W., Janczewski, W.A., Yang, P., Shao, X.M., Callaway, E.M., and Feldman, J.L. (2008). Silencing preBötzinger complex somatostatin-expressing neurons induces persistent apnea in awake rat. Nat. Neurosci. *11*, 538–540.

Thoby-Brisson, M., and Ramirez, J.M. (2001). Identification of two types of inspiratory pacemaker neurons in the isolated respiratory neural network of mice. J. Neurophysiol. *86*, 104–112.

Thoby-Brisson, M., Telgkamp, P., and Ramirez, J.M. (2000). The role of the hyperpolarization-activated current in modulating rhythmic activity in the isolated respiratory network of mice. J. Neurosci. *20*, 2994–3005.

Thoby-Brisson, M., Trinh, J.B., Champagnat, J., and Fortin, G. (2005). Emergence of the pre-Bötzinger respiratory rhythm generator in the mouse embryo. J. Neurosci. *25*, 4307–4318.

Thoby-Brisson, M., Karlén, M., Wu, N., Charnay, P., Champagnat, J., and Fortin, G. (2009). Genetic identification of an embryonic parafacial oscillator coupling to

the preBötzinger complex. Nat. Neurosci. *12*, 1028–1035.

Tresch, M.C., and Kiehn, O. (2000). Motor coordination without action potentials in the mammalian spinal cord. Nat. Neurosci. *3*, 593–599.

Tryba, A.K., Peña, F., and Ramirez, J.-M. (2006). Gasping activity in vitro: a rhythm dependent on 5-HT2A receptors. J. Neurosci. *26*, 2623–2634.

Tupal, S., Huang, W.H., Picardo, M.C.D., Ling, G.Y., Del Negro, C.A., Zoghbi, H.Y., and Gray, P.A. (2014). Atoh1-dependent rhombic lip neurons are required for temporal delay between independent respiratory oscillators in embryonic mice. Elife *3*, e02265.

Turgeon, B., and Meloche, S. (2009). Interpreting neonatal lethal phenotypes in mouse mutants: insights into gene function and human diseases. Physiol. Rev. *89*, 1–26.

Ueno, M., Ueno-Nakamura, Y., Niehaus, J., Popovich, P.G., and Yoshida, Y. (2016). Silencing spinal interneurons inhibits immune suppressive autonomic reflexes caused by spinal cord injury. Nat. Neurosci. *19*, 784–787.

Usiak, M.F., and Landmesser, L.T. (1999). Neuromuscular activity blockade induced by muscimol and d-tubocurarine differentially affects the survival of embryonic chick motoneurons. J. Neurosci. *19*, 7925–7939.

Vann, N.C., Pham, F.D., Hayes, J.A., Kottick, A., and Del Negro, C.A. (2016). Transient suppression of Dbx1 preBötzinger interneurons disrupts breathing in adult mice. PLoS One *11*, e0162418.

Varoqueaux, F., Sons, M.S., Plomp, J.J., and Brose, N. (2005). Aberrant morphology and residual transmitter release at the Munc13-deficient mouse neuromuscular synapse. Mol. Cell. Biol. *25*, 5973–5984.

Viala, D., Vidal, C., and Freton, E. (1979). Coordinated rhythmic bursting in respiratory and locomotor muscle nerves in the spinal rabbit. Neurosci. Lett. *11*, 155–159.

Vong, L., Ye, C., Yang, Z., Choi, B., Chua, S., and Lowell, B.B. (2011). Leptin action on GABAergic neurons prevents Oobesity and reduces inhibitory tone to POMC neurons. Neuron *71*, 142–154.

Wallen-Mackenzie, A., Gezelius, H., Thoby-Brisson, M., Nygard, A., Enjin, A., Fujiyama, F., Fortin, G., and Kullander, K. (2006). Vesicular glutamate transporter 2 is required for central respiratory rhythm generation but not for locomotor central pattern generation. J. Neurosci. *26*, 12294–12307.

Wang, D., Grillner, S., and Wallén, P. (2011). 5-HT and dopamine modulates CaV1.3 calcium channels involved in postinhibitory rebound in the spinal network for locomotion in lamprey. J. Neurophysiol. *105*, 1212–1224.

Wang, H.B., Mullins, M.E., Cregg, J.M., Hurtado, A., Oudega, M., Trombley, M.T., and Gilbert, R.J. (2009a). Creation of highly aligned electrospun poly-L-lactic acid fibers for nerve regeneration applications. J. Neural Eng. *6*.

Wang, H.B., Mullins, M.E., Cregg, J.M., McCarthy, C.W., and Gilbert, R.J. (2010). Varying the diameter of aligned electrospun fibers alters neurite outgrowth and Schwann cell migration. Acta Biomater. *6*.

Wang, S., Polo-Parada, L., and Landmesser, L.T. (2009b). Characterization of rhythmic Ca2+ transients in early embryonic chick motoneurons: Ca2+ sources and effects of altered activation of transmitter receptors. J. Neurosci. *29*, 15232–15244.

Wang, S., Benamer, N., Zanella, S., Kumar, N.N., Shi, Y., Bevengut, M., Penton, D., Guyenet, P.G., Lesage, F., Gestreau, C., et al. (2013). TASK-2 channels contribute to pH sensitivity of retrotrapezoid nucleus chemoreceptor neurons. J. Neurosci. *33*, 16033–16044.

Wang, X., Hayes, J.A., Revill, A.L., Song, H., Kottick, A., Vann, N.C., LaMar, M.D., Picardo, M.C.D., Akins, V.T., Funk, G.D., et al. (2014). Laser ablation of Dbx1 neurons in the pre-Bötzinger complex stops inspiratory rhythm and impairs output in neonatal mice. Elife *3*, e03427.

Warren, P.M., and Alilain, W.J. (2014). The challenges of respiratory motor system recovery following cervical spinal cord injury. In Progress in Brain Research, pp. 173–220.

Warren, P.M., Awad, B.I., and Alilain, W.J. (2014). Drawing breath without the command of effectors: The control of respiration following spinal cord injury. Respir. Physiol. Neurobiol. *203*, 98–108.

Washbourne, P., Thompson, P.M., Carta, M., Costa, E.T., Mathews, J.R., Lopez-Benditó, G., Molnár, Z., Becher, M.W., Valenzuela, C.F., Partridge, L.D., et al. (2002). Genetic ablation of the t-SNARE SNAP-25 distinguishes mechanisms of neuroexocytosis. Nat. Neurosci. *5*, 19–26.

Washburn, C.P., Sirois, J.E., Talley, E.M., Guyenet, P.G., and Bayliss, D.A. (2002). Serotonergic raphe neurons express TASK channel transcripts and a TASK-like pH- and halothane-sensitive K+ conductance. J. Neurosci. *22*, 1256–1265.

Washburn, C.P., Bayliss, D.A., and Guyenet, P.G. (2003). Cardiorespiratory

neurons of the rat ventrolateral medulla contain TASK-1 and TASK-3 channel mRNA. Respir. Physiol. Neurobiol. *138*, 19–35.

Wertheimer, E. (1886). Recherches expérimentales sur les centres respiratoires de la moelleépinière. J L'anat La Physiol *22*, 458–507.

Wojcik, S.M., Katsurabayashi, S., Guillemin, I., Friauf, E., Rosenmund, C., Brose, N., and Rhee, J.S. (2006). A shared vesicular carrier allows synaptic corelease of GABA and glycine. Neuron *50*, 575–587.

Woo, S.H., Ranade, S., Weyer, A.D., Dubin, A.E., Baba, Y., Qiu, Z., Petrus, M., Miyamoto, T., Reddy, K., Lumpkin, E.A., et al. (2014). Piezo2 is required for Merkel-cell mechanotransduction. Nature *509*, 622–626.

Wu, J., Capelli, P., Bouvier, J., Goulding, M., Arber, S., and Fortin, G. (2017). A V0 core neuronal circuit for inspiration. Nat. Commun. *8*, 544.

Yeh, S.Y., Huang, W.H., Wang, W., Ward, C.S., Chao, E.S., Wu, Z., Tang, B., Tang, J., Sun, J.J., Esther van der Heijden, M., et al. (2017). Respiratory network stability and modulatory response to substance P require Nalcn. Neuron *94*, 294–303.

Zhang, J.W., Walker, J.F., Guardiola, J., and Yu, J. (2006). Reflexes from the lungs and airways pulmonary sensory and reflex responses in the mouse pulmonary sensory and reflex responses in the mouse. J Appl Physiol *101*, 986–992.

Zimmer, M.B., and Goshgarian, H.G. (2007). GABA, not glycine, mediates inhibition of latent respiratory motor pathways after spinal cord injury. Exp. Neurol. *203*, 493–501.